UNIVERSITÄT PADERBORN
Die Universität der Informationsgesellschaft

FAKULTÄT FÜR
ELEKTROTECHNIK,
INFORMATIK UND
MATHEMATIK

Selwan Khaleel Ibrahim

Study of Multilevel Modulation Formats for High Speed Digital Optical Communication Systems

Ph.D. Dissertation

Paderborn, July 2007

UNIVERSITÄT PADERBORN
Die Universität der Informationsgesellschaft

FAKULTÄT FÜR
ELEKTROTECHNIK,
INFORMATIK UND
MATHEMATIK

Study of Multilevel Modulation Formats for High Speed Digital Optical Communication Systems

Zur Erlangung des akademischen Grades

DOKTOR-INGENIEUR (Dr.-Ing.)

der Fakultät für Elektrotechnik, Informatik und Mathematik
der Universität Paderborn
vorgelegte Dissertation
von

M.Sc. Selwan Khaleel Ibrahim

Referent:	Prof. Dr.-Ing. Reinhold Noé
Korreferent:	Prof. Dr.-Ing. Reinhold Häb-Umbach

Tag der mündlichen Prüfung: 12.07.2007

Paderborn, den 16.07.2007

Diss. EIM-E/233

Study of Multilevel Modulation Formats for High Speed Digital Optical Communication Systems

A Thesis Submitted to the Faculty of Computer Science
Electrical Engineering and Mathematics

University of Paderborn

in Partial Fulfillment of
the Requirements For The Degree of Doktor-Ingenieur
in Electrical Engineering
(Dr.-Ing.)

By
M.Sc. Selwan Khaleel Ibrahim

Reviewers:
Prof. Dr.-Ing. Reinhold Noé
Prof. Dr.-Ing. Reinhold Häb-Umbach

Date of Thesis Submission: March 1, 2007
Date of Defense Examination: July 12, 2007

Paderborn, Germany
July 2007

Abstract

Spectrally efficient modulation formats can be used to overcome the problems associated with limited channels and bandwidth of Dense Wavelength Division Multiplexing (DWDM) optical systems. Multilevel modulation formats are considered spectrally efficient and can double the transmission capacity by transmitting more information in the amplitude, phase, polarization or a combination of all. Here we have studied and evaluated different multilevel modulation formats in a practical optical transmission system.

Differential Quadrature Phase Shift Keying (DQPSK) doubles the transmission rate by transmitting more information in the phase of the optical carrier signal. DQPSK receivers require more complex and costly components including delay interferometers and balanced detection photodiode receivers. Combining DQPSK with Polarization Division Multiplex (PolDM) would result into 4 times the transmission rate, but a polarization controller would be needed which results into a more complex receiver. A 20 Gbit/s DQPSK signal can be generated by combining two 10 Gbit/s Differential Phase Shift Keying (DPSK) signals in quadrature phases using a QPSK modulator. The receiver sensitivity for 20 Gbit/s NRZ- and RZ-DQPSK signals are measured to be -36.8 dBm and -38.3 dBm, respectively. The chromatic dispersion (CD) tolerance for a 1 dB optical signal to noise ratio (OSNR) penalty for a 20 Gbit/s RZ-DQPSK signal is ~360 ps/nm. When PolDM is used to combine two 20 Gbit/s DQPSK signals, the receiver sensitivity for 40 ($2\times2\times10$) Gbit/s NRZ- and RZ-DQPSK PolDM signals become -33.8 dBm and -34.7 dBm, respectively.

Conventional Quaternary Intensity Modulation (4-IM) doubles the data rate by transmitting more information in the amplitude of the carrier signal. This can be achieved by modulating the optical amplitude with an electrical 4-level Amplitude Shift Keying (ASK) signal. A simple receiver consisting of a single photo diode, three decision circuits and a decoding logic can be used to receive and extract the original transmitted data. It is also possible to generate quaternary intensity modulation signals by different means, such as combining two optical Binary/Duobinary NRZ signals with unequal amplitudes in quadrature phases, or orthogonal polarizations. When optically combining two 10 Gbit/s binary NRZ-ASK signals with unequal amplitudes in quadrature phases using a QPSK modulator a 20 Gbit/s 4-constellation point quaternary intensity signal is generated (QASK) having the same bandwidth as a single 10 Gbit/s binary NRZ-ASK signal. The receiver sensitivity and the 1 dB CD tolerance are measured to be -21.6 dBm and ~130 ps/nm, respectively.

The spectral efficiency of this quaternary intensity modulation signal can be increased even more by combining two 10 Gbit/s optical duobinary signals with unequal amplitudes in quadrature phases using a QPSK modulator resulting in a 20 Gbit/s 9-constellation point Quaternary Duobinary signal (QDB). When combined in orthogonal polarizations using a Polarization Beam Combiner (PBC), a 20 Gbit/s 9-constellation point Quaternary Polarization Duobinary signal (QPolDB) is generated. The receiver sensitivity and CD tolerance of

a 20 Gbit/s QDB signal generated using a duobinary stub filter with a frequency response dip at 5 GHz, are measured to be -21.2 dBm and ~140 ps/nm, respectively. The receiver sensitivity and CD tolerance of a 20 Gbit/s QPolDB signal generated using the same duobinary stub filter, are measured to be -20.5 dBm and ~340 ps/nm, respectively. When using another duobinary stub filter with a frequency response dip at 6 GHz, the receiver sensitivity and CD tolerance of the 20 Gbit/s QPolDB signal became -18.4 dBm and ~530 ps/nm, respectively.

A polarization and phase insensitive direct detection receiver with a single photodiode has been used to detect all generated quaternary signals as 4-IM signals. The 20 Gbit/s QDB and QPolDB quaternary signals that we have reported for the first time, have a narrow spectrum with a bandwidth similar to that of a single 10 Gbit/s duobinary modulation signal. These quaternary intensity modulation formats are attractive for DWDM systems applied for short reach (several kilometers) to medium reach (several hundred kilometers) transmission applications (metro applications). However, for long or ultra long haul optical fiber transmission systems, DQPSK and DQPSK PolDM modulation formats featuring better receiver sensitivities are potential candidates.

Acknowledgments

First, I would like to thank my doctoral adviser Professor Dr.-Ing. Reinhold Noé, for allowing me to work under his supervision in his internationally recognized group. His guidance and support were essential for me to gain a great amount of experience and knowledge in the field of optical communication and high frequency engineering. I would also like to thank Professor Dr.-Ing. Andreas Thiede and Professor Dr. Franz Rammig for acting as my supervisors, Professor Dr.-Ing. Reinhold Häb-Umbach for acting as second reviewer, and Professor Dr.-Ing. Klaus Meerkötter and Professor Dr.-Ing. Rolf Schuhmann for being in my examination committee.

I am also very grateful to the International Graduate School "Dynamic Intelligent Systems" at the University of Paderborn for providing me a fellowship in addition to financially supporting me to attend international conferences that were beneficial for my Ph.D. work. I would like to thank all the staff of the Graduate school for their help and support, especially Dr. Eckhard Steffen and Astrid Canisius.

My Special thanks goes to all of my colleagues and technical staff at the Optical Communications and High Frequency Engineering group at the University of Paderborn for their support and encouragement.

Also I would like to thank Dr. Robert Griffin from Bookham, UK for the loan of the $GaAs/AlGaAs$ oDQPSK modulator and Dr. Henri Porte from Photline Technologies, France for providing the $LiNbO_3$ oDQPSK modulator.

Finally I would like to thank my small and big family including my beloved parents, wife, child and all of my friends for their patience and support.

List of Ph.D. Publications

1. Selwan K. Ibrahim, S. Bhandare, D. Sandel, A. Hidayat, A. Fauzi, R. Noé, "Low-Cost, Signed Online Chromatic Dispersion Detection Scheme Applied to a 2×10 Gb/s RZ-DQPSK Optical Transmission System", IEE Proceedings Optoelectronics, October 2006, Volume 153, Issue 5, pp. 235-239.

2. Selwan K. Ibrahim, Suhas Bhandare, and Reinhold Noé, "Performance of 20 Gbit/s Quaternary Intensity Modulation Based on Binary or Duobinary Modulation in Two Quadratures With Unequal Amplitudes", IEEE Journal of Selected Topics in Quantum Electronics, Vol. 12, No. 4, 2006, pp. 596-602.

3. Selwan K. Ibrahim, Suhas Bhandare, and Reinhold Noé, "20 Gbit/s Quaternary Intensity Modulation Based on Duobinary Modulation with Unequal Amplitude in Two Polarizations", IEEE Photonics Technology Letters, Vol. 18, No. 14, 2006, pp. 1482-1484.

4. Selwan K. Ibrahim, Suhas Bhandare, Reinhold Noé, "Narrowband 2×10 Gbit/s Quaternary Intensity Modulation Based on Duobinary Modulation in Two Polarizations with Unequal Amplitudes", Optical Fiber Communication Conference (OFC 2006), Anaheim, CA, USA, March 2006, paper OThI2.

5. Selwan K. Ibrahim, S. Bhandare, H. Zhang, R. Noé, "2×10 Gbit/s Quaternary Intensity Modulation Generation using an Optical QPSK modulator", Proc. of SPIE, Vol. 6021, Paper 602119, (2005).

6. S. K. Ibrahim, S. Bhandare, H. Zhang, R. Noé, "2×10 Gbit/s Quaternary Intensity Modulation Generation using an Optical QPSK modulator", Asia-Pacific Optical Communications Conference (APOC 2005), Nov. 2005, Shanghai, China, Session 5b, paper 6021-44.

7. S. K. Ibrahim, S. Bhandare, R. Noé, "Narrowband 20 Gbit/s Quaternary Intensity Modulation Generated by Duobinary 10 Gbit/s Modulation in 2 Quadratures", Proc. 31st European Conference on Optical Communication (ECOC 2005), 25-29 September 2005, Glasgow, Scotland, Th2.6.5, Vol. 4, pp. 909-910.

8. Selwan K. Ibrahim, S. Bhandare, D. Sandel, A. Hidayat, A. Fauzi, R. Noé, "Low-Cost, Signed Online Chromatic Dispersion Detection Scheme Applied to a 2×10 Gb/s RZ-DQPSK Optical Transmission System", Conference digest 7th Optical Fibre Measurement Conference (OFMC 2005), 21-23 September 2005, Teddington, UK, pp. 83-86.

9. S. Bhandare, D. Sandel, B. Milivojevic, A. Hidayat, A. Fauzi, H. Zhang, S. K. Ibrahim, F. Wüst, and R. Noé, “5.94 Tbit/s, 1.49 bit/s/Hz (40×2×2×40 Gbit/s) RZ-DQPSK Polarization Division Multiplex C-Band Transmission over 324 km”, IEEE Photonics Technology Letters, Vol. 17, No. 4, 2005, pp. 914-916.

10. S. Bhandare, D. Sandel, B. Milivojevic, A. Hidayat, A. Fauzi, H. Zhang, S. K. Ibrahim, F. Wüst, R. Noé, “5.94 Tbit/s (40×2×2×40 Gbit/s) C-Band Transmission over 324 km using RZ-DQPSK Combined with Polarization Division Multiplex”, 6th ITG-Fachtagung "Photonische Netze", Leipzig, Germany, 2.-3. May 2005, pp. 87-90.

List of Figures

2.1 Schematic of an optical direct detection pre-amplified receiver 6
2.2 Basic digital modulation formats (ASK, PSK, FSK) 9
2.3 Principle of Binary NRZ-ASK modulation generation using intensity MZM 10
2.4 ASK signal constellation diagram 10
2.5 Schematic diagram of an optical DPSK transmission setup 11
2.6 Principle of DPSK modulation generation using a MZM 12
2.7 DPSK signal constellation diagram 13
2.8 10 Gbit/s optical RZ-DPSK generation scheme using two MZMs with resulting NRZ-DPSK (left) and 50% RZ-DPSK (right) eye diagrams. 14
2.9 DPSK receiver 14
2.10 Demodulated 10 Gbit/s NRZ-DPSK (a) and RZ-DPSK (b) intensity eye patterns 15
2.11 Schematic diagram of a standard Duobinary generation and detection scheme (top) and a corresponding practical optical Duobinary transmission setup (bottom) 16
2.12 Principle of Duobinary modulation generation using a MZM and a Duobinary encoder based on the conventional one bit delay and add filter 18
2.13 10 Gbit/s optical Duobinary modulation generation using a MZM and a Duobinary encoder based on a 5th order Bessel filter with cutoff frequency at $2.8\,\mathrm{GHz}$ 19
2.14 Optical Duobinary signal constellation diagram 19

3.1 Schematic of an optical DQPSK transmission system 22
3.2 Schematic of an optical DQPSK modulator 23
3.3 DQPSK signal constellation diagram 24
3.4 NRZ-DQPSK signal eye diagram showing the intensity dips 25
3.5 Schematic of an optical DQPSK decoder 26
3.6 Eye diagram of a demodulated data signal from an NRZ-DQPSK signal . . 26
3.7 Experimental 2×10 Gbit/s DQPSK transmission setup 28
3.8 Eye diagrams of a demodulated data signal I and Q extracted from a 2×10 Gbit/s NRZ-DQPSK signal generated using a Photline DQPSK modulator with PRBS lengths of $2^7 - 1$ (PRBS-7) (top) and $2^{15} - 1$ (PRBS-15) bottom 29
3.9 BER curves for the I and Q received data streams versus received optical power for a 2×10 Gbit/s NRZ-DQPSK signal using a Photline oDQPSK Modulator with PRBS lengths of $2^7 - 1$ (PRBS 7) and $2^{15} - 1$ (PRBS 15) . 30

3.10 Average BER versus received optical power for a 20 Gbit/s NRZ-DQPSK signal using a Photline oDQPSK Modulator with PRBS lengths of $2^7 - 1$ (PRBS 7) and $2^{15} - 1$ (PRBS 15) 30
3.11 Eye diagrams of a demodulated data signal I and Q extracted from a 2×10 Gbit/s RZ-DQPSK signal generated using a Photline DQPSK modulator with PRBS lengths of $2^7 - 1$ (PRBS-7) (top) and $2^{15} - 1$ (PRBS-15) bottom 31
3.12 BER curves for the I and Q received data streams versus received optical power for a 2×10 Gbit/s RZ-DQPSK signal using a Photline oDQPSK Modulator with PRBS lengths of $2^7 - 1$ (PRBS 7) and $2^{15} - 1$ (PRBS 15) . 32
3.13 Average BER versus received optical power for a 20 Gbit/s RZ-DQPSK signal using a Photline oDQPSK Modulator with PRBS lengths of $2^7 - 1$ (PRBS 7) and $2^{15} - 1$ (PRBS 15) 32
3.14 OSNR needed for a BER of 10^{-9} versus CD for a 20 Gbit/s RZ-DQPSK signal 33
3.15 20 Gbit/s RZ-DQPSK signal intensity measurements after transmission over different lengths of SSMF corresponding to different values of CD, (a) Back-to-Back (0 ps/nm), (b) 21.3 km (~362 ps/nm), (c) 32.2 km (~547 ps/nm), and (d) 41.5 km (~706 ps/nm) 34
3.16 2×2×10 Gbit/s RZ-DQPSK PolDM transmission setup 35
3.17 Eye diagrams of 2×2×10 Gbit/s NRZ-DQPSK PolDM signal (left), and RZ-DQPSK PolDM signal (right) 35
3.18 BER curves for the I and Q received data streams in both polarizations X and Y versus the received optical power for 2×2×10 Gbit/s NRZ-DQPSK PolDM signal with PRBS 7 36
3.19 Eye diagram of the demodulated data signals I and Q for both polarizations X and Y extracted from a 2×2×10 Gbit/s NRZ-DQPSK PolDM signal with PRBS 7 37
3.20 BER curves for the I and Q received data streams in both polarizations X and Y versus the received optical power for 2×2×10 Gbit/s NRZ-DQPSK PolDM signal with PRBS 15 37
3.21 Average BER versus received optical power for 2×2×10 Gbit/s NRZ-DQPSK PolDM signal with PRBS 7 and PRBS 15 38
3.22 BER curves for the I and Q received data streams in both polarizations X and Y versus the received optical power for 2×2×10 Gbit/s RZ-DQPSK PolDM signal with PRBS 7 39
3.23 Eye diagram of the demodulated data signals I and Q for both polarizations X and Y extracted from a 2×2×10 Gbit/s RZ-DQPSK PolDM signal with PRBS 7 39
3.24 Average BER versus received optical power for 2×2×10 Gbit/s RZ-DQPSK PolDM signal with PRBS 7 and PRBS 15 40
3.25 2×2×10 Gbit/s DQPSK PolDM transmitter setup photo 40
3.26 2×2×10 Gbit/s RZ-DQPSK Receiver 41
3.27 2×2×10 Gbit/s RZ-DQPSK PolDM transmission setup photo 41

4.1 Electrical 4-ary ASK signal generation 44
4.2 Principle of optical 4-IM generation using intensity MZM 45
4.3 Optical 4-IM signal constellation diagram 46

4.4 Schematic of a 4-IM receiver with decoding logic diagram 46
4.5 20 Gbit/s Quaternary intensity modulation transmission setup 47
4.6 BER curves versus received optical power for the three received eyes (top, middle, and bottom) for a 20 Gbit/s (4-IM) signal 48
4.7 Average BER versus received optical power for a 20 Gbit/s (4-IM) signal . 48
4.8 Optical QASK (2×10 Gbit/s) generation in an optical QPSK modulator, and resulting quaternary intensity eye diagram (bottom) with electrical attenuator setting (b = 1/2) 50
4.9 QASK electrical field signal constellation diagram (top-right) generated using a QPSK modulator driven by binary signals with unequal amplitudes. The resulting intensity eye diagram (bottom-right) shows the 4 intensity levels ($a = 1/\sqrt{2}$). 50
4.10 Heterodyned electrical spectrum for a 2×10 Gbit/s QASK signal 51
4.11 BER curves versus received optical power for the three received eyes (top, middle, and bottom) for a 20 Gbit/s QASK signal 52
4.12 Average BER versus received optical power for a 20 Gbit/s QASK signal . 52
4.13 OSNR needed for a BER of 10^{-9} versus CD for a 20 Gbit/s QASK signal . 53
4.14 Intensity eye diagrams of a 20 Gbit/s QASK signal measured at the sensitivity edge after transmission over different length of SSMF, (a) (Back-to-Back) 0 km (0 ps/nm), (b) 5.34 km (~90.78 ps/nm), (c) 10.9 km (~185 ps/nm), (d) 16.24 km (~276 ps/nm) 53
4.15 Principle of optical QDB modulation generation using duobinary low pass filtering (LPF) and a QPSK modulator (electrical attenuator setting b = 1/2). The resulting quaternary intensity eye diagram (bottom) and the electrical duobinary eye diagram (top) are also shown. 54
4.16 QDB electrical field signal constellation diagram (top-right) generated using a QPSK modulator driven by duobinary signals with unequal amplitudes. The resulting intensity eye diagram (bottom-right) shows the 4 intensity levels ($a = 1/\sqrt{2}$). 55
4.17 Heterodyned electrical spectrum of the 20 Gbit/s QDB signal 56
4.18 BER curves versus received optical power for the three received eyes (top, middle, and bottom) for a 20 Gbit/s QDB signal 56
4.19 Average BER versus received optical power for a 20 Gbit/s QDB signal . . 57
4.20 OSNR needed for a BER of 10^{-9} versus CD for a 20 Gbit/s QDB signal . . 58
4.21 Photo of the 2×10 Gbit/s QDB transmitter based on the Bookham QPSK modulator 58
4.22 Schematic of the optical QPolDB signal generation scheme ($a = 1/\sqrt{2}$) . . 59
4.23 QPolDB electrical field signal constellation diagram (top-right) generated using a polarization division multiplex setup (left) with duobinary signals ($a = 1/\sqrt{2}$) 60
4.24 Schematic of the transmission setup used to generate and detect 2×10 Gbit/s QPolDB signals 61
4.25 Heterodyned electrical spectrum of the 20 Gbit/s QPolDB-6 signal 62
4.26 BER curves versus received optical power for the three received eyes (top, middle, and bottom) for a 20 Gbit/s QPolDB-5 signal 62

4.27 BER curves for the three received eyes (top, middle, and bottom) for a 20 Gbit/s QPolDB-6 signal . . . 63
4.28 Average BER versus received optical power for 20 Gbit/s QPolDB-5 and QPolDB-6 signals . . . 63
4.29 Average BER versus received optical power for 20 Gbit/s QPolDB-6 signal with PRBS 7, 10 and 15 . . . 64
4.30 OSNR needed for a BER of 10^{-9} versus CD in ps/nm for 20 Gbit/s QPolDB-5 and QPolDB-6 signals . . . 65
4.31 Intensity eye diagrams of the 20 Gbit/s QPolDB-5 signal measured at the sensitivity edge after transmission over (a) 0 km (back-to-back), (b) 10.9 km, (c) 16.24 km, (d) 26.65 km, and (e) 37.55 km of SSMF . . . 66
4.32 Intensity eye diagrams of the 20 Gbit/s QPolDB-6 signal measured at the sensitivity edge after transmission over (a) 0 km (back-to-back), (b) 10.9 km, (c) 16.24 km, (d) 26.65 km, (e) 37.55 km, and (f) 41.54 km of SSMF . 67
4.33 Photo of the PolDM transmitter setup used to generate the QPolDB signals 67
4.34 Schematic of the optical QPolASK signal generation scheme ($a = 1/\sqrt{2}$), eye diagram of 2×10 Gbit/s QPolASK signal (top-right). . . . 68
4.35 QPolASK electrical field signal constellation diagram (top-right) generated using a polarization division multiplex setup with binary signals ($a = 1/\sqrt{2}$) 69
4.36 Schematic of quaternary DP-ASK transmitter and receiver . . . 70
4.37 DP-ASK signal constellation diagram . . . 70

5.1 Average BER curves versus received optical power for 20 Gbit/s quaternary modulation signals (4-IM, QASK, QDB, QPolDB-5, and QPolDB-6). . . . 72
5.2 OSNR needed for a BER of 10-9 versus CD in ps/nm for 20 Gbit/s quaternary modulation signals (QASK, QDB, QPolDB-5, and QPolDB-6). . . . 73

A.1 Schematic drawing of a Mach-Zehnder interferometer . . . 75
A.2 Mach-Zehnder modulator (push-pull) structure using $x - \mathrm{cut}\ LiNbO_3$ . . . 77
A.3 Typical transfer characteristic curve of a Mach-Zehnder modulator . . . 77

B.1 Schematic of a DQPSK transmission system . . . 79
B.2 QPSK modulator and generated phase states $\phi(k)$ . . . 80
B.3 Karnaugh-maps for the DQPSK precoder outputs $I(k)$ and $Q(k)$ . . . 82
B.4 DQPSK precoder circuit diagram . . . 82

C.1 Schematic of a 4-ary ASK receiver . . . 83
C.2 Karnaugh-maps for the 4-ary ASK decoder outputs D1 and D2 . . . 84
C.3 4-ary ASK decoder circuit diagram . . . 84

D.1 Schematic of the one bit delay-and-add duobinary encoder versus the stub filter duobinary encoder . . . 85
D.2 Photo of constructed electrical stub LPFs, (a) Stub-5, (b) Stub-6 . . . 86
D.3 Frequency response of the electrical stub LPF (Stub-5) and eye diagram of a generated 10 Gbit/s electrical duobinary signal . . . 87
D.4 Frequency response of the electrical stub LPF (Stub-6), and eye diagram of a generated 10 Gbit/s electrical duobinary signal . . . 87
D.5 Frequency response of a Stub-5 filter and 5th order Bessel LPF (3dB@2.8GHz) 88

D.6 Frequency response of a Stub-6 filter and 5th order Bessel LPF (3dB@2.8GHz) 88

List of Tables

2.1 Transmitted bit stream "01010011" for DPSK modulation 13
2.2 Transmitted and received bit stream "01010011" for Duobinary modulation 20

3.1 Mapping of the input signals (I_k and Q_k) to the output electric field (E_o) and generated phase state (ϕ_k) of the o(D)QPSK modulator 24
3.2 Mapping of data signals (U_k and V_k) to transmitted symbol (d_k), and corresponding phase changes ($\triangle\phi_k$) for DQPSK modulation 25
3.3 Transmitted and received data bit streams U_k = "01010011" and V_k = "10011010" for an optical DQPSK system 27

4.1 Mapping of input binary data to output levels of a 4-ary ASK signal 45

5.1 Comparison between different modulation formats at 20 Gbit/s 74

B.1 Mapping of the phase change ($\triangle\phi_k$) to received data ($u(k)$ and $v(k)$) for DQPSK signals 80
B.2 Mapping of the input signals ($I(k)$ and $Q(k)$) to the output electric field (E_o) and generated phase state ($\phi(k)$) of the o(D)QPSK modulator 80
B.3 DQPSK precoder look up table 81

C.1 Mapping of the input levels and the 3 received patterns to the decoded outputs for a 4-ary ASK receiver 84

Contents

Abstract iii

Acknowledgments v

List of Ph.D. Publications vii

List of Figures ix

List of Tables xv

Contents xvii

1 Introduction 1
- 1.1 Background . . . 1
- 1.2 Motivation . . . 3
- 1.3 Organization of the Thesis . . . 3

2 Digital Modulation Formats for Optical Communication Systems 5
- 2.1 Introduction . . . 5
- 2.2 Performance Evaluation Parameters . . . 5
  - 2.2.1 Receiver Sensitivity . . . 5
  - 2.2.2 Chromatic Dispersion Tolerance . . . 6
  - 2.2.3 Spectral Efficiency . . . 7
- 2.3 Digital Optical Modulation Formats . . . 8
  - 2.3.1 Binary Intensity Modulation (IM) . . . 9
  - 2.3.2 Differential Phase Shift Keying (DPSK) . . . 11
    - 2.3.2.1 DPSK Precoder . . . 11
    - 2.3.2.2 DPSK Transmitter . . . 12
    - 2.3.2.3 DPSK Receiver . . . 14
  - 2.3.3 Duobinary Modulation (DB) . . . 15
    - 2.3.3.1 Duobinary Precoder . . . 16
    - 2.3.3.2 Duobinary Encoder . . . 17
    - 2.3.3.3 Duobinary Decoder . . . 18

3 Differential Quadrature Phase Shift Keying (DQPSK) 21
- 3.1 Introduction . . . 21
- 3.2 Differential Quadrature Phase Shift Keying (DQPSK) . . . 21

3.2.1 DQPSK Precoder . . . 22
3.2.2 DQPSK Optical Encoder . . . 22
3.2.3 DQPSK Optical Decoder . . . 26
3.3 DQPSK Transmission System at 2×10 Gbit/s . . . 27
3.4 DQPSK PolDM Transmission System at 2×2×10 Gbits/s . . . 34

4 Quaternary Intensity Modulation 43
4.1 Introduction . . . 43
4.2 Conventional Quaternary Intensity Modulation (4-IM) . . . 43
4.2.1 Generation of Conventional 2×10 Gbit/s Quaternary 4-IM Signals . 44
4.2.2 Quaternary 4-IM Signal Detection . . . 45
4.2.3 Experimental Transmission System for 2×10 Gbit/s Quaternary Modulation . . . 46
4.3 Quaternary Amplitude Shift Keying (QASK) . . . 49
4.3.1 Generation and Detection of 2×10 Gbit/s QASK Signals . . . 49
4.3.2 Experimental Results Measured for 2×10 Gbit/s QASK . . . 51
4.4 Quaternary Duobinary Modulation (QDB) . . . 54
4.4.1 Generation and Detection of 2×10 Gbit/s QDB signals . . . 54
4.4.2 Experimental Results Measured for 2×10 Gbit/s QDB . . . 55
4.5 Quaternary Polarization Duobinary Modulation (QPolDB) . . . 59
4.5.1 Generation and Detection of 2×10 Gbit/s QPolDB Signals . . . 59
4.5.2 Experimental Results Measured for 2×10 Gbit/s QPolDB . . . 60
4.6 Other Quaternary Multilevel Modulation Formats . . . 68
4.6.1 Quaternary Polarization Amplitude Shift Keying (QPolASK) . . . 68
4.6.2 Quaternary Differential-Phase ASK Modulation (DP-ASK) . . . 69

5 Results Discussion and Conclusion 71
5.1 Introduction . . . 71
5.2 Results Discussion . . . 71
5.3 Conclusion . . . 74

A Optical Intensity Mach-Zehnder Modulator (MZM) 75

B DQPSK Precoder 79

C 4-ary ASK Decoder 83

D Duobinary Filters 85

Bibliography 89

Chapter 1

Introduction

1.1 Background

The growth increase in the number of Internet users and the high demand for multimedia applications such as audio and video will cause a need to upgrade the existing Internet backbone communication networks to operate at higher transmission rates. Currently, virtually most or all of the telephone conversations, cellular phone calls, and Internet packets must pass through an optical fiber communication network between the source and destination. While initial deployment of optical fiber networks were mainly for long-haul or submarine transmission, optical fiber networks are currently in virtually all metro networks [1]. These optical communication networks widely use Dense Wavelength Division Multiplexed (DWDM) transmission systems to increase the transmission capacity by transmitting different data streams on different wavelengths (channels). It is possible to increase the throughput of such DWDM transmission systems by using wider optical bandwidths per channel so that the data rate per channel can be increased, or by using advanced modulation formats with higher spectral efficiency (SE) that can be used to transmit more information using the same bandwidth, or by using a combination of both mentioned methods [2, 3, 4, 5, 6]. Using wider optical bandwidths per channel will lead to a limited number of DWDM channels due to a limitation by the spectral bandwidth of optical amplifiers and fiber transmission lines [5]. Higher spectral efficiency can be achieved by doubling the transmission capacity by transmitting more information in the amplitude, phase, polarization or a combination of all [2, 6, 7]. Multilevel modulation formats are considered as advanced modulation formats that can be used to overcome the problems associated with limited channels and bandwidth of DWDM systems by lowering the signaling speed by carrying several information bits on a single symbol. Multilevel modulation formats are widely used in highly efficient electrical communication systems such as wireless communications [5]. Some examples of such optical advanced multilevel modulation formats that can double the data rate are:

1. Conventional Quaternary Intensity Modulation (4-IM) or also called 4-ary ASK can double the data rate by transmitting more information in the amplitude of the carrier signal by modulating the amplitude with an electrical 4-level ASK signal. To receive and extract the original transmitted data, a single photo diode, three decision circuits and a decoding logic is needed at the receiver side [8, 9, 10, 11, 12].

2. Differential Quadrature Phase Shift Keying (DQPSK) doubles the data rate by trans-

mitting information in two quadrature phases. To receive and extract the original transmitted data, two balanced receiver structures each similar to a Differential Phase Shift Keying (DPSK) receiver are needed at the receiver side. Each receiver consists of two photo diodes and a Mach Zehnder Delay Interferometer (MZDI) [13, 14, 15].

3. Differential Polarization Phase Shift Keying (DPolPSK) doubles the data rate by transmitting information in the carrier phase and two orthogonal polarizations. To receive and extract the original transmitted data, a balanced receiver structure, consisting of two photodiodes and a MZDI (DPSK receiver) in addition to a similar receiver used for the 4-IM signal are needed [16, 17].

4. Differential Phase Amplitude Shift Keying (DP-ASK) doubles the data rate by transmitting information in both the phase and amplitude of the carrier signal. To receive and extract the original transmitted data, a balanced receiver structure, consisting of two photo diodes and a MZDI (DPSK receiver) to detect one data stream in addition to a single photo diode (ASK receiver) to detect the other transmitted data stream are needed at the receiver [18, 19].

Combining DQPSK with Polarization Division Multiplex (PolDM) would improve the spectral efficiency but would require a more complex receiver. The multilevel 4-IM modulation format can be considered as a cost-effective single-channel implementation of high-capacity links and can result in increased capacity when combined with DWDM. However, its inherent degradation of the receiver sensitivity suggests that it is not suitable for ultra-long distance transmission. Therefore, it can be suitable for short reach (several kilometers) to medium reach (several hundreds kilometers) transmission applications [5]. A quaternary 4-ary (4-IM) modulation signal can also be generated using different generation techniques than the conventional method by:

1. Optically combining two binary intensity modulated signals with unequal amplitudes in quadrature phases using a QPSK modulator (QASK) [20, 21, 6]. To receive and extract the original transmitted data, the same receiver structure of the conventional 4-IM method is used.

2. Optically combining two binary intensity modulated signals with unequal amplitudes in orthogonal polarizations using a polarization beam splitter (QPolASK) [22, 23]. To receive and extract the original transmitted data, the same receiver structure of the conventional 4-IM method is also used.

All of the previous mentioned methods double the transmission capacity and are spectrally efficient to one extent, but still do not have the best spectral efficiency. Another limitation for high speed optical transmission systems is the chromatic dispersion (CD) in single mode fibers which is the optical frequency dependence of the group delay. It is possible to overcome the CD limitation by using other modulation formats that have higher CD tolerance such as Duobinary modulation. Duobinary modulation outperforms all the other previously mentioned quaternary modulation formats in term of CD tolerance. Although Duobinary modulation does not double the transmission rate, it is also spectrally efficient [24, 25, 26]. Combining Duobinary modulation and Quaternary modulation could result in even a higher spectral efficient modulation format. It is possible to reduce the spectral bandwidth of the

QASK and QPolASK modulation formats to an extent where it outperforms all the other mentioned multilevel modulation formats in terms of spectral efficiency, by using Duobinary modulation instead of binary modulation in the generation scheme. A 9-constellation point optical quaternary intensity signal can be generated by combining two optical Duobinary signals with unequal amplitudes in quadrature phases using a QPSK modulator resulting in a Quaternary Duobinary signal (QDB)/(9-QAM QPSK) [27, 28, 21, 6] or in orthogonal polarizations using a Polarization Beam Combiner (PBC) resulting in a Quaternary Polarization Duobinary signal (QPolDB)/(9-QAM PolDM) [29, 7, 6], respectively. Both of these modulation formats have higher spectral efficiency compared to the binary, Duobinary, and the other quaternary modulation formats. The QPolDB format had higher CD tolerance compared to binary modulation and other quaternary modulation formats operating all at the same bit rate.

1.2 Motivation

The motivation of the work performed in this dissertation was to implement different optical quaternary modulation formats at 10 Gbaud and 20 Gbit/s data rate, measure their performance regarding to their sensitivities, CD tolerance, and spectral bandwidth and compare them with each other and to other intensity modulation schemes at the same bit rate. The quaternary modulation formats used throughout this work were DQPSK, DQPSK with PolDM, 4-IM, QASK, and the newly proposed QDB and QPolDB. All these modulation formats are known to be advanced modulation formats with higher spectral efficiency compared to binary Non-Return-to-Zero amplitude modulation (NRZ-ASK). The experimental results obtained in this thesis gives the reader or designer useful information that can be used to select between different modulation formats a suitable one that can match the requirements of a specific optical transmission system for short to medium reach transmission applications.

1.3 Organization of the Thesis

The thesis is organized into five main chapters as follows:

- The first chapter is a general introduction to the work performed in this thesis and the motivation.

- The second chapter in its first part gives a brief description of some of the performance parameters used to compare between different modulation formats. The second part introduces some digital modulation formats that are used for optical communication systems such as binary (NRZ-ASK), differential phase shift keying (DPSK), and Duobinary modulation (DB). For each of these modulation formats a brief explanation will be given on their generation and detection schemes and expected signal constellation diagram. Measured eye diagrams at 10 Gbit/s obtained by experimental implementation of each modulation format will also be presented. These modulation formats will be useful to understand the multilevel modulation formats mentioned later in chapters three and four.

- The third chapter will introduce the optical DQPSK modulation format describing the generation and detection scheme, and the expected signal constellation diagram. Experimental data will be presented for 20 Gbit/s DQPSK and 40 Gbit/s DQPSK PolDM transmission system showing the receiver sensitivity and eye diagrams. Also the CD tolerance for 20 Gbit/s RZ-DQPSK will be evaluated.

- The fourth chapter will introduce different quaternary modulation formats implemented at 20 Gbit/s including conventional 4-IM, QASK, QDB, and QPolDB. The generation and detection scheme and the expected signal constellation diagram for each of these modulation formats will be explained. Also the practical hardware system setup and the experimental measured results obtained such as the eye diagrams, receiver sensitivity, and measured CD tolerances will be presented for the quaternary modulation formats. The last section of this chapter will introduce and briefly explain some other previously reported quaternary modulation formats such as QPolASK, and DP-ASK.

- The fifth chapter is the last chapter of the thesis that will discusses the results obtained from chapter three and four with a full comparison based on the performance parameters given in chapter two. A conclusion of the work is given in this chapter.

Chapter 2

Digital Modulation Formats for Optical Communication Systems

2.1 Introduction

This chapter gives a short introduction to the basic concepts and performance evaluation parameters used to compare the different modulation formats presented in this thesis. The parameters covered in this chapter are the receiver sensitivity, chromatic dispersion tolerance, and spectral efficiency (SE). The last section of this chapter will introduce some standard digital optical modulation formats such as binary amplitude shift keying (ASK), Differential phase shift keying (DPSK), and Duobinary modulation (DB). The generation and detection schemes for each modulation format will be explained in details showing the corresponding signal constellation and eye diagrams. These modulation formats are useful to fully understand the multilevel modulation formats later mentioned in chapters three and four.

2.2 Performance Evaluation Parameters

The commonly used linear parameters that will be used to compare the performance of different optical transmission systems based on different modulation formats mentioned in this thesis are the receiver sensitivity, dispersion, and spectral efficiency. A brief explanation for each parameter will be given in the following:

2.2.1 Receiver Sensitivity

An important parameter to indicate the receiver performance in an optical transmission system is called the receiver sensitivity. It is usually defined as the minimum average received optical power for which the Bit Error Rate (BER) of the optical receiver is 10^{-9}. Figure 2.1 shows the main components of a simple optical pre-amplified direct detection receiver used for an optical transmission system consisting of an optical pre-amplifier, optical band-pass filter (BPF), a photodiode, an electrical amplifier and an electrical low-pass filter (LPF).

The BER depends on the signal to noise ratio (SNR), which depends on various noise sources that degrade the received optical signal. The important noise contributions are the

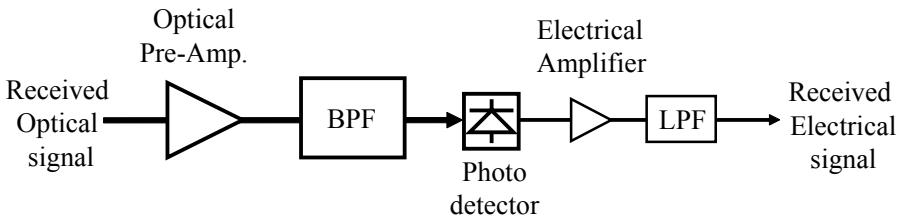

Figure 2.1: Schematic of an optical direct detection pre-amplified receiver

Amplified Spontaneous Emission (ASE), Shot noise and Thermal noise [30]. It should be noted that the photons at the output of the optical amplifier obey noncentral or central negative bionomial distributions for transmitted one or zero, respectively. If there is no gain, these become Poisson distributions. If the gain is infinite, these become chi-square distributions [31]. The receiver sensitivity can also be degraded due to the fiber dispersion that leads to power penalties and depends on both the bit rate and the fiber length. The performance of an optical receiver can also be measured using the eye diagram. The closing of the eye is a measure of degradation in receiver performance and is associated with a corresponding increase in the BER [32].

2.2.2 Chromatic Dispersion Tolerance

Chromatic dispersion (CD) is one of the most basic characteristics of optical fibers [33]. It is also known as group-velocity dispersion (GVD) which is caused by the wavelength dependence of the refractive index. In optical transmission systems when an optical carrier is modulated and transmitted over a fiber, the modulated signal occupies a certain optical spectral bandwidth. Signal from different parts of the spectrum propagates with different speed due to chromatic dispersion [33, 1]. When operating at higher bit rates over long lengths of optical fiber, the chromatic dispersion causes broadening of a single transmitted pulse in addition to interference between adjacent pulses which is known as inter-symbol-interference (ISI), hence producing distortions in the received signals [34, 35].

To understand better the chromatic dispersion, we will use the complex field transfer function of an optical fiber with a length L in the frequency domain

$$\underline{H}\left(\omega\right) = e^{j\varphi} = e^{-j\beta(\omega)L}, \tag{2.1}$$

where $\beta\left(\omega\right)$ is the propagation constant , ω is the optical angular frequency and the attenuation has been neglected. It is useful to approximate its phase φ by a truncated Taylor series around the carrier frequency ω_0,

$$\varphi = -\beta\left(\omega\right)L = -n\left(\omega\right)\frac{\omega}{c}L = -(\beta_0 + \beta_1(\omega-\omega_0) + \frac{1}{2}\beta_2(\omega-\omega_0)^2 + ...)L, \tag{2.2}$$

where c is the speed of light in vacuum and $n\left(\omega\right)$ is the refractive index. At ω_0 the propagation constant $\beta\left(\omega\right)$ assumes the value β_0, and its first and second derivatives with respect to ω are β_1, and β_2, respectively as follows:

$$\beta_1 = \beta' = \frac{1}{\upsilon_g} = \left.\frac{d\beta}{d\omega}\right|_{\omega=\omega_0}, \tag{2.3}$$

$$\beta_2 = \beta'' = \frac{d}{d\omega}\left(\frac{1}{\upsilon_g}\right) = \left.\frac{d^2\beta}{d\omega^2}\right|_{\omega=\omega_0}, \tag{2.4}$$

where β' is the inverse of the group velocity υ_g, β'' is the first order dispersion, λ is the optical wavelength, and $\omega = 2\pi c/\lambda$. The group delay is:

$$\tau_g = -\varphi' = \frac{d\varphi}{d\omega} = (\beta' + (\omega - \omega_0)\beta'')\, L. \tag{2.5}$$

It is a linear function of ω. Its derivative with respect to wavelength λ and length L is the chromatic dispersion coefficient:

$$D = \frac{d^2\tau_g}{d\lambda.dL} = \frac{d}{d\lambda}\left(\frac{1}{\upsilon_g}\right) = -\frac{2\pi c}{\lambda^2}\beta'' = -\frac{2\pi}{\lambda^2}\left(2\frac{d\bar{n}}{d\omega} + \omega\frac{d^2\bar{n}}{d\omega^2}\right), \tag{2.6}$$

in the units of ps/(km.nm) [36, 37, 1, 32]. The wavelength dependence of D is governed by the frequency dependence of the mode index $\bar{n}$. Standard single mode fiber (SSMF) has a dispersion coefficient from 16 to 19 ps/(nm.km) at the low-loss window of 1550 nm. Due to chromatic dispersion in optical fiber, the level of intersymbol interference that limits the maximum transmission distance depends on the chromatic dispersion index factor γ [34, 38] given as :

$$\gamma = \frac{R^2 L D \lambda^2}{\pi c}, \tag{2.7}$$

where R is the data rate of the system, and L is the transmission length. It can be seen that the limit of transmission length due to the waveform distortion by the chromatic dispersion of the fiber is inversely proportional to the chromatic dispersion and the square of the system data rate. The chromatic dispersion tolerance curve shows the required optical signal-to-noise ratio OSNR [dB/0.1nm] for a $BER = 10^{-9}$ versus the residual chromatic dispersion. The OSNR [dB/0.1nm] is usually measured with an Optical Spectrum Analyzer (OSA) by subtracting the noise power (dBm) measured with the OSA resolution bandwidth (RB) set to 0.1 nm from the signal peak power (dBm) measured with the OSA RB set to 1 nm. Normally the CD tolerance of a modulation format corresponds to the maximum residual dispersion where the OSNR penalty is 1dB [39].

2.2.3 Spectral Efficiency

The throughput of a dense wavelength-division multiplexed (DWDM) transmission system can be increased by using a wider optical bandwidth, increasing the spectral efficiency SE, or by some combination of both [2]. Utilizing a wider bandwidth typically requires additional amplifiers and other optical components. So a better solution is to efficiently use the available optical bandwidth by reducing the channel spacing to increase the number of channels within a fixed optical bandwidth. This can be achieved by reducing the spectral occupancy for the modulation signal by using alternative advanced modulation formats with

high spectral efficiency [4, 3, 10, 40, 41, 42]. The spectral efficiency (SE) limit in a DWDM system is defined as:

$$SE = \frac{C}{\triangle f}, \tag{2.8}$$

where $\triangle f$ is the channel spacing and C is the capacity per channel. C and S have units of bits per second (b/s) and b/s/Hz, respectively. Advanced modulation formats such as multilevel modulation formats have higher spectral efficiency due to the narrower optical spectrum with respect to that of binary NRZ signal with identical bit rate [40, 39, 43].

2.3 Digital Optical Modulation Formats

For designing digital optical communication links, there exist a wide variety of modulation formats to choose from. The electric field of the optical carrier is given by [32]:

$$E\left(t\right) = \hat{\mathrm{e}} A e^{-j(\omega t + \phi)}. \tag{2.9}$$

Four properties of an optical signal can be modulated: A is the amplitude of the optical field, ϕ is the optical phase, ω is the optical angular frequency, and $\hat{\mathrm{e}}$ is the polarization vector of the laser source [44, 45, 46, 47]. Each of these parameters can be modulated by an electrical binary baseband signal $q(t)$:

$$q\left(t\right) = \sum_{i=-\infty}^{\infty} I_i q\left(t - iT_b\right), \tag{2.10}$$

with the $i-$ th information coefficient $I \in [0, 1]$ and the baseband pulse shape $q(t)$ delayed by multiples of the bit period T_b. Depending on which parameter of the laser source is modulated, the modulation is mainly differentiated as: amplitude shift keying (ASK) [48, 24, 49, 50], frequency shift keying (FSK) [51, 52, 53, 54], phase shift keying (PSK) [55, 56, 49, 57, 58, 15, 59], or polarization shift keying (PolSK) [60, 61, 62]. Figure 2.2 shows an electrical binary data stream "01010011" used to modulate the amplitude, frequency, and phase of an optical carrier signal, resulting in the generation of the standard optical digital modulation formats ASK, PSK and FSK respectively.

Most systems today use the binary amplitude modulation format amplitude-shift-keying (ASK) because it is simple and cheap to implement. Recently, and in the previous years, novel advanced modulation formats with improved performance with respect to binary modulation have been suggested and investigated. However, these advanced modulation formats may add further complexity to the transmitter and receiver hardware of the optical transmission system [45, 46, 63, 15]. Some of these advanced modulation formats such as Duobinary and DPSK feature enhanced robustness to chromatic dispersion, optical filtering, and/or nonlinearities [15].

Other advanced modulation formats such as multilevel modulation formats can even have higher spectral efficiency than standard binary modulation due to the doubling of the transmission capacity by transmitting more information in the amplitude, phase, polarization or a combination of all [6]. Some of the previous published multilevel modulation formats

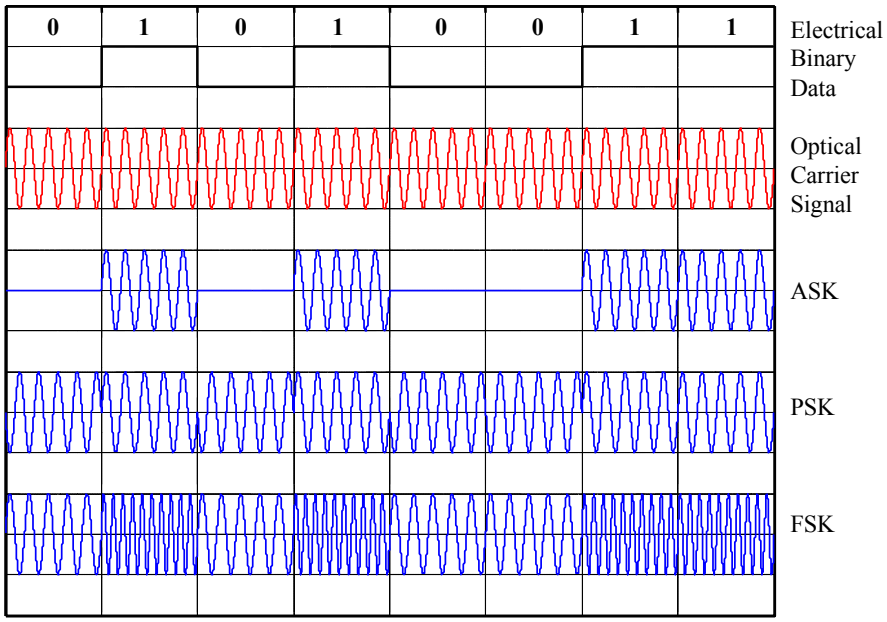

Figure 2.2: Basic digital modulation formats (ASK, PSK, FSK)

are quaternary intensity modulation (4-IM) or also called 4-ary ASK [8, 9, 10, 11, 12], differential quadrature phase-shift-key (DQPSK) [14, 15, 13], Differential Polarization-Phase-Shift Keying (DPolPSK) [16, 17], Quaternary polarization amplitude-shift-keying (QPolASK) [23, 22], Differential-phase amplitude-shift-keying (DP-ASK) [18, 19], and quaternary amplitude-shift-keying (QASK) [20, 28, 6, 21].

In the following sections the principle of operation will be given for generating and detecting standard optical modulation formats such as Binary Intensity Modulation (IM), Differential Phase Shift Keying (DPSK), and Duobinary Modulation (DB). These modulation formats will be used as a base to generate more advanced quaternary modulation formats such as DQPSK, 4-IM, QASK, QDB, and QPolDB that will be explained in more details in the following chapters.

2.3.1 Binary Intensity Modulation (IM)

Binary intensity modulation (IM) or also called Amplitude Shift Keying (ASK) is the most common used modulation format in the deployed optical transmission systems currently available today. This modulation technique is well known from classical telecommunication theory [64, 65, 42]. It is also known as On-Off-keying (OOK) because it is a result of switching ON and OFF the amplitude of an optical carrier signal. This can be achieved by directly modulating the current of the laser source or by using an external optical modulator to modulate the amplitude of the laser carrier signal [66]. The most common generation scheme is externally modulating the laser signal using an intensity Mach-Zehnder Modulator (MZM) biased at the quadrature point of the modulator power transfer function, and driven by an electrical binary NRZ-ASK signal with peak-to-peak (p-p) amplitude of V_π as shown in figure 2.3. More details and explanation on the principle of operation of the intensity Mach-Zehnder modulator are given in appendix A.

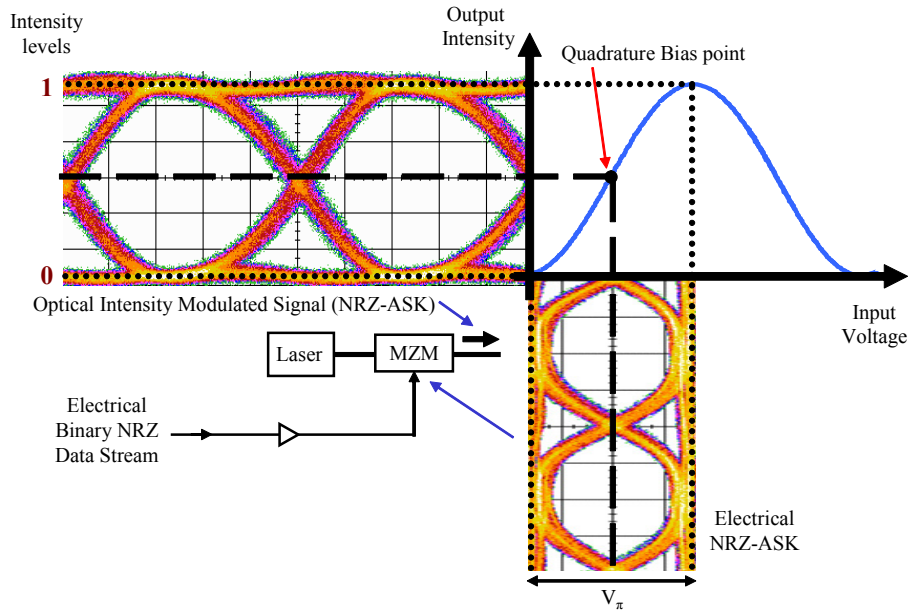

Figure 2.3: Principle of Binary NRZ-ASK modulation generation using intensity MZM

The intensity eye diagram of a detected 10 Gbit/s binary NRZ-ASK signal is also shown in figure 2.3 (left). Figure 2.4 shows the resulting constellation diagram of the optical ASK signal consisting of the OFF state “0” and the ON state “1”.

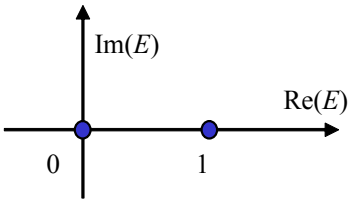

Figure 2.4: ASK signal constellation diagram

The ASK modulation format can also be characterized by the extinction ratio (ER) which is defined as the ratio between the intensities of the ON and OFF states [35]:

$$ER = 10 \log \left(\frac{I_{ON}}{I_{OFF}} \right). \tag{2.11}$$

The binary NRZ-ASK signal can be detected using a simple photo diode at the receiver (direct detection) similar to the receiver shown in figure 2.1. The spectrum of a binary NRZ-ASK signal contains a carrier and has a bandwidth equal to twice the bit rate ($\frac{2}{T_b}$), where the bandwidth will be defined as the null-to-null bandwidth of the main lobe spectrum [42].

2.3.2 Differential Phase Shift Keying (DPSK)

Differential-phase-shift-keying (DPSK) signal format is a promising technique to improve the system performance of optical communication systems [55]. In the DPSK modulation format, the information is carried by the phase of the optical carrier signal. The optical power in a DPSK signal appears in each bit slot, with the binary data encoded as either a 0 or π optical phase shift between adjacent bits. In NRZ-DPSK the optical power can occupy the entire bit slot. In RZ-DPSK the optical power can appear as an optical pulse. RZ-DPSK can be implemented by using a DPSK modulator in combination with an RZ pulse carver [55, 47]. The most benefit of DPSK signals when compared to the conventional ASK format is the high receiver sensitivity due to the ~3dB lower OSNR required to achieve a given BER [67, 55, 59, 68]. DPSK can be used to extend the transmission distance, reduce optical power requirements, and relax component specifications [15]. A critical element in any DPSK system is the demodulator, which converts the phase modulation of the received signal into intensity modulation [68]. The advantage of DPSK over ASK is obtained at the expense of increased complexity and cost in the transmitter and receiver structure, such as a need of a differential encoder at the transmitter, a delay- interferometer and its stabilization at the receiver side and two photodiodes to construct a balanced receiver [55, 59]. An extension of DPSK to Differential quadrature phase-shift keying (DQPSK) should enable higher spectral efficiency and greater chromatic-dispersion tolerance [69, 70].

A standard DPSK transmission system is shown in figure 2.5. It consists of a CW laser source, a precoder circuit, an electrical modulator driver amplifier, a DPSK transmitter (optical modulator) which encodes the data in the phase of the optical signal, and a DPSK receiver which demodulates the received data [59].

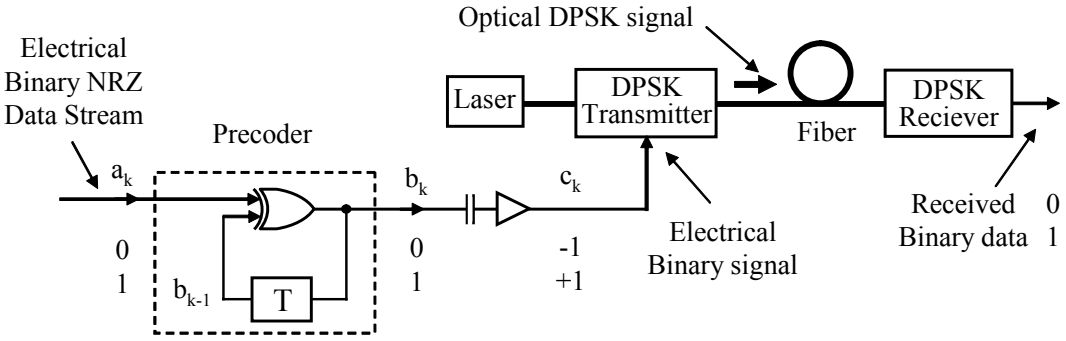

Figure 2.5: Schematic diagram of an optical DPSK transmission setup

A description for each block of the optical DPSK setup will be given in the following subsections:

2.3.2.1 DPSK Precoder

A precoder must be used at the transmitter side in order to recover the original transmitted data at the receiver side by using a differential detection receiver with out the need of a special decoding circuit [1, 47]. Generally, the precoder differentially encodes the original binary bit sequence using a logic XOR gate with a feedback tap with one bit delay. The precoding function can be written as:

$$b_k = a_k \oplus b_{k-1}, \tag{2.12}$$

where $a_k \in \{0, 1\}$ is the original transmitted binary data sequence, $b_k \in \{0, 1\}$ is the precoded binary sequence, and $\oplus$ is the logic instruction "XOR". The encoded symbol b_k is then transmitted in a bipolar fashion $c_k \in \{-1, +1\}$.

2.3.2.2 DPSK Transmitter

A commonly used NRZ-DPSK transmitter setup consists of an external MZM biased at minimum transmission and driven with a precoded binary data with twice the switching voltage required for ASK modulation $2V_\pi$ as shown in figure 2.6.

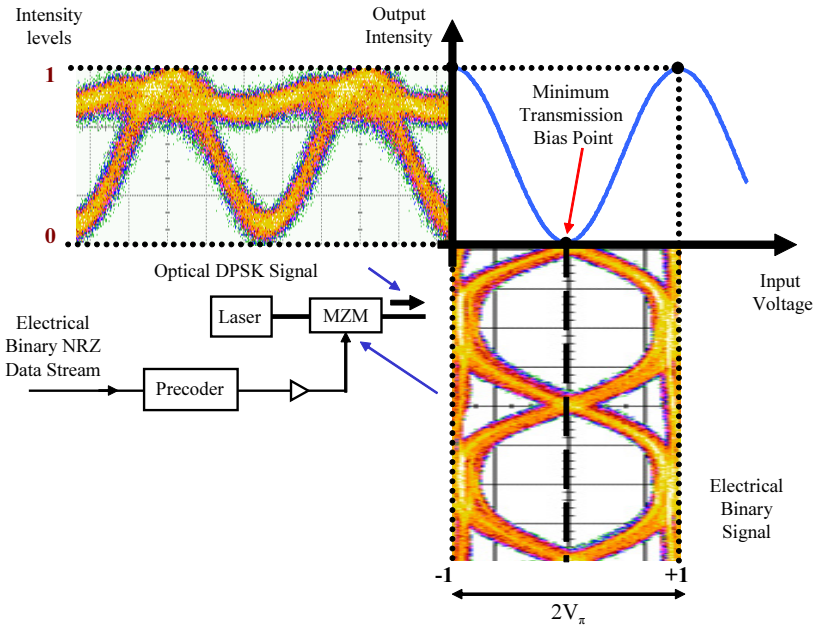

Figure 2.6: Principle of DPSK modulation generation using a MZM

Figure 2.6 also shows the eye diagram (bottom-right) for a 10 Gbit/s electrical binary NRZ signal obtained from a pseudo-random bit sequences (PRBS) pattern generator and the resulting 10Gbit/s optical DPSK signal eye diagram (top-left) detected using a photodiode. A phase modulator (PM) can also be used instead of the intensity MZM by only modulating the phase of the optical field, which results in a constant-envelope optical signal [15]. A drawback of this scheme is that the waveform ripples of the electrical driving signals are converted into phase modulation and will eventually degrade the receiver sensitivity. This is not the case with the MZM since the phase of the optical field changes its sign when a transition is occurred through the minimum point of the MZMs power transmission curve, therefore, the two neighboring intensity transmission maxima points will have an opposite phase, resulting in a near-perfect π phase shift independent of the drive voltage swing [59, 15]. Table 2.1 illustrates the different digital signals in a DPSK transmitter, for an input bit pattern $a_k =$ "01010011". For differential encoding a reference bit is needed to initiate the encoding process. This reference bit could arbitrarily be set to logic "1" or logic "0". In the table the reference bit b_k at instant $k = -1$ was set to logic "0".

Table 2.1: Transmitted bit stream "01010011" for DPSK modulation

Time instant k	-1	0	1	2	3	4	5	6	7
Transmitted data a_k		0	1	0	1	0	0	1	1
Diff. Encoded data b_k	0	0	1	1	0	0	0	1	0
Bipolar encoded c_k	-1	-1	+1	+1	-1	-1	-1	+1	-1
I/P voltage to MZM $\pm V_\pi$	$-V_\pi$	$-V_\pi$	$+V_\pi$	$+V_\pi$	$-V_\pi$	$-V_\pi$	$-V_\pi$	$+V_\pi$	$-V_\pi$
O/P Electrical Field $\pm E$	$+E$	$+E$	$-E$	$-E$	$+E$	$+E$	$+E$	$-E$	$+E$
Transmitted phase ϕ	0	0	π	π	0	0	0	π	0
Phase difference $\|\phi\|$		0	π	0	π	0	0	π	π

The optical spectrum of a DPSK signal has the same bandwidth of an ASK signal but without containing any carrier frequency component. Figure 2.7 shows the resulting signal constellation diagram of the DPSK signal.

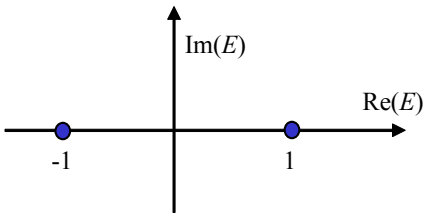

Figure 2.7: DPSK signal constellation diagram

For the generation of RZ-DPSK signals, the transmitter setup will consist of two external modulators as shown in figure 2.8. The first modulator is used for phase modulation which is mostly based on a MZM biased at minimum transmission and driven with precoded binary data with a voltage swing of $2V_\pi$ [59, 15] thus generating an NRZ-DPSK signal as shown in figure 2.8 (Top-Left). The second MZM is used as a pulse carver and is driven by a sinusoidal signal. When the pulse carver MZM is biased at the quadrature point (similar to ASK) and driven with a clock frequency signal with voltage swing amplitude of V_π, a 50% RZ-DPSK signal will be generated as shown in figure 2.8 (Top-Right). Different duty cycle ratios can be obtained for the RZ-DPSK signals depending on the driving conditions of the pulse carver such as the modulation frequency, bias position, and driving voltage [59].

It is also noticed that the generated NRZ-DPSK signal shown in Figure 2.8 has a non-constant optical intensity. This is due to the fact that the signal intensity returns to zero at every transition between marks "1" and spaces "0", which results in a residual amplitude modulation. The width of the resulting intensity dips depends on the driving signal bandwidth and voltage [59, 55]. However, since DPSK encodes information in the optical phase rather than in the intensity, these dips are of reduced importance, especially for RZ-DPSK, where the pulse carver cuts out the amplitude-modulation-free center portions of the bits only, and thus largely eliminates any residual dips [15].

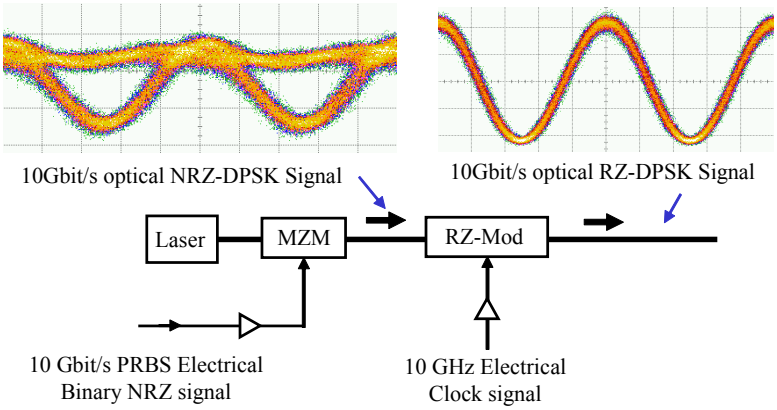

Figure 2.8: 10 Gbit/s optical RZ-DPSK generation scheme using two MZMs with resulting NRZ-DPSK (left) and 50% RZ-DPSK (right) eye diagrams.

2.3.2.3 DPSK Receiver

The most commonly used DPSK receiver is shown in figure 2.9 . It consists of an optical pre-amplifier, an optical filter, a Mach-Zehnder interferometer with a 1-bit delay in one arm, and a dual photodiode balanced receiver [71, 68, 59, 55, 15, 44]. The critical component of the DPSK receiver is the one bit delay Mach-Zehnder delay-interferometer (MZDI) which acts as the demodulator.

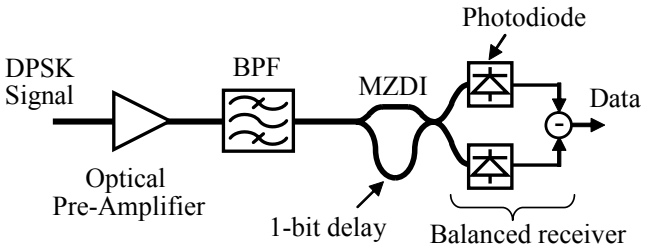

Figure 2.9: DPSK receiver

The one bit delay MZDI can be constructed using two 3dB 2×2 couplers. One coupler is used at the input and the other at the output [44]. The two optical branches connecting the two couplers have unequal optical path lengths. The difference in the optical path lengths correspond to one bit duration. If the input optical field to the MZDI shown in figure 2.9 is $E(t)$, the output optical fields at both the output arms of MZDI are $E_1(t)$ and $E_2(t)$ [44, 72] as follows:

$$E_1(t) = \frac{1}{2}\left[E(t) + E(t-T)\right] \tag{2.13}$$

$$E_2(t) = -j\frac{1}{2}\left[E(t) - E(t-T)\right]. \tag{2.14}$$

The MZDI lets two adjacent bits interfere with each other at its output ports. This interference leads to the presence of power at a MZDI output port when there is constructive interference between two adjacent bits, or the absence of power when there is destructive

interference between two adjacent bits. Therefore, the previous bit in a DPSK encoded bit stream acts as the phase reference for demodulating the current bit [55, 15]. At the MZDI outputs, the two output ports will carry identical, but logically inverted data streams under DPSK modulation. The optically demodulated signal measured at the constructive port is similar to Duobinary modulation, and at the destructive port is similar to alternate-mark inversion (AMI) modulation signal [15, 73, 74, 59]. After the MZDI, direct detection can be achieved by using a single photo-diode (single ended detection) to receive the signal by detecting it at one of the interferometer output ports, or by using two photo receivers (balanced detection) to receive the signal by detecting the difference between the constructive and destructive interferometer output ports [56, 68]. For balanced detection the photocurrent difference is proportional to the difference of the intensities at the two photodiode outputs:

$$|E_1(t)|^2 - |E_2(t)|^2 = Re\left(E^*(t)\, E(t-T)\right). \tag{2.15}$$

Figure 2.10 shows the eye diagram patterns for a demodulated 10 Gbit/s NRZ-DPSK and RZ-DPSK signal at the output of a DPSK receiver with balanced detection. The MZDI used in the receiver had a differential delay of 100 ps. The two high speed photodiodes used for balanced detection had approximately equal fiber length. An electrical RF variable delay line was used to fine tune the path delay difference between the outputs of the two photodiodes. An electrical differential amplifier was used to measure the current difference between the two photodiodes.

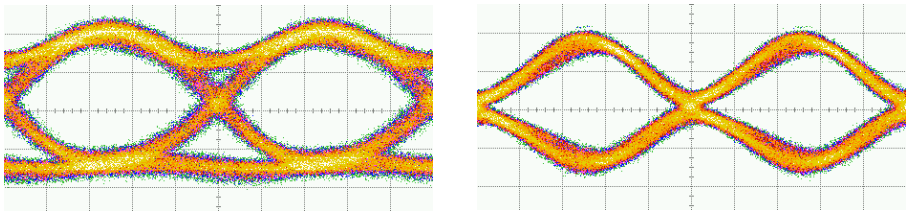

a b

Figure 2.10: Demodulated 10 Gbit/s NRZ-DPSK (a) and RZ-DPSK (b) intensity eye patterns

2.3.3 Duobinary Modulation (DB)

Waveform distortion due to fiber chromatic dispersion in high-speed optical transmission systems is a serious problem. Optical Duobinary modulation is an effective way to avoid such distortion resulting in an increased dispersion tolerance compared to binary NRZ modulation format [75]. Duobinary modulation is also spectrally efficient due to the reduced occupied spectral bandwidth which is about half the spectrum bandwidth of a conventional binary NRZ intensity modulation (IM) [24, 25, 76]. The cost of an optical transmission link over long-haul distances can be reduced by using Duobinary modulation due to the better CD tolerance and therefore no need of dispersion compensation which adds to the total cost [47, 77]. An optical Duobinary signal can be generated by modulating the optical carrier signal with a three level electrical Duobinary signal. The most common type of optical Duobinary modulation is the Amplitude Modulation Phase Shift Keying (AM-PSK) type

[75]. Duobinary is interesting for Dense Wavelength Division Multiplexing (DWDM) applications, since it has been optimized to reduce the channel bandwidth [47]. It should also be noted that Duobinary and DPSK have similarities. The DPSK demodulator which is a Mach-Zehnder delay interferometer (MZDI) can be viewed as a narrow-band optical filter with sinusoidal shape. If the MZDI is used at the transmitter side after the intensity Mach-Zehnder modulator, the signal obtained at the output of the MZDI constructive port has most of the features of a Duobinary signal [47]. A standard Duobinary transmitter and receiver consist of a precoder, Duobinary encoder, and decoder. The corresponding practical optical Duobinary transmission setup consists of the precoder logical circuit, a Duobinary filter as an encoder, an electrical modulator driver amplifier used to amplify to electrical Duobinary signal to drive the optical MZM, and a decoder to extract the data from the demodulated optical Duobinary signal as shown in figure 2.11.

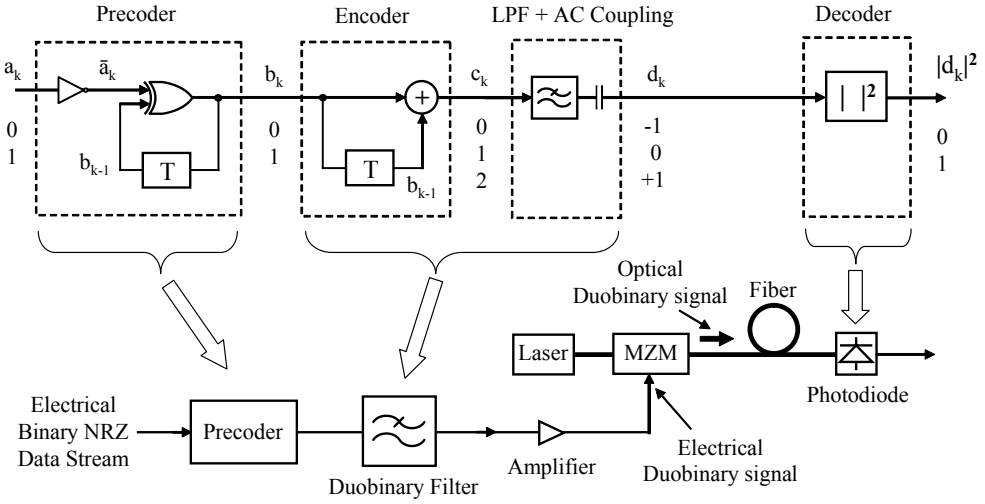

Figure 2.11: Schematic diagram of a standard Duobinary generation and detection scheme (top) and a corresponding practical optical Duobinary transmission setup (bottom)

A description for each block of the optical Duobinary setup will be given in the following subsections:

2.3.3.1 Duobinary Precoder

The Duobinary encoder at the transmitter side scrambles the original binary data; therefore an electrical precoder is needed to be inserted before the encoder to recover the original transmitted binary data at the receiver side using a conventional NRZ receiver. This precoder normally is a differential encoder which is also used for a DPSK system [47]. The differential encoder (precoder) is used to avoid recursive decoding in the receiver thus avoiding error propagation and reducing hardware complexity [76, 78, 75]. The precoder is basically constructed using a logic XOR gate with a feedback tap with one bit delay. The precoding function for Duobinary coding can be written as:

$$b_k = \bar{a}_k \oplus b_{k-1}, \tag{2.16}$$

where a_k is the transmitted binary data sequence, b_k is the precoded binary sequence, and $\oplus$ is the logic instruction "XOR". In a laboratory environment, most of the optical

Duobinary transmission experiments are performed without a precoder. This is due to the properties of the commonly used pseudo-random bit sequences (PRBS) where the precoder output bit stream is in fact a time-delayed version of the input PRBS bit stream. Therefore, the information is maintained and the functionality of the precoder can be omitted. Also the transmitted PRBS pattern is inverted at the input of the precoder in order to receive a non-inverted PRBS at the receiver [26, 76, 45].

2.3.3.2 Duobinary Encoder

To generate an optical Duobinary signal two common types of Duobinary encoding schemes are well known, a low-pass filtering (LPF) method [24, 79, 80] and the conventional method by using an electrical one-bit delay and add method [24, 25, 26]. The electrical LPF used to generate a Duobinary signal usually has approximately a 3dB bandwidth equal to quarter of the data bit rate. This LPF filter is equivalent to a one-bit delay-and-add operation similar to the conventional scheme. The Duobinary encoder is mainly used to convert an electrical binary NRZ signal to a three-level electrical Duobinary signal, producing the logic levels {0, 1, 2} by adding the current bit to the previous bit [78] as shown in figure 2.11 based on the following equation:

$$c_k = b_k + b_{k-1}. \tag{2.17}$$

The DC offset is removed from the electrical Duobinary signal c_k using a DC-block capacitor resulting in the electrical Duobinary signal d_k with the normalized levels {-1 , 0, +1}. To generate an optical Duobinary signal in practice an intensity MZM biased at minimum transmission is used and driven by an electrical Duobinary signal with the peak-to-peak swing voltage (V_{p-p}) equal to $2V_\pi$. The generated electric fields are $\{-E\ ,\ 0,\ +E\}$ which corresponds to the normalized intensities {0, 1} as shown in figure 2.12. Figure 2.12 shows the optical Duobinary generation method using the conventional one bit delay-and-add encoding scheme. The eye diagrams shown in figure 2.12 are for a 10Gbit/s electrical binary NRZ signal obtained from a PRBS pattern generator (bottom-left), the generated electrical 10Gbit/s Duobinary signal (bottom-right), and finally the resulting 10 Gbit/s optical Duobinary signal detected using a photodiode (top-left).

The ON state corresponding to the normalized intensity "1" can have one of the two optical phases, 0 and π depending on the input levels "-1" and "+1" of the electrical Duobinary encoded signal, respectively. The OFF state corresponds to the intensity "0" and depends on the input level "0" of the electrical Duobinary encoded signal [25]. Figure 2.13 shows another optical Duobinary modulation generation scheme based on driving an intensity MZM biased at transmission minimum with an electrical Duobinary signal with a voltage swing amplitude of $2V_\pi$ generated using a 5th order Bessel LPF with a cutoff frequency at $2.8\,\mathrm{GHz}$. The measured eye diagrams shown in figure 2.13 are for an electrical 10Gbit/s binary NRZ signal (left) generated using a PRBS pattern generator, an electrical Duobinary signal (bottom-right) generated using the Bessel filter, and finally the intensity eye diagram of the generated 10 Gbit/s optical Duobinary signal (top-right). It can be noticed that the intensity profile of the conventional delay-and-add type optical Duobinary signal [24, 25, 26] shown in figure 2.12 (top-left) is more similar to that of a binary NRZ signal, while the intensity diagram shown for optical Duobinary signal using the LPF generation method shown in figure 2.13 (top-right) [24, 79, 80] leaves a small fraction of light

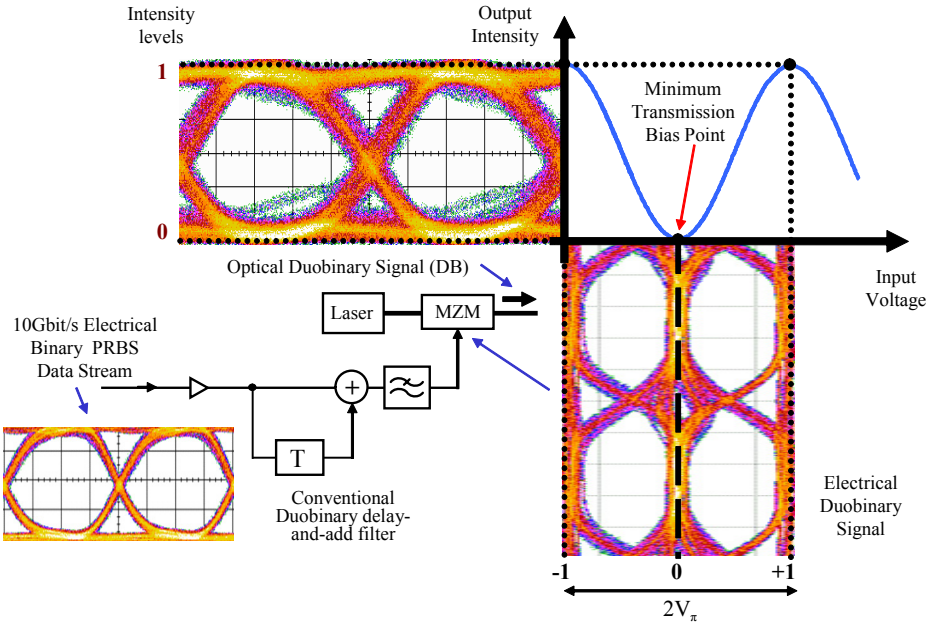

Figure 2.12: Principle of Duobinary modulation generation using a MZM and a Duobinary encoder based on the conventional one bit delay and add filter

within "0" symbols, which incorporate π phase shifts in their center. Due to this property, this type of Duobinary modulation has also been named Phase-Shaped Binary Transmission (PSBT) [47, 81, 82]. The optical Duobinary signal generated using the LPF method suppresses the optical spectrum side-lobes better than the Duobinary one-bit delay and add method. Therefore it tolerates more chromatic dispersion. A drawback of the LPF method generated optical Duobinary signal is that it has worse eye opening, poor tolerance to noise, and worse back-to-back receiver sensitivity compared to the one-bit-delay and add method [24, 48, 83, 84, 82, 47].

The optical spectrum of a Duobinary signal has two special characteristics. One is that most of the signal power is concentrated within a narrow bandwidth approximately half of the binary NRZ-ASK IM signal spectrum. Such a narrow band signal can be expected to achieve high tolerance to chromatic dispersion [79]. The other is that the optical Duobinary signal has no carrier frequency component in contrast with the binary NRZ-ASK IM signal[26]. Figure 2.14 shows the resulting signal constellation diagram of the optical Duobinary signal.

2.3.3.3 Duobinary Decoder

A simple decoder can be used to detect the received Duobinary signals by using a square-law device which can be a photo-diode used for detecting binary intensity modulated signals [78, 26]. The photodiode will convert the received optical Duobinary signal d_k with electrical field levels {-E, 0, +E} to an electrical binary signal $|d_k|^2$ with normalized amplitudes {0, 1}. Due to the inverter and precoder used at the transmitter side the demodulated electrical binary signal will be identical to the original transmitted binary data stream [26, 76, 45]. It is also possible invert the data at the receiver side instead of the transmitter side. Table 2.2 illustrates the different digital signals in a Duobinary system, for an input bit pattern a_k

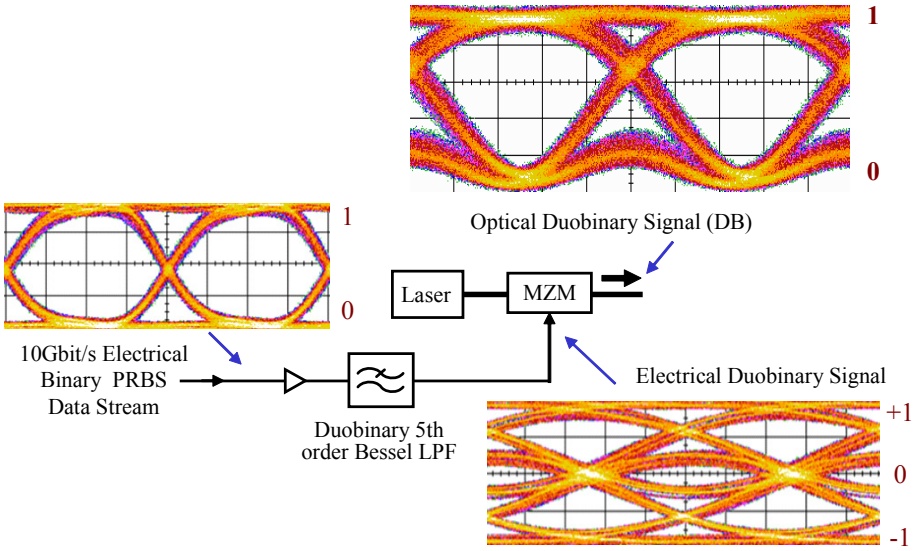

Figure 2.13: 10 Gbit/s optical Duobinary modulation generation using a MZM and a Duobinary encoder based on a 5th order Bessel filter with cutoff frequency at 2.8 GHz

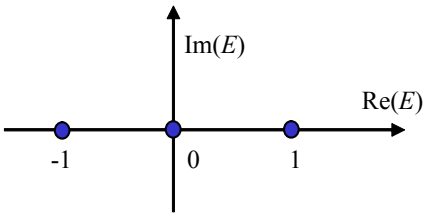

Figure 2.14: Optical Duobinary signal constellation diagram

= “01010011”. For differential encoding a reference bit is needed to initiate the encoding process. This reference bit could arbitrarily be set to logic “1” or logic “0”. In table 2.2 the reference bit b_k at instant $k = -1$ was set to logic “0”. To prove the precoding, encoding, and decoding functions are correct, it is shown in table 2.2 that the received data $|d_k|^2$is identical to the original transmitted data a_k.

Table 2.2: Transmitted and received bit stream “01010011” for Duobinary modulation

Time instant k	-1	0	1	2	3	4	5	6	7
Transmitted data a_k		0	1	0	1	0	0	1	1
Inverted Data $\bar{a}_k$		1	0	1	0	1	1	0	0
Diff. Encoded Data b_k	0	1	1	0	0	1	0	0	0
Duobinary Encoded c_k		1	2	1	0	1	1	0	0
Transmitted Duobinary d_k		0	+1	0	-1	0	0	-1	-1
I/P voltage to MZM $\pm V_\pi$		0	$+V_\pi$	0	$-V_\pi$	0	0	$-V_\pi$	$-V_\pi$
O/P Electrical Field $\pm E$		0	$-E$	0	$+E$	0	0	$+E$	$+E$
Optical Power (Intensity)		0	E^2	0	E^2	0	0	E^2	E^2
Received data $\|d_k\|^2$		0	1	0	1	0	0	1	1

Chapter 3

Differential Quadrature Phase Shift Keying (DQPSK)

3.1 Introduction

In this chapter, the Differential Quadrature Phase Shift Keying (DQPSK) modulation format will be introduced. DQPSK is a multilevel (quaternary) modulation format that can be used for long haul optical communication systems. The following sections of this chapter will cover the generation and detection scheme of DQPSK. Experimental data will be presented for 20 Gbit/s DQPSK and 40 Gbit/s DQPSK PolDM transmission system showing the receiver sensitivity and eye diagrams. Also the CD tolerance for 20 Gbit/s RZ-DQPSK will be evaluated.

3.2 Differential Quadrature Phase Shift Keying (DQPSK)

Differential quadrature phase-shift keying (DQPSK) is one of the interesting advanced modulation formats that has received intense study and is seen as an alternative modulation format for high bit rate long haul optical transmission systems [85, 69, 13, 70, 86, 87, 88]. DQPSK is a four-level (quaternary) phase modulation format and can be considered as an extension of the DPSK modulation format introduced in the previous chapter. For DQPSK two bits are transmitted for each symbol. Each transmitted symbol is mapped into four (quaternary) possible phase change transitions. Since two bits are transmitted for each symbol, the symbol rate is half of the bit rate which results in reduced spectral occupancy and bandwidth requirements for the transmitter and receiver components. Another advantage of DQPSK are the extended chromatic dispersion and PMD tolerances [15]. The high spectral efficiency of DQPSK can be even doubled by using polarization multiplexing [44, 89]. For DQPSK, the required OSNR to reach a given BER compared to DPSK measured at the same bit rate, is increased by about 1-2 dB [90, 15, 91]. Combined with RZ coding its robustness against non linear effects is increased because the intensity is not modulated by the data but is rather modulated by a pulse carver [44]. The main components needed to build an optical DQPSK (oDQPSK) system [13, 69, 92] are the digital precoder, optical encoder and the optical decoder as shown in the schematic in figure 3.1.

A description for each block of the optical DQPSK system will be given in the following

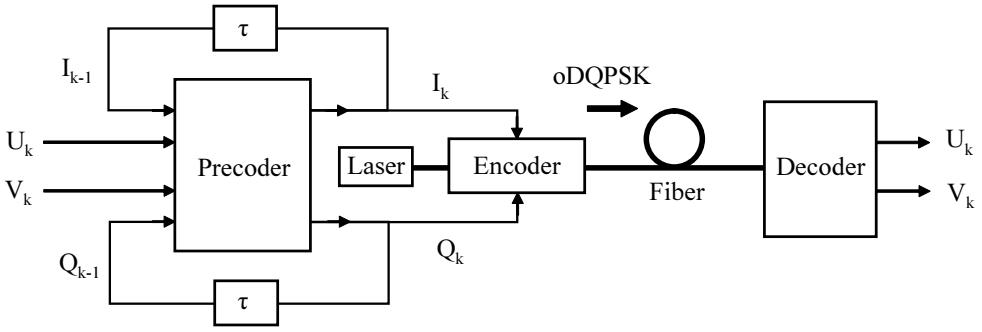

Figure 3.1: Schematic of an optical DQPSK transmission system

subsections:

3.2.1 DQPSK Precoder

Due to the differential nature of decoding in DQPSK, a precoding function is required to provide a direct mapping of the data from the input to the output [13] taking care that the received data streams are identical to the original transmitted data streams. The precoder for the DQPSK transmitter can operate at a clock rate which is half of the total transmission data rate. The precoder block shown in figure 3.1 has four inputs and two outputs. Two of the four inputs are the input data streams (U_k and V_k) and the other two are the time delayed version of the precoder outputs (I_{k-1} and Q_{k-1}). The two output precoded signals (I_k and Q_k) are used to drive the optical encoder resulting in the transmitted symbol (d_k). Every transmitted symbol is coded into one of four possible phase levels, representing one of the four combinations of the two transmitted signals I_k and Q_k. The input signals U_k and V_k can be demultiplexed from a signal operating at the total transmitted bit rate, or can be two independent data inputs at half the total transmitted bit rate. For the DQPSK encoder based on the parallel MZM transmitter, the operation of the precoder is described by the following set of logic equations [13, 93, 1]:

$$I_k = \overline{U}_k\overline{V}_k\overline{I}_{k-1} + \overline{U}_kV_kQ_{k-1} + U_kV_kI_{k-1} + U_k\overline{V}_k\overline{Q}_{k-1} \tag{3.1}$$

$$Q_k = \overline{U}_k\overline{V}_k\overline{Q}_{k-1} + \overline{U}_kV_k\overline{I}_{k-1} + U_kV_kQ_{k-1} + U_k\overline{V}_kI_{k-1}. \tag{3.2}$$

A more detailed explanation on how to derive the precoder equations is given in appendix B. For DQPSK experimental test measurements, the precoding is normally not implemented in hardware [45]. By transmitting a binary PRBS data stream and a time-shifted binary PRBS data stream by using an optical DQPSK modulator, the expected received pattern at the receiver side can be calculated by software means. These calculated patterns are then used to program a programmable bit error detector (BER) with the corresponding expected received patterns enabling BER measurements for the received data.

3.2.2 DQPSK Optical Encoder

A preferred and most widely used implementation of the optical encoder is the oDQPSK modulator based on two parallel MZMs as shown figure 3.2 [13, 86].

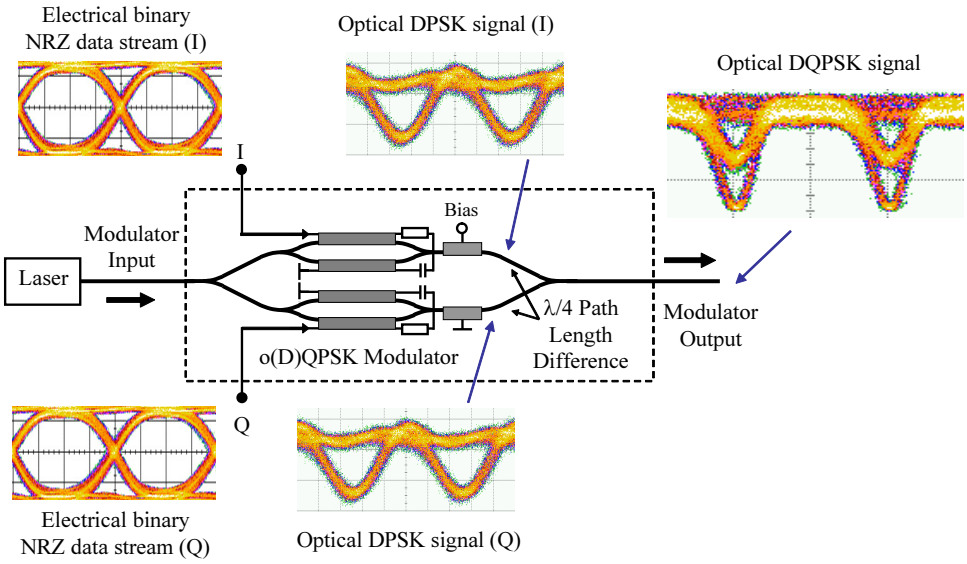

Figure 3.2: Schematic of an optical DQPSK modulator

The oDQPSK modulator consists of two parallel DPSK modulators that are integrated together in order to achieve phase stability [15]. These two DPSK modulators are mainly two Mach-Zehnder modulators (MZMs), placed in two arms of another interferometer that forms a Mach-Zehnder superstructure. The superstructure has quadrature control electrodes in both arms for phase control enabling an adjustment of the optical phase difference $\frac{\pi}{2}$ between the upper and lower arms. Each of the MZMs are biased for minimum transmission and driven by a Binary NRZ data signal with peak-to-peak amplitude of $2V_\pi$. Two binary NRZ data streams in-phase I and quadrature Q can be transmitted simultaneously. One binary NRZ data signal I with a full $2V_\pi$voltage swing generates in one MZM the in-phase optical field $Re(E)$ with normalized field amplitudes {-1, +1} which is similar to a differential phase shift keying (DPSK) signal. The other arm MZM is driven with another binary NRZ data signal Q with also a full $2V_\pi$ voltage swing therefore generating the quadrature optical field component $Im(E)$ with normalized field amplitudes {-1, +1}, which is also similar to a DPSK signal. The DPSK signal generated in one arm is combined with a $\frac{\pi}{2}$ phase shifted version of the other DPSK signal in the other arm. Since the output field of the oDQPSK modulator is $E_o = Re(E) + jIm(E)$, the generated fields at the output are $\{\pm 1 \pm j\}$ resulting in a four-level phase modulated signal with resulting phase values within $\{\frac{\pi}{4}, \frac{3\pi}{4}, \frac{5\pi}{4}, \frac{7\pi}{4}\}$ and labeled { “00”, “10”, “11”, “01”} respectively. The mapping of the input signals (I_k and Q_k) to the output electric field (E_o) and generated phase state (ϕ_k) of the optical (D)QPSK modulator is shown in table 3.1 . The modulation resulting signal constellation diagram is shown in figure 3.3.

Table 3.1: Mapping of the input signals (I_k and Q_k) to the output electric field (E_o) and generated phase state (ϕ_k) of the o(D)QPSK modulator

I_k	Q_k	E_o	ϕ_k
0	0	$+1+j$	$\frac{\pi}{4}$
0	1	$+1-j$	$\frac{7\pi}{4}$
1	0	$-1+j$	$\frac{3\pi}{4}$
1	1	$-1-j$	$\frac{5\pi}{4}$

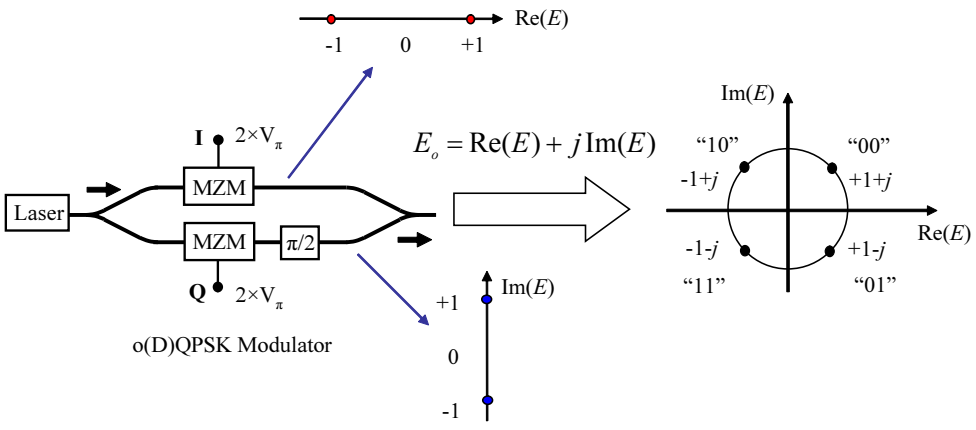

Figure 3.3: DQPSK signal constellation diagram

Figure 3.4 shows a generated 2×10 Gbit/s NRZ-DQPSK signal eye diagram generated using the same DQPSK modulator given in figure 3.2. It can be noticed that the NRZ-DQPSK signal contains residual intensity dips at the transition between two symbols. The width of the intensity dips depends on the drive signal voltage and bandwidth [15]. The strong intensity dip is a result of the optical power drop to zero when both I and Q change value at the same time (e.g., "00" $\longleftrightarrow$ "11"). The smaller intensity dip is a result of the optical power drop to half when either I or Q changes value (e.g., "00" $\longleftrightarrow$ "01" or "00" $\longleftrightarrow$ "10") [45]. Since DQPSK modulation encodes the information in the optical phase rather than in the amplitude, the intensity dip has negligible effect on the transmitted data, especially for RZ-DQPSK signals where the pulse carver largely eliminates the residual dips [15]. The spectrum of the generated DQPSK signal is just as broad as for a single DPSK modulation signal although the capacity is doubled [45].

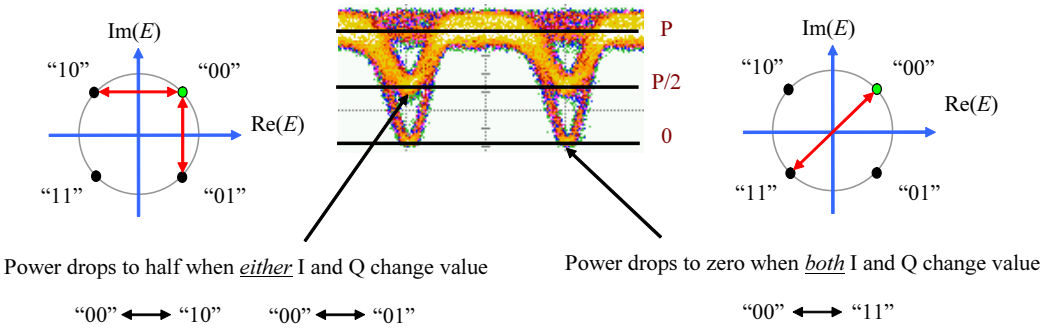

Figure 3.4: NRZ-DQPSK signal eye diagram showing the intensity dips

With the use of a digital precoder before the optical encoder (DQPSK modulator) at the transmitter side the original input data signals (U_k and V_k) corresponding to a transmitted symbol (d_k) will map to the phase changes ($\triangle\phi_k$) as shown in table 3.2 . The phase change $\triangle\phi_k$ corresponds to the phase difference between the current phase (ϕ_k) generated by (I_k and Q_k) driving the DQPSK modulator and the previous phase (ϕ_{k-1}) generated by (I_{k-1} and Q_{k-1}) driving the DQPSK modulator. It contains the transmitted information that can be extracted at the receiver side by the DQPSK decoder which is used to demodulate the received signal.

Table 3.2: Mapping of data signals (U_k and V_k) to transmitted symbol (d_k), and corresponding phase changes ($\triangle\phi_k$) for DQPSK modulation

U_k	V_k	d_k	$\triangle\phi_k$
1	1	0	0
1	0	1	$\frac{\pi}{2}$
0	0	2	π
0	1	3	$\frac{3\pi}{2}$

3.2.3 DQPSK Optical Decoder

The DQPSK signals can be decoded optically using an optical delay and add interferometer structure. To simultaneously receive the two transmitted data streams, the decoder needs two Mach-Zehnder delay interferometers (MZDI) and two balanced detectors which is similar to using two DPSK demodulators as shown in figure 3.5 [13]. Both interferometers need a 1 bit delay in one of their arms. The differential optical phase between the interferometer arms is to be set to $+\pi/4$ and $-\pi/4$ for the upper and lower branches respectively in order to receive the two transmitted data streams [15]. If the input signal to the MZDI has the form $E_o e^{-j(\omega_o + \triangle\phi_k)}$, the output signals after balanced detection for each MZDI are proportional to $[\cos(\triangle\phi_k) + \sin(\triangle\phi_k)]$ and $[\cos(\triangle\phi_k) - \sin(\triangle\phi_k)]$, respectively where $\triangle\phi_k$ is the phase difference between consecutive bits [13, 45, 44, 94]. The balanced detection used after each interferometer provides a 3dB improvement in the receiver sensitivity [14].

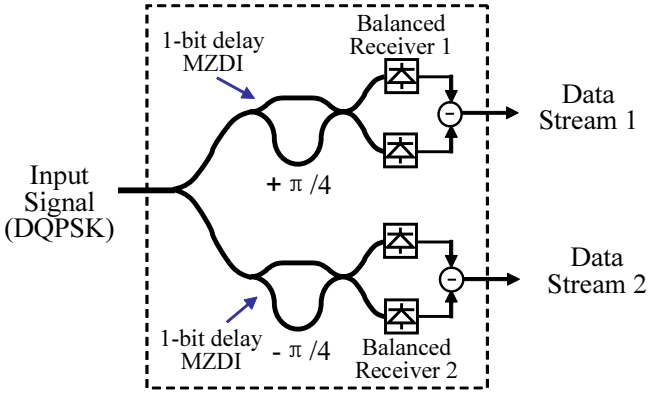

Figure 3.5: Schematic of an optical DQPSK decoder

The received phase modulated DQPSK signal is converted into an amplitude modulated signal after demodulation. Figure 3.6 shows the eye diagram of a demodulated 2×10 Gbit/s NRZ-DQPSK signal after balanced detection. Standard clock and data recovery circuits can be used to extract the clock and data from the demodulated signal [44, 13, 45]. DQPSK demodulators suffer from stability problems due to small temperature drift in the interferometer may cause a phase change between the two arms. Therefore, the interferometer needs to be temperature stabilized [45].

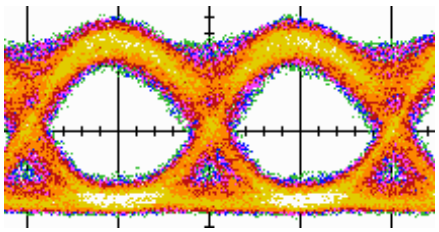

Figure 3.6: Eye diagram of a demodulated data signal from an NRZ-DQPSK signal

Table 3.3 illustrates the different digitally precoded, optically encoded and optically decoded DQPSK signals for two transmitted binary data streams U_k "01010011" and V_k

"10011010" in the optical DQPSK system shown in figure 3.1. The precoder function is based on the precoder equations 3.1 and 3.2. The optical encoder is based on the parallel MZM oDQPSK modulator shown in figure 3.2. The decoder is based on the two MZDI and two balanced receivers as shown in figure 3.5. For the precoder both the initial values of I_k and Q_k at time instant $k = -1$ were set to logic "0". It can be seen that the received data is identical to the transmitted data, therefore verifying that the precoding and decoding functions are correct.

Table 3.3: Transmitted and received data bit streams U_k = "01010011" and V_k = "10011010" for an optical DQPSK system

Time instant k	-1	0	1	2	3	4	5	6	7
Binary data U_k		0	1	0	1	0	0	1	1
Binary data V_k		1	0	0	1	1	0	1	0
Precoded data I_k	0	0	0	1	1	1	0	0	0
Precoded data Q_k	0	1	0	1	1	0	1	1	0
I/P voltage to MZM (I)	-V_π	-V_π	-V_π	+V_π	+V_π	+V_π	-V_π	-V_π	-V_π
I/P voltage to MZM (Q)	-V_π	+V_π	-V_π	+V_π	+V_π	-V_π	+V_π	+V_π	-V_π
O/P Electrical Field E_0	+1+j	+1-j	+1+j	-1-j	-1-j	-1+j	+1-j	+1-j	+1+j
Transmitted phase ϕ_k	$\frac{\pi}{4}$	$\frac{7\pi}{4}$	$\frac{\pi}{4}$	$\frac{5\pi}{4}$	$\frac{5\pi}{4}$	$\frac{3\pi}{4}$	$\frac{7\pi}{4}$	$\frac{7\pi}{4}$	$\frac{\pi}{4}$
Phase difference $\triangle\phi$		$\frac{3\pi}{2}$	$\frac{\pi}{2}$	π	0	$\frac{3\pi}{2}$	π	0	$\frac{\pi}{2}$
Received data u_k		0	1	0	1	0	0	1	1
Received data v_k		1	0	0	1	1	0	1	0

3.3 DQPSK Transmission System at 2×10 Gbit/s

Figure 3.7 shows the details of an experimental DQPSK transmission setup used to generate and detect 2×10 Gbit/s NRZ-, RZ-DQPSK signals. NRZ-DQPSK signals are generated when the RZ modulator is bypassed. RZ-DQPSK signals can be generated by placing the RZ modulator (pulse carver) before or after the DQPSK modulator. RZ coding is widely used in optical communication systems due to its superior performance and improved receiver sensitivity [45, 16]. RZ-DQPSK is known to have an approximately 2 dB advantage in the OSNR over NRZ-DQPSK [45].

A 192.5 THz DFB laser was used at the transmitter. A fiber-pigtailed $LiNbO_3$ oDQPSK Modulator (from Photline) with a structure similar to that given in figure 3.2 was used to generate the DQPSK signals. A pattern generator was used to generate a 10 Gbit/s Pseudo Random Bit Sequence (PRBS) Binary NRZ data stream. The 10 Gbit/s NRZ data stream was split and delayed by 31 bit durations to emulate two decorrelated patterns (I and Q). Each MZM modulator in both arms of the oDQPSK modulator was biased at minimum transmission and driven by the two 10 Gbit/s binary NRZ data stream patterns (I and Q) with each signal having a $2V_\pi$ signal peak-to-peak voltage amplitude corresponding to 10V ($V_\pi \simeq 5\mathrm{V}$). No DQPSK precoder was implemented. The intensity eye diagram of the

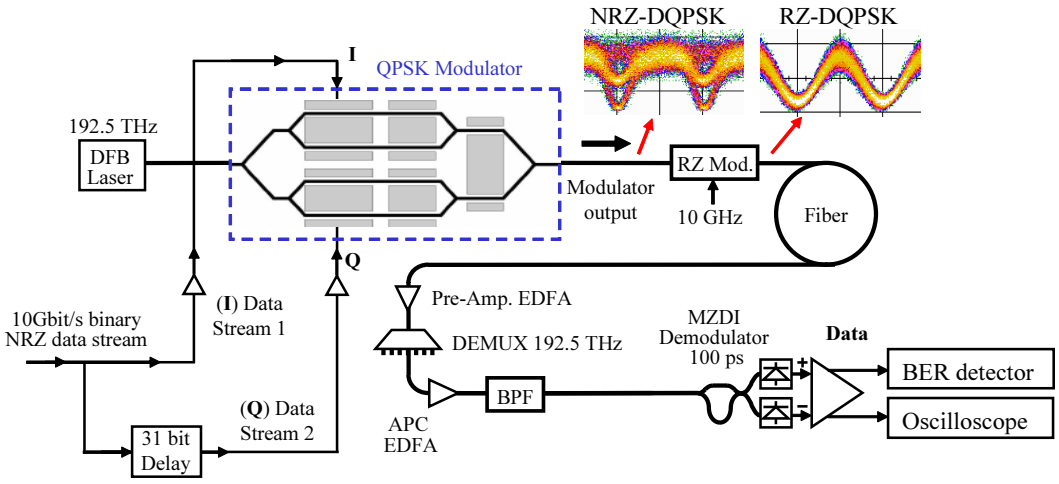

Figure 3.7: Experimental 2×10 Gbit/s DQPSK transmission setup

generated 2×10 Gbit/s NRZ-DQPSK signal is shown in figure 3.7 (top-left). The DQPSK modulator was followed by a $LiNbO_3$ Mach-Zehnder modulator. The latter was biased at the quadrature point and driven by a 10 GHz clock signal with peak-to-peak voltage amplitude of V_π to generate 50% duty cycle Return-to-Zero (RZ) pulses, thereby completing a 2×10 Gbit/s RZ-DQPSK signal. The intensity eye diagram of the generated 2×10 Gbit/s RZ-DQPSK signal is shown in figure 3.7 (top-right).

The receiver employed an Erbium Doped Fiber Amplifier (EDFA) as an optical preamplifier followed by a 40-channel Dense Wavelength Division Multiplexing (DWDM) Arrayed-Waveguide Grating (AWG) Demultiplexer (DEMUX) with 100 GH_z channel spacing and Gaussian top characteristics. The DEMUX acted as a narrow bandpass optical filter to remove the broadband optical noise. After the DEMUX another EDFA operated in an automatic power control (APC) mode was used to amplify the received signal to a level where it can be detected with high sensitivity. The received signal was then split to the demodulator and an optical front end based on a p-type intrinsic n-type (PIN) photodiode followed by a Trans-Impedance Amplifier (PIN-TIA). This photo-receiver was used to stabilize a feedback loop (not shown) that controlled the pump current of the last EDFA for automatic power control (APC). The other part of the received RZ-DQPSK signal after the last BPF was connected to the demodulator which was an integrated Planar Lightwave Circuit (PLC) Mach-Zehnder interferometer (from NEL) with a 100 ps (1 bit) differential delay. The NEL PLC MZDI was based on silica waveguide technology and was temperature stabilized using a PI controller. By adjusting the differential optical phase between the interferometer arms by controlling the differential micro-heaters of the MZDI, it was possible to select either of the transmitted patterns I and Q. The demodulator outputs were connected to two optical front ends (PIN-TIA) (from NORTEL) having a bandwidth (BW) of 11 GHz and photodiode responsitivity (R) of 0.88 A/W. The outputs of the two optical front ends were then subtracted by connecting them to a high sensitivity differential limiting amplifier iT3011 (from iTerra). The outputs of the differential amplifier were connected to an oscilloscope for signal monitoring and a bit error rate (BER) detector for measuring the BER and receiver sensitivity. To allow BER measurements, the error detector was programmed with the expected data sequence received at the output of the demodulator.

Figure 3.8 shows the demodulated eye diagram measured at the output of the differential amplifier for the I and Q channels extracted from a 2×10 Gbit/s NRZ-DQPSK signal generated with PRBS lengths of $2^7 - 1$ and $2^{15} - 1$ for the top (PRBS-7) and bottom (PRBS-15) eyes, respectively.

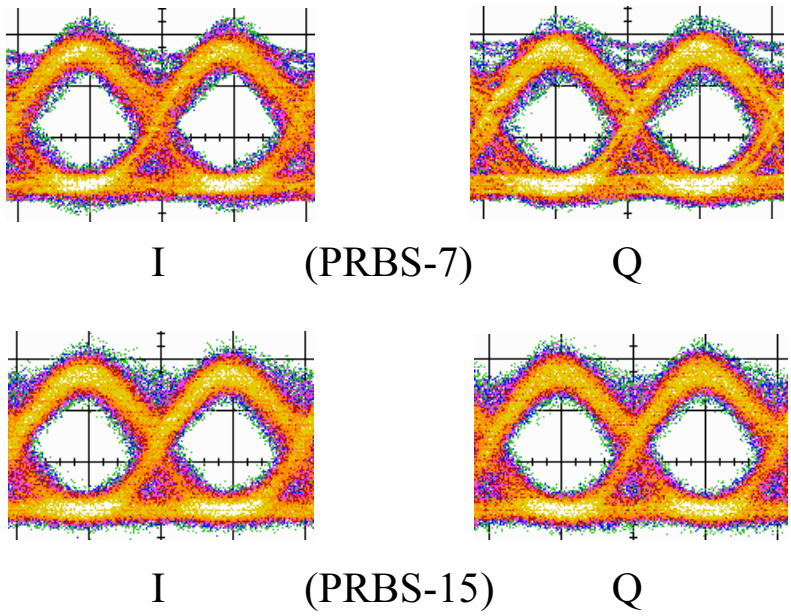

Figure 3.8: Eye diagrams of a demodulated data signal I and Q extracted from a 2×10 Gbit/s NRZ-DQPSK signal generated using a Photline DQPSK modulator with PRBS lengths of $2^7 - 1$ (PRBS-7) (top) and $2^{15} - 1$ (PRBS-15) bottom

The measured BER curves versus the received optical power measured at the input of the optical preamplifier for both the received patterns I and Q are plotted in figure 3.9 for a 2×10 NRZ-DQPSK signal generated with PRBS lengths of $2^7 - 1$ (PRBS 7) and $2^{15} - 1$ (PRBS 15). Figure 3.10 shows the average BER of the received 2×10 NRZ-DQPSK data streams I and Q versus the received optical power for both PRBS 7 and PRBS 15. From the curve in figure 3.10 the measured receiver sensitivity for the 20 (2×10) Gbit/s NRZ-DQPSK signal at a BER of 10^{-9} was ~-36.8 dBm and ~-36.4 dBm for both PRBS 7 and PRBS 15, respectively.

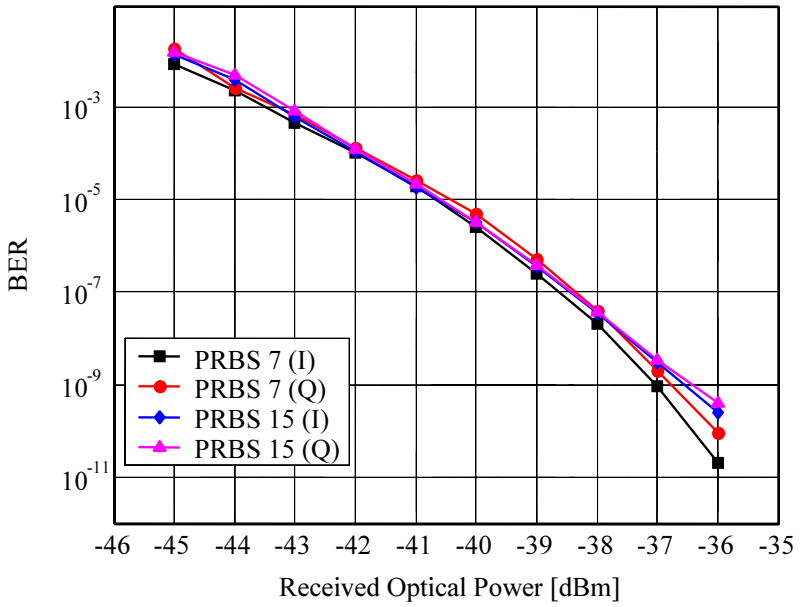

Figure 3.9: BER curves for the I and Q received data streams versus received optical power for a 2×10 Gbit/s NRZ-DQPSK signal using a Photline oDQPSK Modulator with PRBS lengths of $2^7 - 1$ (PRBS 7) and $2^{15} - 1$ (PRBS 15)

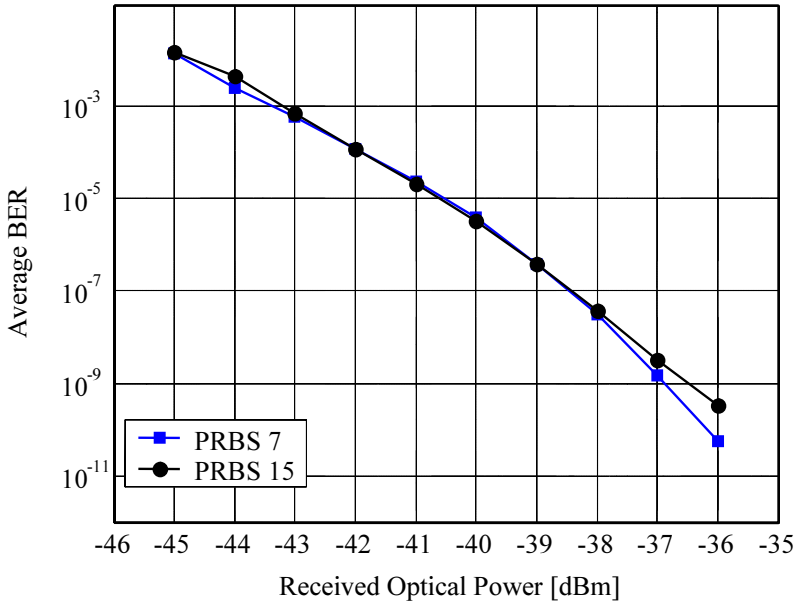

Figure 3.10: Average BER versus received optical power for a 20 Gbit/s NRZ-DQPSK signal using a Photline oDQPSK Modulator with PRBS lengths of $2^7 - 1$ (PRBS 7) and $2^{15} - 1$ (PRBS 15)

Figure 3.11 shows the demodulated eye diagram measured at the output of the differential amplifier for the I and Q channels extracted from a 2×10 Gbit/s RZ-DQPSK signal generated with PRBS lengths of 2^7-1 and $2^{15}-1$, for the top (PRBS-7) and bottom (PRBS-15) eyes respectively.

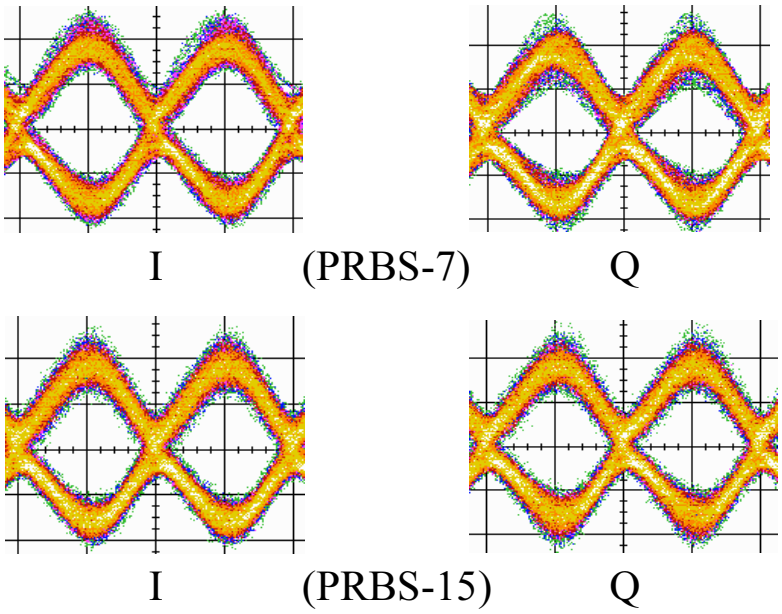

Figure 3.11: Eye diagrams of a demodulated data signal I and Q extracted from a 2×10 Gbit/s RZ-DQPSK signal generated using a Photline DQPSK modulator with PRBS lengths of 2^7-1 (PRBS-7) (top) and $2^{15}-1$ (PRBS-15) bottom

The measured BER curves versus the received optical power measured at the input of the optical preamplifier for both the received patterns I and Q are plotted in figure 3.12 for a 2×10 Gbit/s RZ-DQPSK signal generated with PRBS lengths of 2^7-1 (PRBS 7) and $2^{15}-1$ (PRBS 15). Figure 3.13 shows the average BER of the received 2×10 Gbit/s RZ-DQPSK data streams I and Q versus the received optical power for both PRBS 7 and PRBS 15. From the curve in figure 3.13 the measured receiver sensitivity for the 20 (2×10) Gbit/s RZ-DQPSK signal at a BER of 10^{-9} was ~-38.3 dBm and ~-37.3 dBm for both PRBS 7 and PRBS 15, respectively. In [14] the receiver sensitivity for 2×10 Gbit/s RZ-DQPSK signal with PRBS length of 2^9-1 was measured ~-34.3 dBm.

From our measurements RZ-DQPSK had an improved receiver sensitivity over NRZ-DQPSK by about (1-1.5) dB. It has been reported that the receiver sensitivity would be improved by 2-3 dB depending on the exact implementation, but for theoretically optimal DQPSK signals the OSNR sensitivity difference between RZ and NRZ pulse shaping is limited to about 1dB [95].

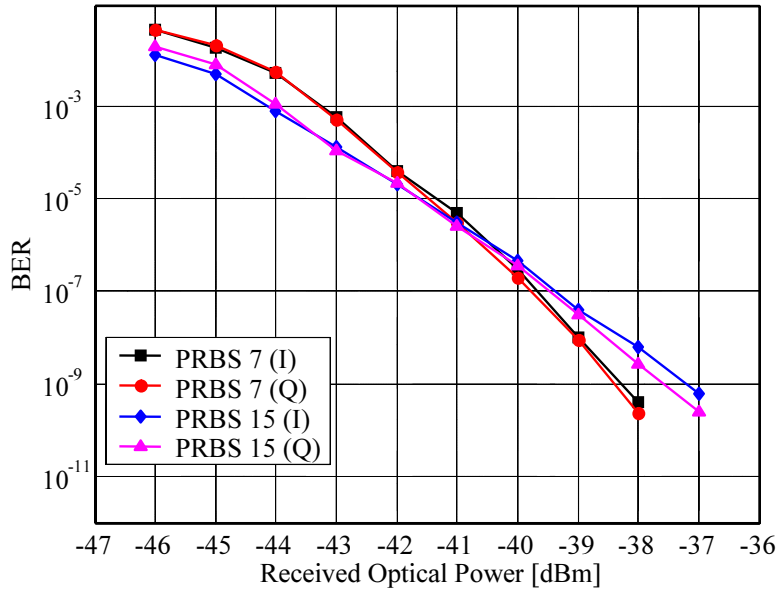

Figure 3.12: BER curves for the I and Q received data streams versus received optical power for a 2×10 Gbit/s RZ-DQPSK signal using a Photline oDQPSK Modulator with PRBS lengths of $2^7 - 1$ (PRBS 7) and $2^{15} - 1$ (PRBS 15)

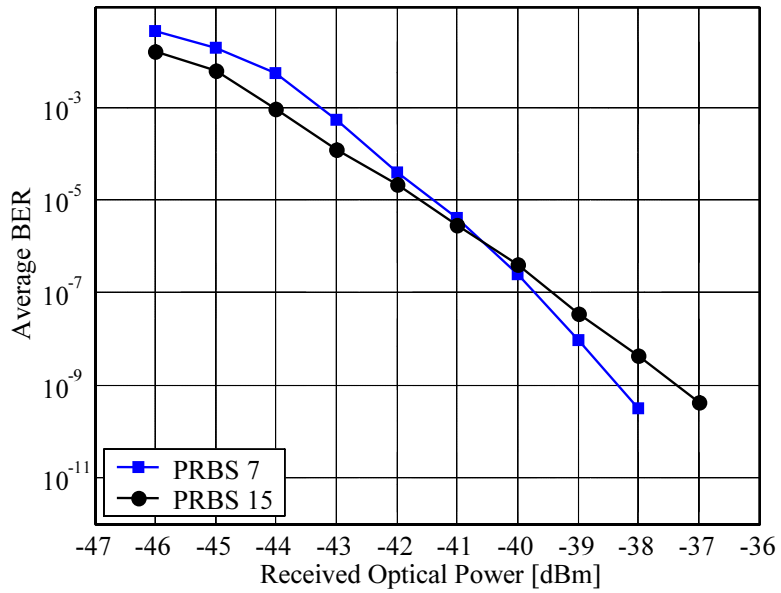

Figure 3.13: Average BER versus received optical power for a 20 Gbit/s RZ-DQPSK signal using a Photline oDQPSK Modulator with PRBS lengths of $2^7 - 1$ (PRBS 7) and $2^{15} - 1$ (PRBS 15)

Figure 3.14 is the chromatic dispersion (CD) tolerance curve showing the required optical signal-to-noise ratio (OSNR) for a BER of 10^{-9} versus the residual chromatic dispersion. A fiber-pigtailed Bookham $GaAs/AlGaAs$ oDQPSK modulator was used to generate the DQPSK signals in the RZ-DQPSK setup shown in figure 3.7. The measured CD tolerance for the 20 Gbit/s RZ-DQPSK signal corresponding to a 1-dB OSNR penalty at a BER of 10^{-9} was measured to be ~360 ps/nm.

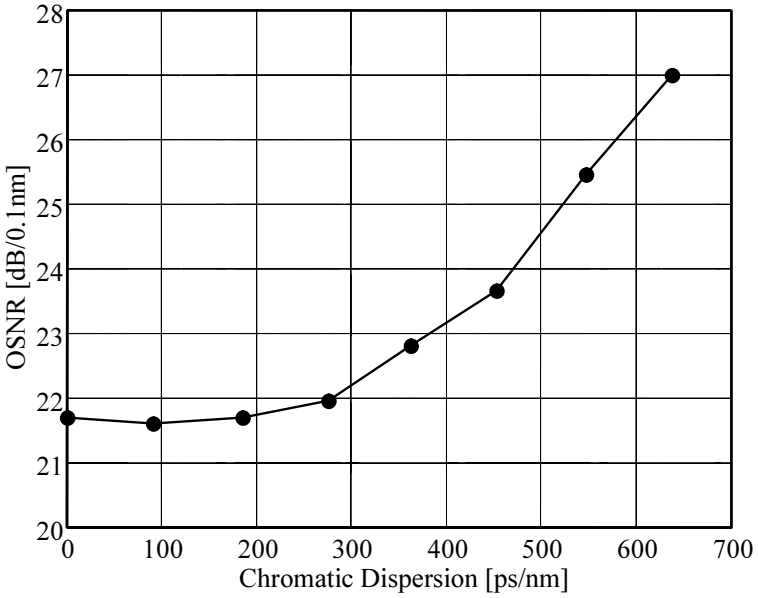

Figure 3.14: OSNR needed for a BER of 10^{-9} versus CD for a 20 Gbit/s RZ-DQPSK signal

Figure 3.15 shows the intensity measurements versus time for a 2×10 Gbit/s RZ-DQPSK signal measured before the MZDI Demodulator of figure 3.7 after different lengths of standard single mode fiber, corresponding to different values of chromatic dispersion.

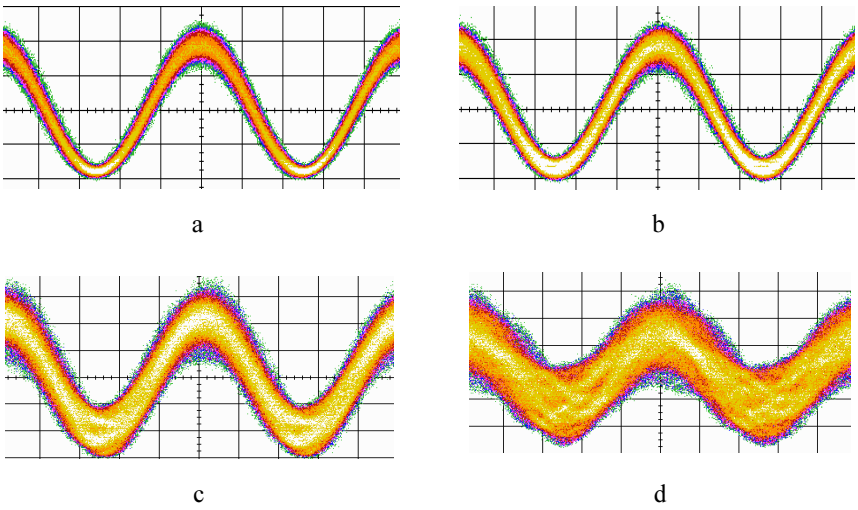

Figure 3.15: 20 Gbit/s RZ-DQPSK signal intensity measurements after transmission over different lengths of SSMF corresponding to different values of CD, (a) Back-to-Back (0 ps/nm), (b) 21.3 km (~362 ps/nm), (c) 32.2 km (~547 ps/nm), and (d) 41.5 km (~706 ps/nm)

3.4 DQPSK PolDM Transmission System at $2\times2\times10$ Gbits/s

Combining DQPSK modulation and Polarization division multiplex (PolDM) results in a doubled transmission rate, improved spectral efficiency and chromatic dispersion tolerance [89, 96, 44, 97, 98, 99, 100, 87]. Figure 3.16 shows an RZ-DQPSK PolDM setup operating at $2\times2\times10$ Gbit/s. At the transmitter a MZM biased at the quadrature point and driven with a 10 GHz clock signal was used to generate 50% RZ pulses. The optical signal is then split into two polarizations (X and Y) through the polarization beam splitter (PBS), and each signal is then modulated by a Photline DQPSK modulator driven by two 10 Gbit/s PRBS data streams with 31 bit mutual delay resulting in the generation of an optical DQPSK signal similar to that generated in section 3.3.2. The two resultant DQPSK signals having a mutual delay of 22 bit are then combined in orthogonal polarizations in a polarization beam combiner (PBC). The resultant signal is a $2\times2\times10$ Gbit/s RZ-DQPSK PolDM signal. If the RZ modulator is removed or switched off, NRZ-DQPSK PolDM signal will be generated. Figure 3.17 shows the intensity eye diagrams measured at the output of the DQPSK PolDM setup for $2\times2\times10$ Gbit/s NRZ-DQPSK PolDM signals (left), and RZ-DQPSK PolDM signals (right).

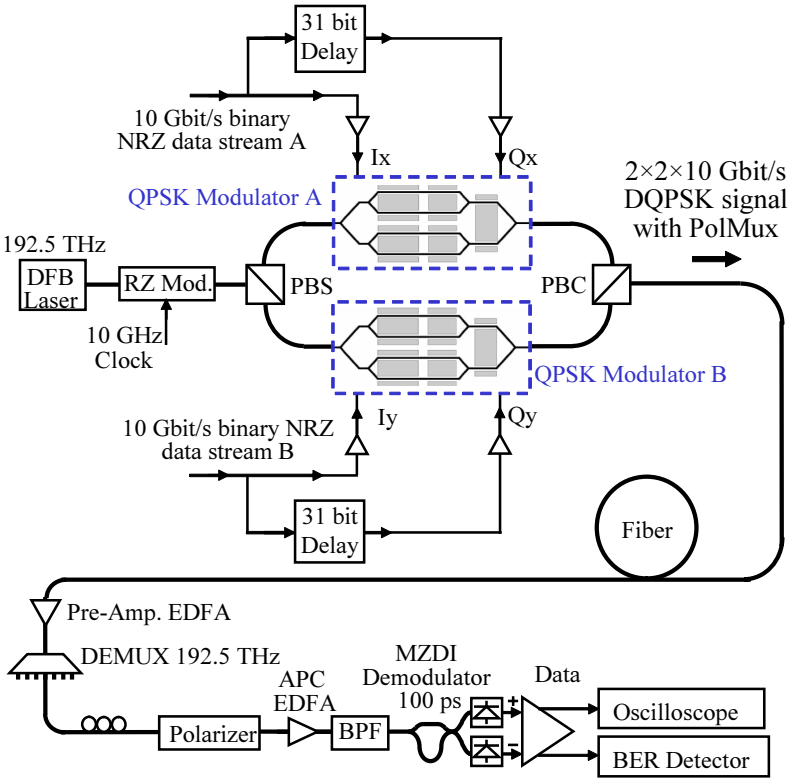

Figure 3.16: 2×2×10 Gbit/s RZ-DQPSK PolDM transmission setup

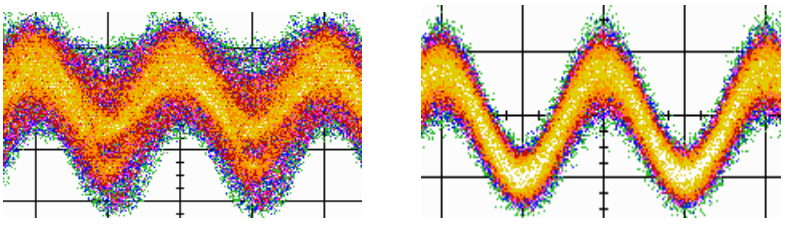

Figure 3.17: Eye diagrams of 2×2×10 Gbit/s NRZ-DQPSK PolDM signal (left), and RZ-DQPSK PolDM signal (right)

To extract the information from the received DQPSK PolDM signals a DQPSK receiver similar to that in section 3.3 was used with a polarization controller and polarizer placed before the last APC EDFA in order to select the received polarization as shown in figure 3.16. In a practical implementation, a PBS would be used instead of the Polarizer in order to receive the signals in both polarizations simultaneously where each signal will be then connected to a separate DQPSK receiver to extract the transmitted information. The measured BER curves versus the received optical power measured at the input of the optical preamplifier for the received patterns I and Q in both polarizations X and Y for 2×2×10 Gbit/s NRZ-DQPSK PolDM signal with PRBS 7 are plotted in figure 3.18. Figure 3.19 shows the demodulated eye diagrams measured at the sensitivity limit for the I and Q channels in both polarizations X and Y extracted from the 2×2×10 Gbit/s NRZ-DQPSK PolDM signal with PRBS 7.

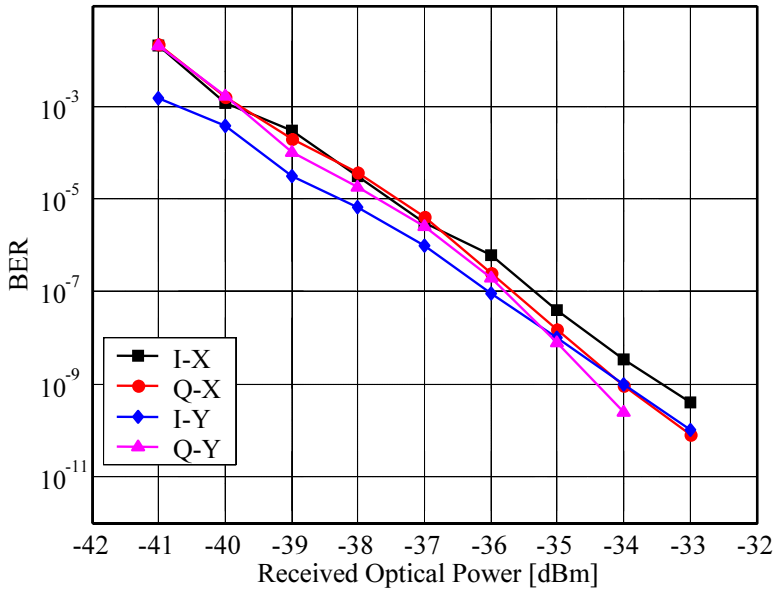

Figure 3.18: BER curves for the I and Q received data streams in both polarizations X and Y versus the received optical power for 2×2×10 Gbit/s NRZ-DQPSK PolDM signal with PRBS 7

The measured BER curves versus the received optical power measured at the input of the optical preamplifier for the received patterns I and Q in both polarizations X and Y for 2×2×10 Gbit/s NRZ-DQPSK PolDM signal with PRBS 15 are plotted in figure 3.20. Figure 3.21 shows the average BER of the received data streams I and Q in both polarizations versus the received optical power for 2×2×10 Gbit/s NRZ-DQPSK PolDM signal with PRBS 7 and PRBS 15. From the curve in figure 3.21 the measured receiver sensitivity for the 2×2×10 Gbit/s NRZ-DQPSK PolDM signal at a BER of 10^{-9} for PRBS 7 and PRBS 15, was ~-33.8 dBm and ~-32.4 dBm, respectively.

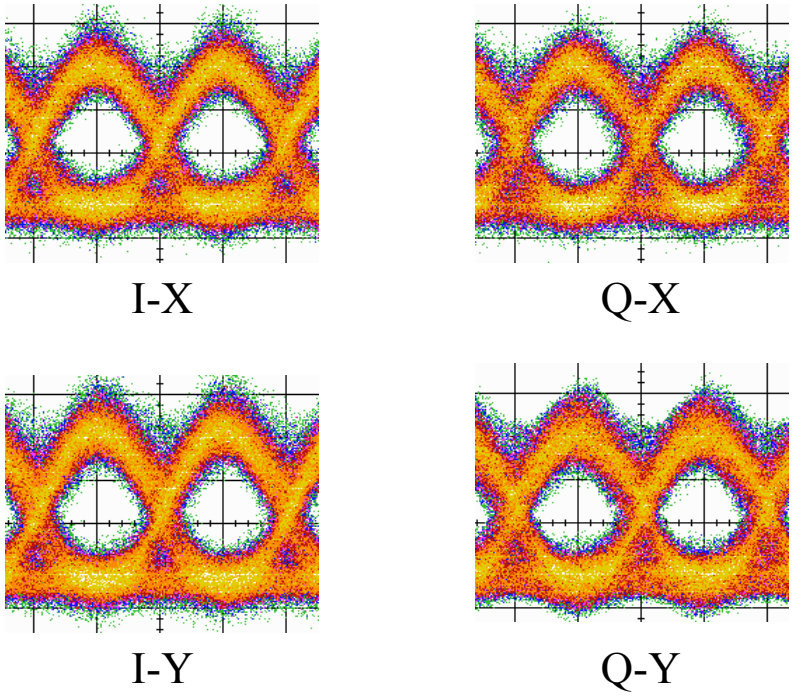

Figure 3.19: Eye diagram of the demodulated data signals I and Q for both polarizations X and Y extracted from a 2×2×10 Gbit/s NRZ-DQPSK PolDM signal with PRBS 7

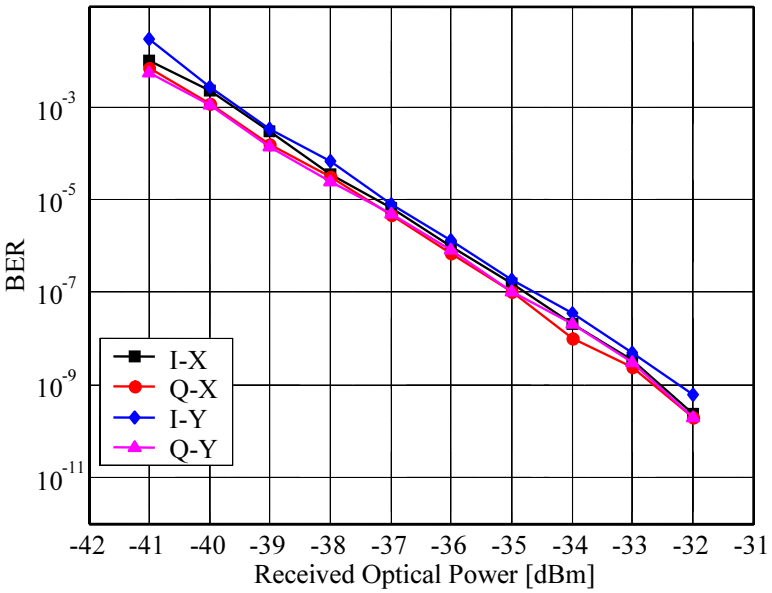

Figure 3.20: BER curves for the I and Q received data streams in both polarizations X and Y versus the received optical power for 2×2×10 Gbit/s NRZ-DQPSK PolDM signal with PRBS 15

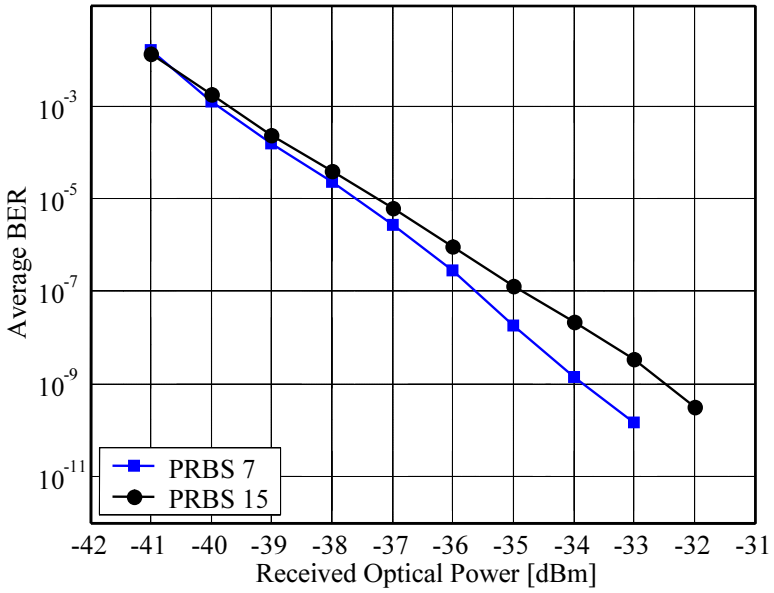

Figure 3.21: Average BER versus received optical power for 2×2×10 Gbit/s NRZ-DQPSK PolDM signal with PRBS 7 and PRBS 15

When the RZ modulator is used, the measured BER curves versus the received optical power measured at the input of the optical preamplifier for the received patterns I and Q in both polarizations X and Y for 2×2×10 Gbit/s RZ-DQPSK PolDM signal with PRBS 7 are plotted in figure 3.22. Figure 3.23 shows the demodulated eye diagrams measured at the sensitivity limit for the I and Q channels in both polarizations X and Y extracted from the 2×2×10 Gbit/s NRZ-DQPSK PolDM signal with PRBS 7.

Figure 3.24 shows the average BER of the received data streams I and Q in both polarizations versus the received optical power for 2×2×10 Gbit/s RZ-DQPSK PolDM signal. From the curve in figure 3.24 the measured receiver sensitivity for the 2×2×10 Gbit/s RZ-DQPSK PolDM signal at a BER of 10^{-9} with PRBS 7 and PRBS 15 was ~-34.7 dBm and ~-34.3 dBm, respectively. In [87] the receiver sensitivity for 2×2×10 Gbit/s RZ-DQPSK PolDM signal at a BER of 10^{-9} with PRBS 15 was measured ~-30.4 dBm.

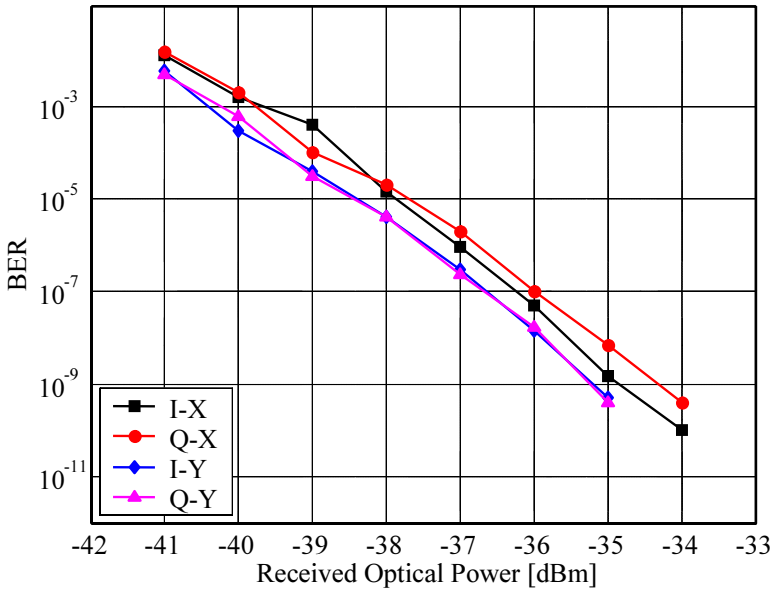

Figure 3.22: BER curves for the I and Q received data streams in both polarizations X and Y versus the received optical power for 2×2×10 Gbit/s RZ-DQPSK PolDM signal with PRBS 7

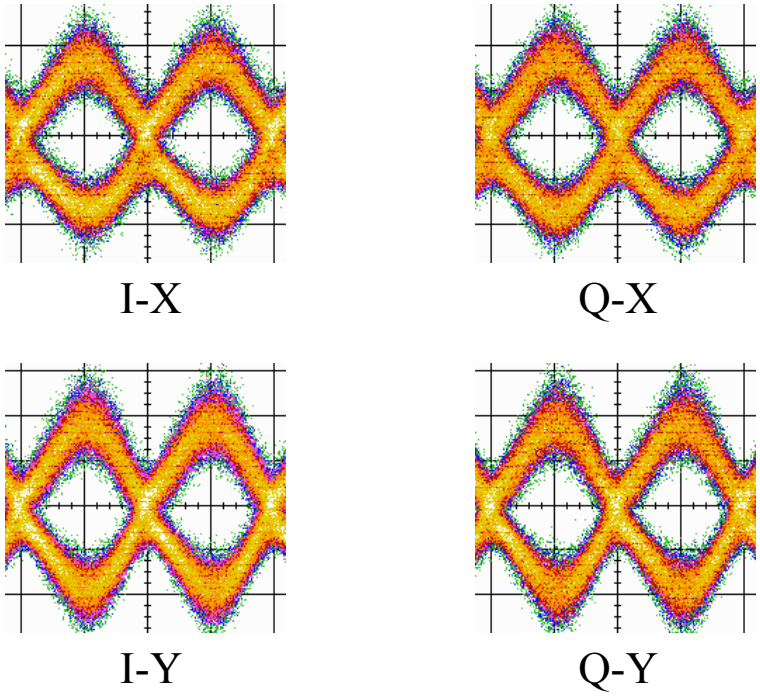

Figure 3.23: Eye diagram of the demodulated data signals I and Q for both polarizations X and Y extracted from a 2×2×10 Gbit/s RZ-DQPSK PolDM signal with PRBS 7

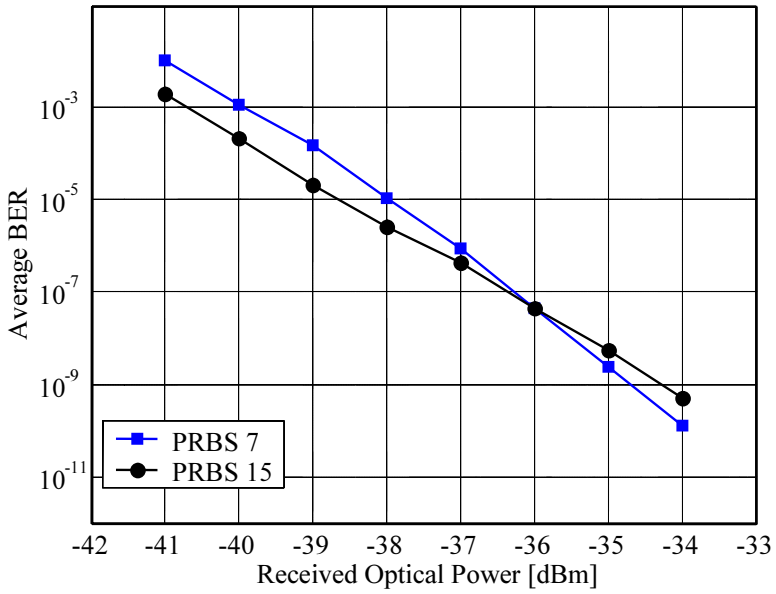

Figure 3.24: Average BER versus received optical power for 2×2×10 Gbit/s RZ-DQPSK PolDM signal with PRBS 7 and PRBS 15

Figure 3.25 shows a photo of the 2×2×10 Gbit/s DQPSK PolDM transmitter setup based on two Photline DQPSK modulators and two polarization beam splitters (PBS). Figures 3.26 show the main components used to construct the experimental 2×2×10 Gbit/s DQPSK PolDM receiver setup including the 2×10 Gbit/s DQPSK receiver. Figure 3.27 shows a photo of the full 2×2×10 Gbit/s RZ-DQPSK PolDM transmission setup that was used to perform the BER measurements.

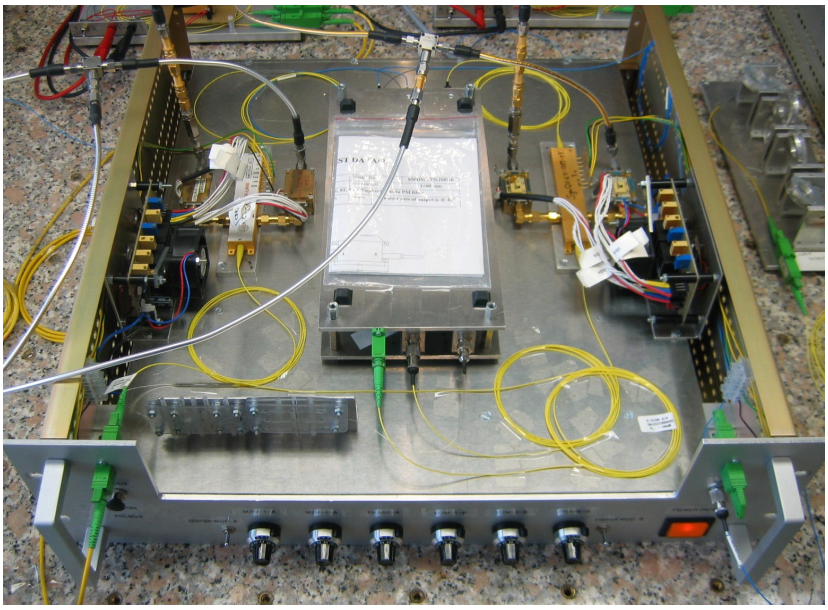

Figure 3.25: 2×2×10 Gbit/s DQPSK PolDM transmitter setup photo

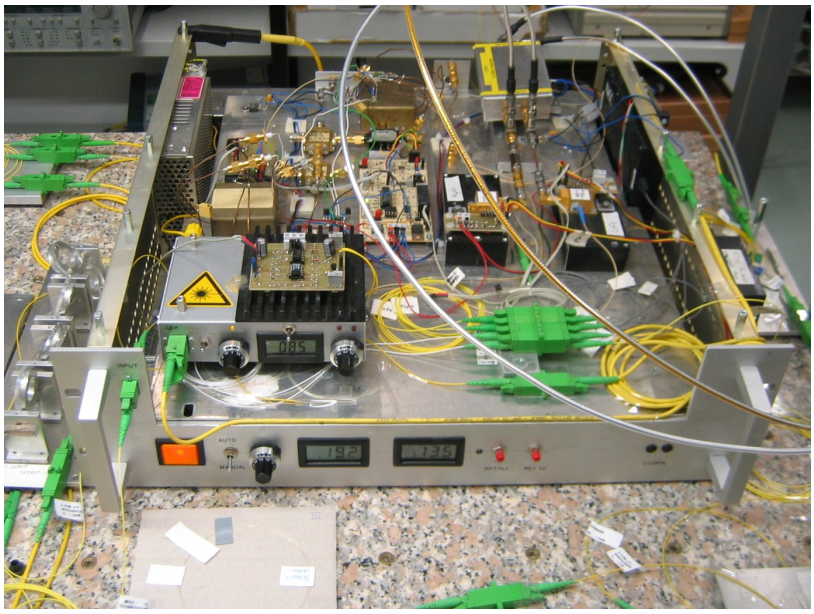

Figure 3.26: 2×2×10 Gbit/s RZ-DQPSK Receiver

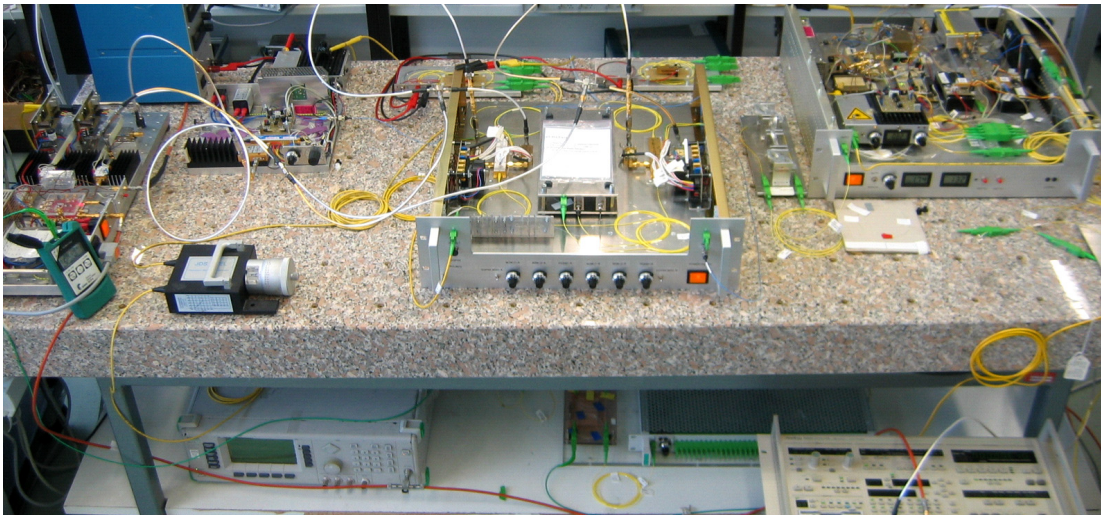

Figure 3.27: 2×2×10 Gbit/s RZ-DQPSK PolDM transmission setup photo

Chapter 4

Quaternary Intensity Modulation

4.1 Introduction

This chapter will introduce several types of multilevel quaternary modulation formats used for 2×10 (20 Gbit/s) optical communication systems. These multilevel modulation formats are Conventional Quaternary Intensity Modulation (4-IM), Quaternary intensity modulation based on combining two binary signals with unequal amplitudes in quadrature phases (QASK), Quaternary intensity modulation based on combining two Duobinary signals with unequal amplitudes in quadrature phases (QDB), and Quaternary intensity modulation based on combining two duobinary signals with unequal amplitudes in orthogonal polarizations (QPolDB). The generation and detection scheme for each modulation format will be explained in details with an evaluation of their performances based on experimental results obtained from their implementation in a practical 20 Gbit/s optical transmission system. The last section of this chapter will briefly cover other reported quaternary modulation formats Quaternary Polarization ASK (QPolASK) and Quaternary Differential-Phase ASK Modulation (DP-ASK).

4.2 Conventional Quaternary Intensity Modulation (4-IM)

An electrical binary ASK signal has an amplitude switching between two levels "0" and "1", while an electrical multilevel ASK signal (M-ary ASK) has an amplitude switching between different levels where each level can represent two or more bits of information [101]. The number of levels required for each transmitted symbol is $\mathrm{M} = 2^n$, where n is the number of bits transmitted for each symbol. If the number of bits transmitted for each symbol is two ($n = 2$), then an electrical 4-ary ASK signal (M=4) will result. This electrical 4-level ASK signal can be used to drive an optical intensity modulator resulting in the generation of an optical quaternary intensity modulation signal (4-IM) [10, 11, 8, 9, 12].

An advantage of using optical 4-IM signals is that it needs electrical and optical components operating at half the bit rate when compared to a binary signal operating at the same bit rate, which may reduce the cost of the required components of an optical transmission system. Also a 4-IM signal has a narrower spectrum width than a binary signal (reduced by a factor of 2), resulting in improved spectral efficiency which can be useful in a DWDM transmission system [20].

A disadvantage of using optical 4-IM signals is that it is has an eye closure penalty due to the more closely spaced levels than binary modulation. This makes it more sensitive to noise and distortion than a binary signal, therefore requiring larger optical power at the receiver side [101, 10].

A conventional quaternary 4-IM signal generation and detection scheme used for a digital optical communication system will be explained in the following subsections.

4.2.1 Generation of Conventional 2×10 Gbit/s Quaternary 4-IM Signals

A conventional quaternary 4-IM signal is generated by modulating a laser carrier signal with an electrical 4-level ASK signal (4-ASK) by directly modulating the laser current or using an external intensity modulator. The electrical 4-ASK signal can be obtained by adding two electrical binary signals with unequal amplitudes. In order to obtain an equally spaced electrical 4-ASK signal, the amplitude of one of the original electrical Binary NRZ signals (Data stream 1) is halved by using an electrical attenuator with 6 dB attenuation, then combined with the second electrical Binary NRZ signal (Data stream 2) in an electrical power combiner as shown in figure 4.1 (left). The eye diagrams shown in figure 4.1 are; Data stream 1 (top-left) which is a 10 Gbit/s electrical binary NRZ-ASK signal, Data stream 2 (bottom) which is also a 10 Gbit/s electrical binary NRZ-ASK but with half the amplitude of data stream 1, and finally the generated 10 Gbaud (2×10 Gbit/s) electrical 4-ary ASK signal (top-right).

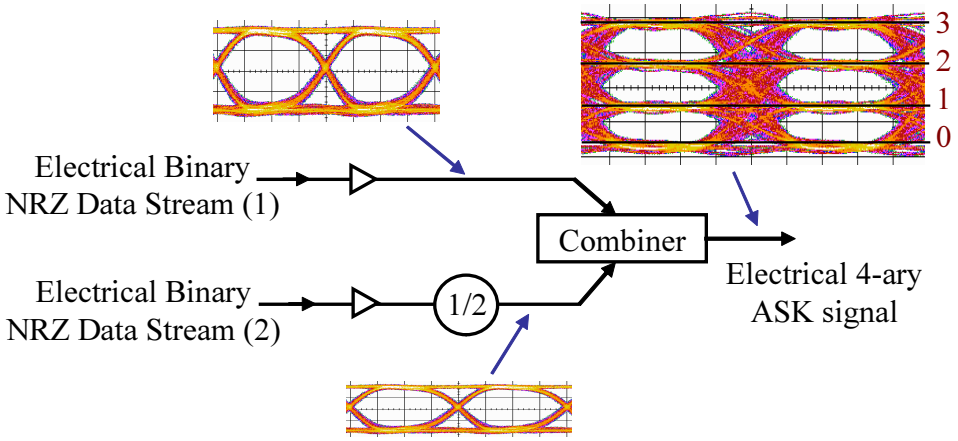

Figure 4.1: Electrical 4-ary ASK signal generation

The mapping between the input data and corresponding output levels for the 4-ary ASK signal generated in figure 4.1 is shown in table 4.1.

In practice the original binary data streams should be gray encoded before generating the quaternary signal. The gray encoder is useful because the most likely error to occur in the received quaternary signal is between the adjacent levels of the received signal which only differ by one binary digit, therefore the gray encoder would force only one bit error when decision errors are made between adjacent levels [101, 65, 64]. Figure 4.2 shows a common method to generate an optical quaternary intensity signal (4-IM) by driving an external intensity Mach-Zehnder modulator (MZM) biased at the quadrature point (half power

Table 4.1: Mapping of input binary data to output levels of a 4-ary ASK signal

Data Stream 1	Data Stream 1	Output Level
0	0	0
0	1	1
1	0	2
1	1	3

point) with an electrical 4-ary signal having a V_π peak-to-peak voltage amplitude [10, 20]. Since the intensity transfer function of a MZM modulator normally has a $\cos^2(x)$ transfer characteristics (See Appendix A), it is necessary to optimally adjust the amplitude ratio of the two transmitted electrical binary data streams to obtain an equally spaced 4-level optical quaternary intensity signal (4-IM) by adjusting the attenuator (b) shown in figure 4.2.

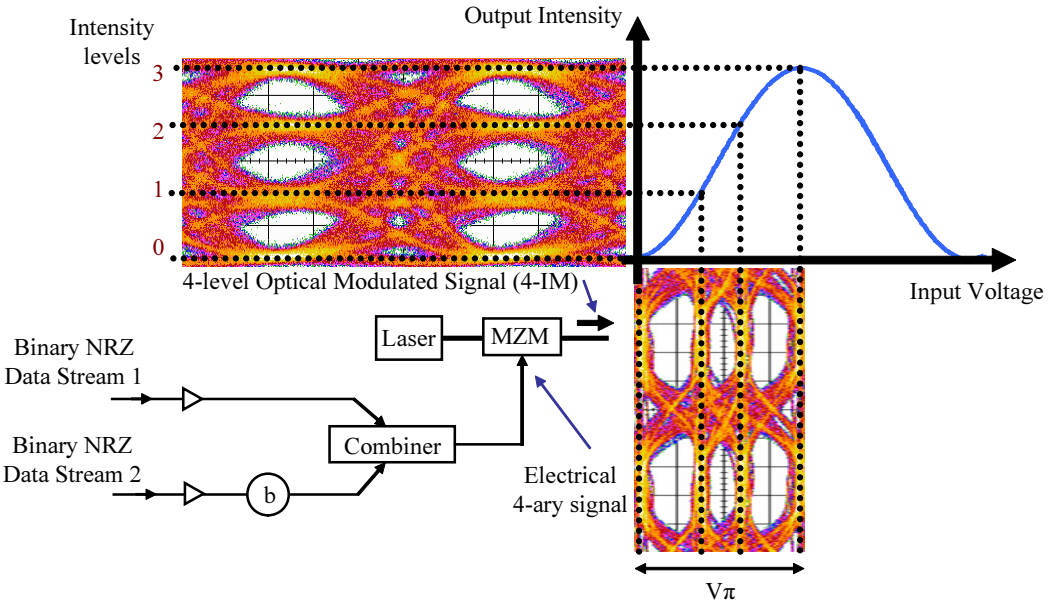

Figure 4.2: Principle of optical 4-IM generation using intensity MZM

The eye diagrams shown in figure 4.2 are for a 2×10 Gbit/s electrical 4-ary ASK signal (bottom-right) and the resulting optical 2×10 Gbit/s quaternary intensity modulation signal (4-IM) (top-left). The 4-IM signal constellation diagram is shown in figure 4.3. The optical field E has four different constellation points with normalized field amplitudes {0, 1, $\sqrt{2}$, $\sqrt{3}$}, which results into four different intensity levels {"0", "1", "2", "3"}.

4.2.2 Quaternary 4-IM Signal Detection

Figure 4.4 shows a schematic of a four level 4-IM receiver [10]. A single photodiode (direct detection) is used at the receiver to convert the optical quaternary intensity modulated signal (4-IM) to a 4-ary electrical signal. The received quaternary signal contains three eye

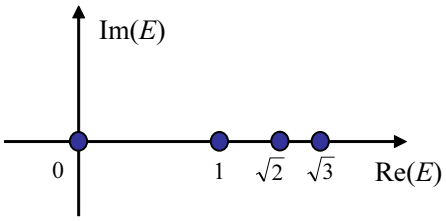

Figure 4.3: Optical 4-IM signal constellation diagram

openings corresponding to three different patterns $\{Q_1, Q_2, Q_3\}$ representing the bottom, middle, and top eyes respectively. These three patterns are separated at the receiver by three decision circuits (D flip-flops). Suitable decoding is then needed to recover the two original transmitted data streams from the three detected patterns [101, 10, 6]. The decoding logic functions used to extract Data stream 1 and Data stream 2 are:

$$Data\,Stream\,1 = Q_2 \tag{4.1}$$

$$Data\,Stream\,2 = Q_3 + Q_1\overline{Q}_2. \tag{4.2}$$

The schematic of the decoding logic circuit is also shown in the figure 4.4. A more detailed explanation showing how to derive the receiver logic equations and decoder circuit is given in appendix B.

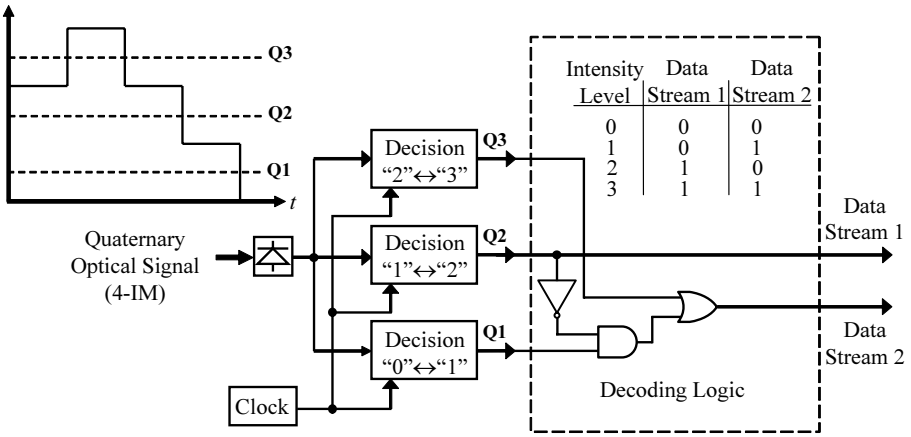

Figure 4.4: Schematic of a 4-IM receiver with decoding logic diagram

4.2.3 Experimental Transmission System for 2×10 Gbit/s Quaternary Modulation

Figure 4.5 shows the details of an experimental transmission setup used to generate and detect a 2×10 Gbit/s quaternary 4-IM signal. The transmitter (Tx) used in the figure is based on the conventional 4-IM generation scheme shown in figure 4.2. A 193.5 THz DFB laser was used. A pattern generator was used to generate a 10 Gbit/s pseudo random bit sequence (PRBS) binary NRZ data stream with a PRBS data length of $2^7 - 1$. The 10

Gbit/s binary NRZ data stream was split and delayed by 31 bit durations to emulate two decorrelated patterns (Data stream 1 and Data stream 2). Both data streams were amplified using 10 GHz optical modulator drivers from JDS-UNIPHASE. The amplitude of one of the electrical binary NRZ signals (Data stream 1) was attenuated and then combined with the second electrical binary NRZ signal (Data stream 2) in an electrical power combiner, therefore generating a 4-ary electrical signal with a peak-to-peak voltage amplitude of V_π. No Gray encoding was implemented. The electrical 4-ary signal was used to drive a fiber-pigtailed $LiNbO_3$ Mach-Zehnder intensity modulator (MZM) biased at the quadrature point (half power point) to generate an optical quaternary intensity signal. Figure 4.2 (top-left) shows the 4-level eye diagram of the generated optical quaternary intensity modulated signal, detected at the modulator output at 10 Gbaud (20 Gbit/s). The generated 2×10 Gbit/s 4-IM signal spectrum contains a carrier and is just as broad as for a single binary 10 Gbit/s NRZ-ASK modulation signal although the capacity is doubled.

The receiver employed in figure 4.5 is similar to that for receiving DQPSK signals in figure 3.7, but without the MZDI and balanced receiver. Also the error detector was programmed, using different thresholds, to receive all the three patterns, corresponding to the top, middle, and bottom eye diagram. Proper BER averaging is performed to represent the mean BER of the received patterns.

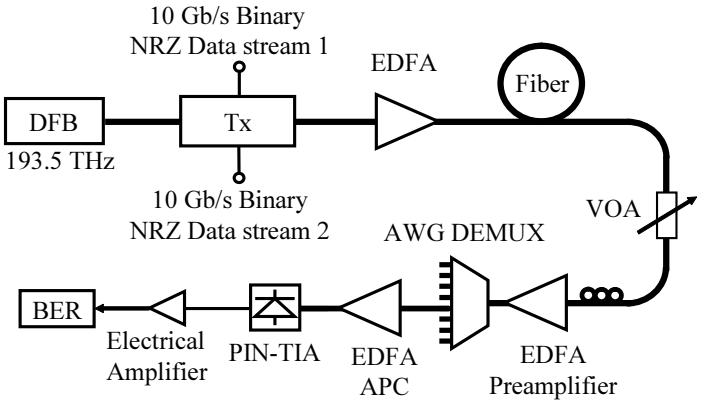

Figure 4.5: 20 Gbit/s Quaternary intensity modulation transmission setup

The BER of the three received eye patterns (top, middle, and bottom) versus the received power measured at the optical preamplifier input is shown in figure 4.6.

The average BER versus the received power measured at the optical preamplifier input is shown in figure 4.7. The measured receiver sensitivity for the 2×10 Gbit/s 4-IM signal with a PRBS length of 2^7-1 at a BER of 10^{-9} is ~-13 dBm.

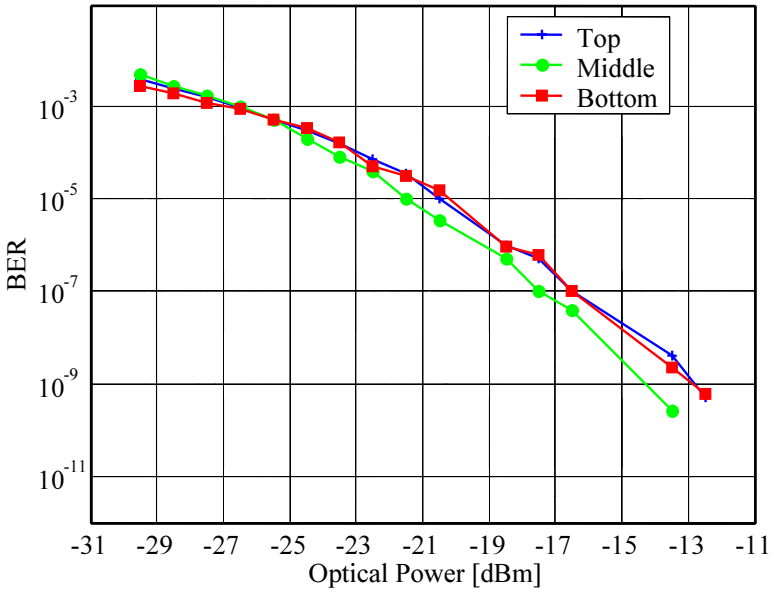

Figure 4.6: BER curves versus received optical power for the three received eyes (top, middle, and bottom) for a 20 Gbit/s (4-IM) signal

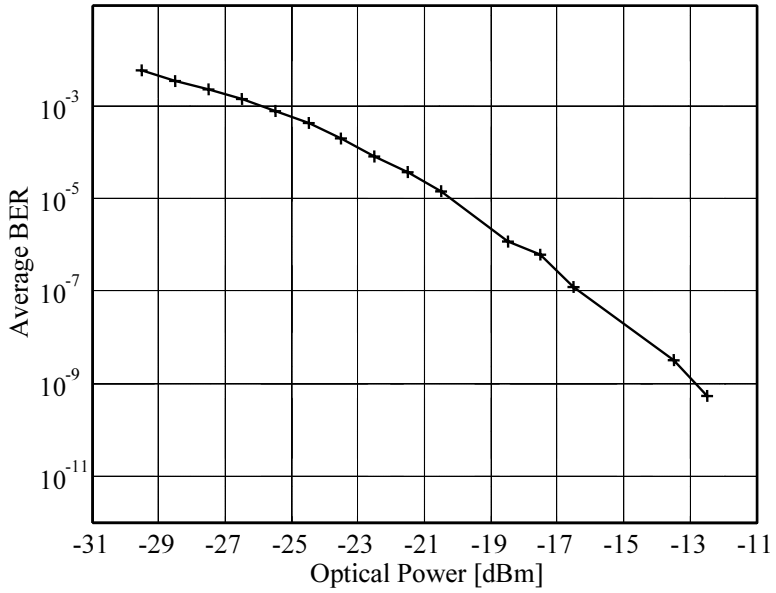

Figure 4.7: Average BER versus received optical power for a 20 Gbit/s (4-IM) signal

4.3 Quaternary Amplitude Shift Keying (QASK)

In the conventional quaternary intensity modulation (4-IM) generation scheme explained in the previous section, an optical 4-IM signal was generated by modulating a continuous lightwave carrier signal with an electrical 4-ary ASK signal that was obtained by combining an electrical binary signal with another one with reduced amplitude in an electrical RF power combiner. Such configuration results into transforming any amplitude distortion in the original electrical binary signals into significant distortion in the optical 4-IM signal [20]. This amplitude distortion can result in receiver sensitivity degradation. It is possible to suppress the amplitude distortion by using a different generation scheme by optically combining one binary signal and another intensity-halved binary signal in two quadrature phases generating an optical quaternary ASK signal (QASK) [20, 28, 6, 21]. This generation scheme has been proposed in [20] to generate a 2×5 Gbit/s QASK signal by using two parallel MZM modulators, an optical phase control section, and an optical intensity control section all integrated on lithium niobate ($LiNbO_3$) substrate. In the following subsections a 2×10 Gbit/s QASK signal has been generated with a similar method, but by using an integrated $GaAs/AlGaAs$ Optical QPSK modulator based on two parallel MZM modulators, and an optical phase control section, without using any optical intensity control section. The optical QPSK modulator was driven by two 10 Gbit/s binary NRZ data streams with unequal amplitudes, to generate an optical 4-constellation-point 20 Gbit/s quaternary intensity signal (QASK). The receiver sensitivity for the proposed QASK signal generated at 2×5 Gbit/s [20] and 2×10 Gbit/s [6, 21] was found to be improved when compared to a the conventional 4-IM signal at the same bit rate. The generation scheme, receiver sensitivity and CD tolerance of a 20 Gbit/s QASK modulation format will be discussed in the following subsections.

4.3.1 Generation and Detection of 2×10 Gbit/s QASK Signals

The optical QPSK modulator shown in figure 4.8 contains two Mach-Zehnder modulators (MZMs), placed in the two arms of another interferometer that forms a Mach-Zehnder superstructure. The superstructure has quadrature control electrodes in both arms for phase trimming. Throughout the experiments in this section and in the next section, a fiber-pigtailed Bookham $GaAs/AlGaAs$ o(D)QPSK modulator [92, 13] was used.

The two MZMs are driven by two electrical 10 Gbit/s binary NRZ-ASK signals. The drive amplitude of the NRZ-ASK signal in one of the MZMs equals V_π. This generates an in-phase optical field $Re(E)$ with normalized field amplitudes {0, +1}. The other MZM is driven by another binary NRZ-ASK signal with voltage amplitude of $V_\pi/2$. This results into the generation of a quadrature optical field $Im(E)$ with normalized field amplitudes {0, $+a$}. The total output electric field is $E_o = Re(E) + jIm(E)$ with the generated fields are {0, $+ja$, +1, and $+1 + ja$} corresponding to four different constellation points as shown in figure 4.9. The four constellation points results into four different intensities {0, a^2, 1, 1+a^2}. For $a = 1/\sqrt{2}$, corresponding to 6 dB of electrical attenuation (b = 1/2), the intensities are equidistant and are now labeled as "0", "1", "2", "3" as shown in figure 4.9 (bottom-right). To receive the original transmitted patterns from the QASK signal, decoding is needed identical to that of the 4-IM decoder shown in figure 4.4.

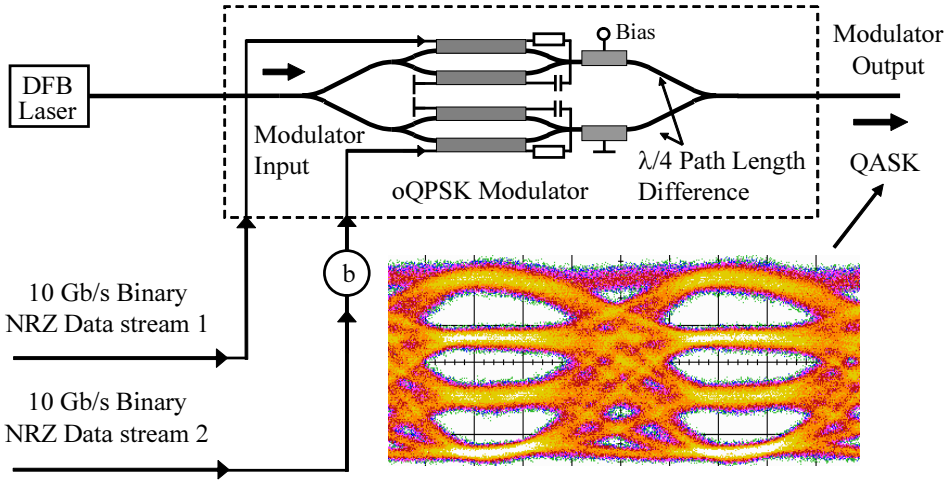

Figure 4.8: Optical QASK (2×10 Gbit/s) generation in an optical QPSK modulator, and resulting quaternary intensity eye diagram (bottom) with electrical attenuator setting (b = 1/2)

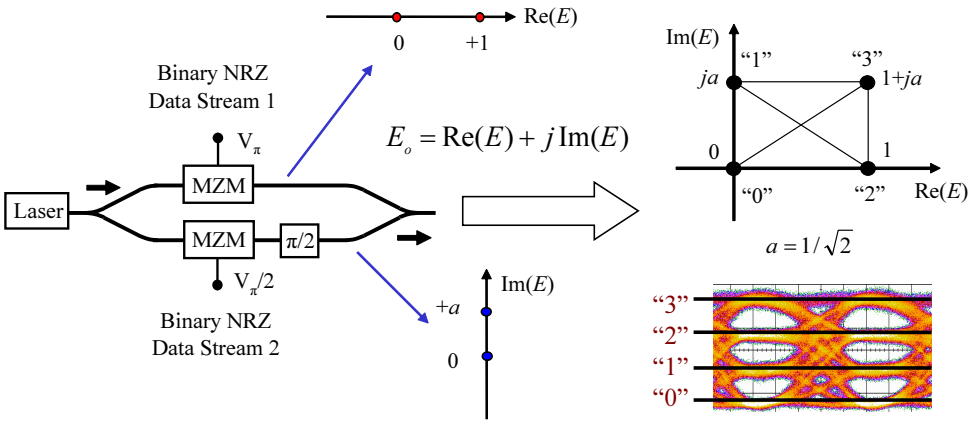

Figure 4.9: QASK electrical field signal constellation diagram (top-right) generated using a QPSK modulator driven by binary signals with unequal amplitudes. The resulting intensity eye diagram (bottom-right) shows the 4 intensity levels ($a = 1/\sqrt{2}$).

4.3.2 Experimental Results Measured for 2×10 Gbit/s QASK

The experimental transmission setup used to generate and detect a 2×10 Gbit/s quaternary QASK signal was similar to the setup used for generating and detecting the 4-IM signal shown in figure 4.5 in the previous section. The transmitter used in the setup is the same given in figure 4.8. The 10 Gbaud (2×10 Gbit/s) QASK signal represents a 4-IM and its spectrum is just as broad as for a single binary 10 Gbit/s NRZ-ASK modulation signal although the capacity is doubled. Figure 4.10 shows the heterodyned electrical spectrum of the 10 Gbaud optical QASK signal. There exists a carrier component in the spectrum which is identical to that of a 4-IM signal.

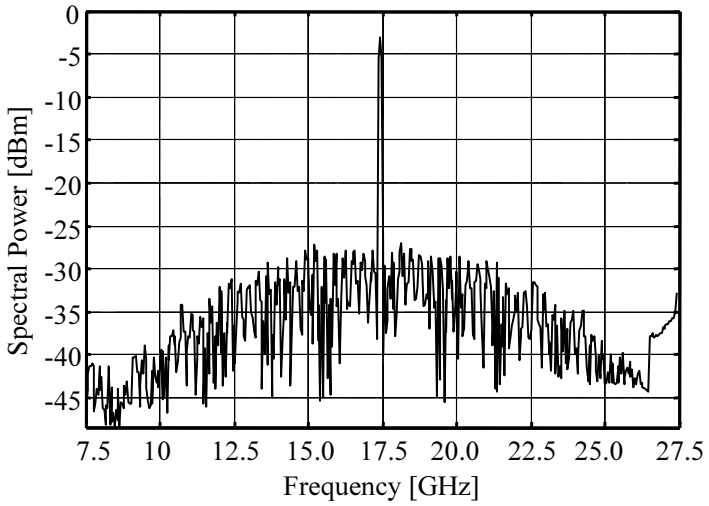

Figure 4.10: Heterodyned electrical spectrum for a 2×10 Gbit/s QASK signal

Figure 4.11, shows the BER curves for the three received eyes (top, middle, and bottom) of the 2×10 Gbit/s QASK signal.

The average BER versus the received optical power measured at the optical preamplifier input is shown in figure 4.12. The measured receiver sensitivity for the 2×10 Gbit/s QASK signal with a PRBS $2^7 - 1$ at a BER of 10^{-9} is ~-21.6 dBm.

The chromatic dispersion (CD) tolerance was measured for the generated 20 Gbit/s QASK signal. Figure 4.13 shows the OSNR after the optical preamplifier needed for a BER of 10^{-9} versus CD. An optical attenuator was used to vary the OSNR. The 1-dB tolerance at a BER of 10^{-9} was found to be ~130 ps/nm for 20 Gbit/s QASK.

Figure 4.14 shows the intensity eye diagrams of a 20 Gbit/s QASK signal at the sensitivity edge after transmission over 0, 5.34, 10.9, and 16.24 km of SSMF.

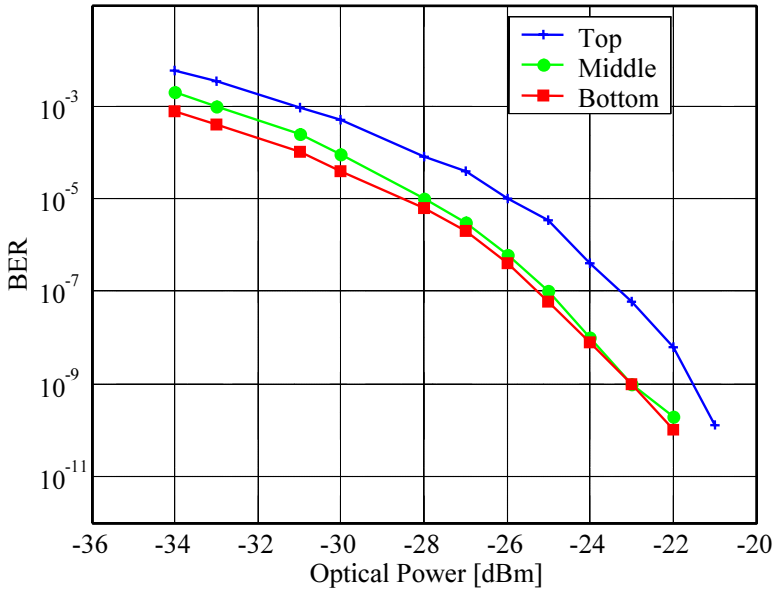

Figure 4.11: BER curves versus received optical power for the three received eyes (top, middle, and bottom) for a 20 Gbit/s QASK signal

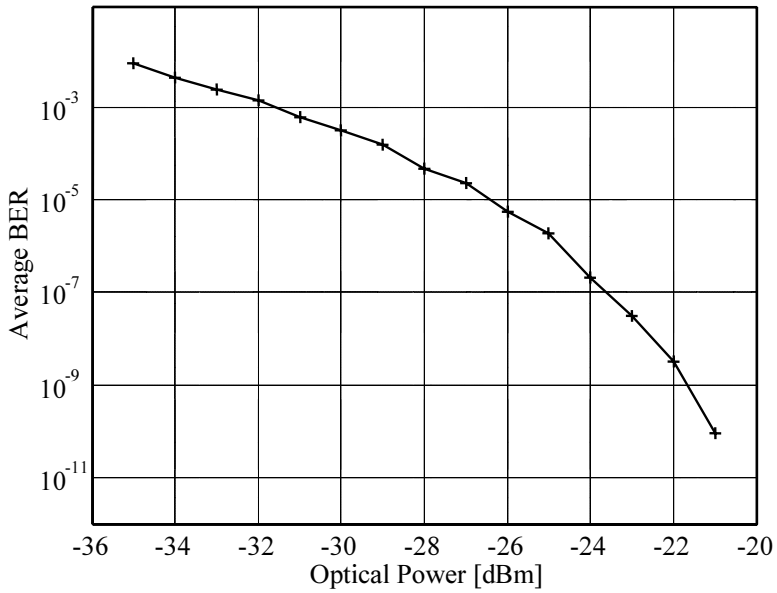

Figure 4.12: Average BER versus received optical power for a 20 Gbit/s QASK signal

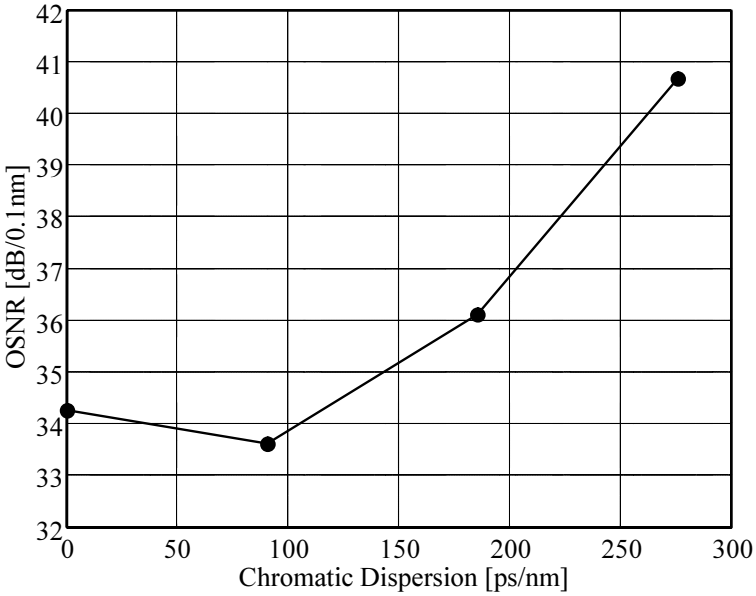

Figure 4.13: OSNR needed for a BER of 10^{-9} versus CD for a 20 Gbit/s QASK signal

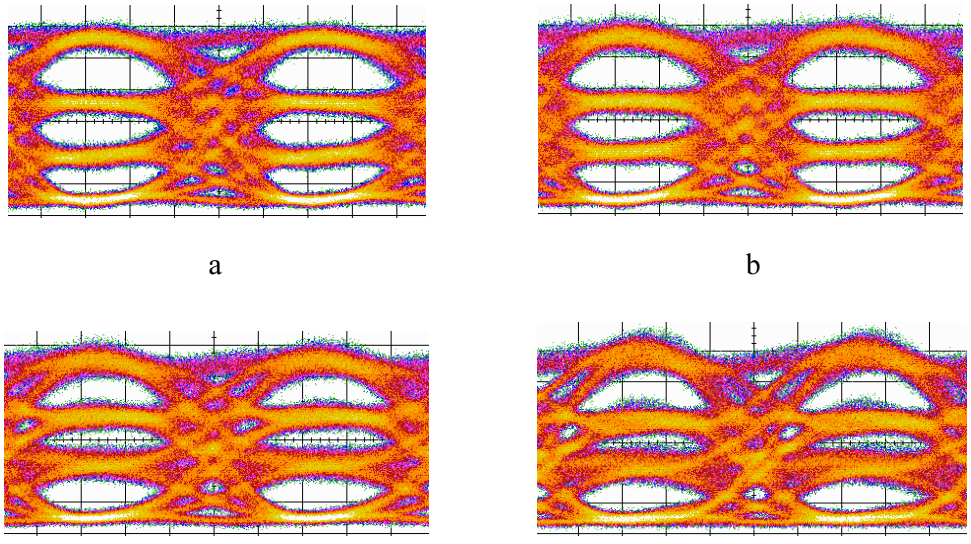

Figure 4.14: Intensity eye diagrams of a 20 Gbit/s QASK signal measured at the sensitivity edge after transmission over different length of SSMF, (a) (Back-to-Back) 0 km (0 ps/nm), (b) 5.34 km (~90.78 ps/nm), (c) 10.9 km (~185 ps/nm), (d) 16.24 km (~276 ps/nm)

4.4 Quaternary Duobinary Modulation (QDB)

In the previous section on QASK we used an optical QPSK modulator, driven by two binary 10 Gbit/s NRZ data streams with unequal amplitudes, to generate an optical 4-constellation-point 20 Gbit/s quaternary amplitude shift keying (QASK) signal, which has an identical spectral bandwidth of a 4-IM signal. It is possible to further increase the spectral efficiency by replacing the binary data streams by duobinary data streams in order to generate an optical 9-constellation-point 20 Gbit/s quaternary duobinary (QDB) signal [28, 27, 6, 21]. This QDB signal has a spectral bandwidth which is about half of that for 4-IM and QASK. The generation scheme, receiver sensitivity and CD tolerance of the proposed QDB modulation format at 20 Gbit/s will be discussed in the following subsections.

4.4.1 Generation and Detection of 2×10 Gbit/s QDB signals

The same QASK generation scheme shown in figure 4.8 was used after replacing the binary data streams with duobinary data streams as shown in figure 4.15. Both MZMs were biased at minimum transmission. Since differential encoding was not available, two mutually delayed PRBS 10 Gbit/s binary NRZ electrical signals were lowpass-filtered (LPF) to generate the duobinary signals. The lowpass filters were constructed using open stubs with single-path delays of 50 ps. Each stub filter (LPF) responds to an impulse by two impulses of equal height and 100 ps mutual delay, thereby forming an idealized duobinary one-bit-delay and add filter [25, 24]. The simulated frequency response of the LPF stub used in this experiment had a ~ 35dB dip at the frequency 5 GHz. The frequency response of this stub filter (stub-5) and a comparison with the frequency response of a duobinary Bessel LPF is given in appendix D.

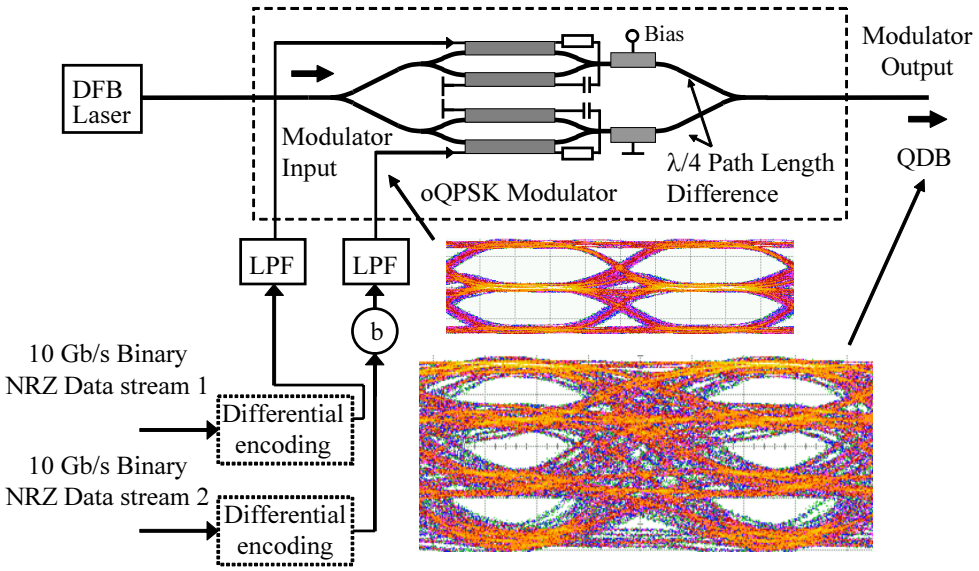

Figure 4.15: Principle of optical QDB modulation generation using duobinary low pass filtering (LPF) and a QPSK modulator (electrical attenuator setting b = 1/2). The resulting quaternary intensity eye diagram (bottom) and the electrical duobinary eye diagram (top) are also shown.

A duobinary signal with a full $2V_\pi$ voltage swing generates in one MZM the in-phase optical field $Re(E)$ with normalized field amplitudes {-1, 0, +1}. The other arm MZM is driven with a duobinary signal with a V_π voltage swing and generates the quadrature component $Im(E)$ with normalized field amplitudes $\{-a, 0, +a\}$. The total output field is $E_o = Re(E) + jIm(E)$. The generated QDB signal constellation diagram is shown in figure 4.16 (top-right). The generated fields are $\{0, \pm ja, \pm 1, \pm 1 \pm ja\}$, corresponding to 9-constellation points and are mapped into four different intensities $\{0, a^2, 1, 1 + a^2\}$. Illustrating the case $a = 1/\sqrt{2}$ (b = 1/2), the intensities are again labeled "0", "1", "2", "3" corresponding to the 4 levels of the generated 10 Gbaud (20 Gbit/s) QDB signal as shown in figure 4.16 (bottom-right). Not only differential encoding is needed at the transmitter side, but also 4-IM decoding at the receiver side.

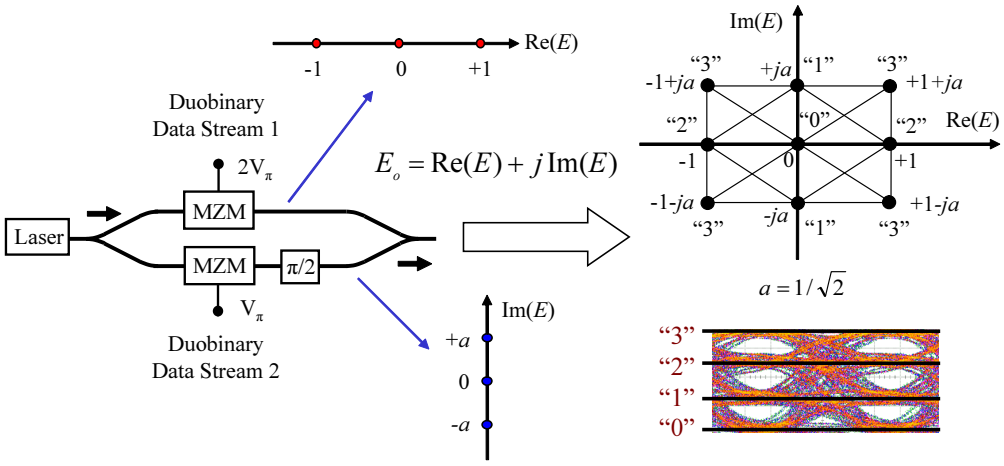

Figure 4.16: QDB electrical field signal constellation diagram (top-right) generated using a QPSK modulator driven by duobinary signals with unequal amplitudes. The resulting intensity eye diagram (bottom-right) shows the 4 intensity levels ($a = 1/\sqrt{2}$).

4.4.2 Experimental Results Measured for 2×10 Gbit/s QDB

The experimental transmission setup used to generate and detect the 2×10 Gbit/s quaternary QDB signal is similar to that used for 4-IM and QASK signals as shown in figure 4.5. The transmitter used in the setup is the QDB transmitter given in figure 4.15. The spectrum of the generated 10 Gbaud (2×10 Gbit/s) QDB signal is just as broad as a single 10 Gbit/s duobinary modulation signal although the capacity is doubled. Its spectral bandwidth is also equivalent to half of that for 2×10 Gbit/s 4-IM and QASK signals. Figure 4.17 shows the heterodyned electrical spectrum of the 10 Gbaud optical QDB signal. There exists no carrier in the spectrum which is the case for duobinary modulation.

Figure 4.18, shows the BER curves for the three received eyes (top, middle, and bottom) of the 2×10 Gbit/s QDB signal. The average BER curve versus the received optical power measured at the input of the receiver optical preamplifier is shown in figure 4.19. The measured receiver sensitivity for 20 Gbit/s QDB with a PRBS $2^7 - 1$ at a BER of 10^{-9} is ~-21.2 dBm.

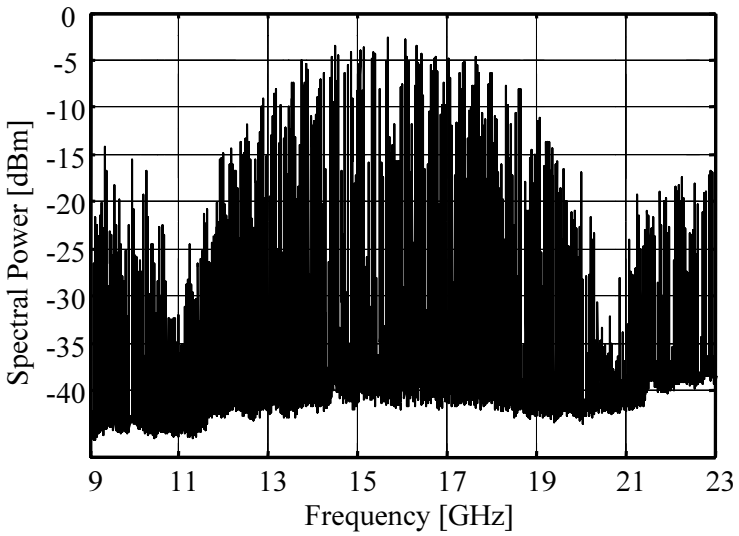

Figure 4.17: Heterodyned electrical spectrum of the 20 Gbit/s QDB signal

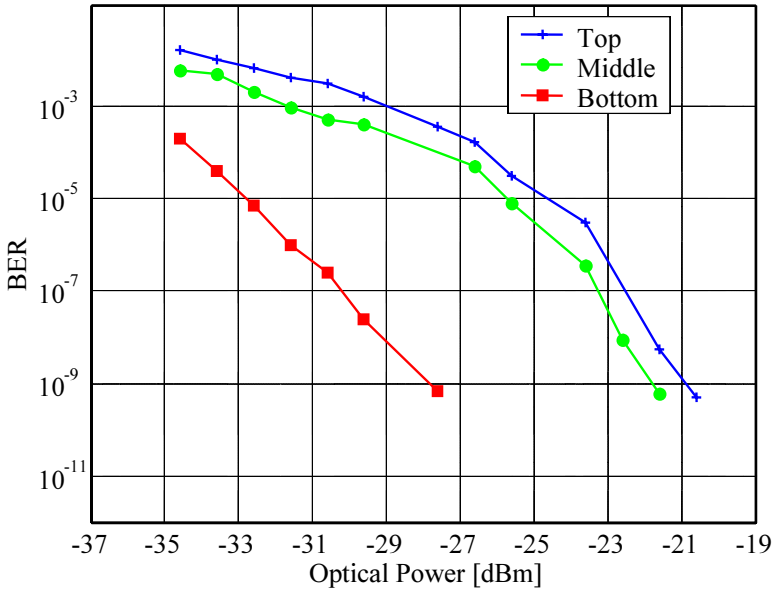

Figure 4.18: BER curves versus received optical power for the three received eyes (top, middle, and bottom) for a 20 Gbit/s QDB signal

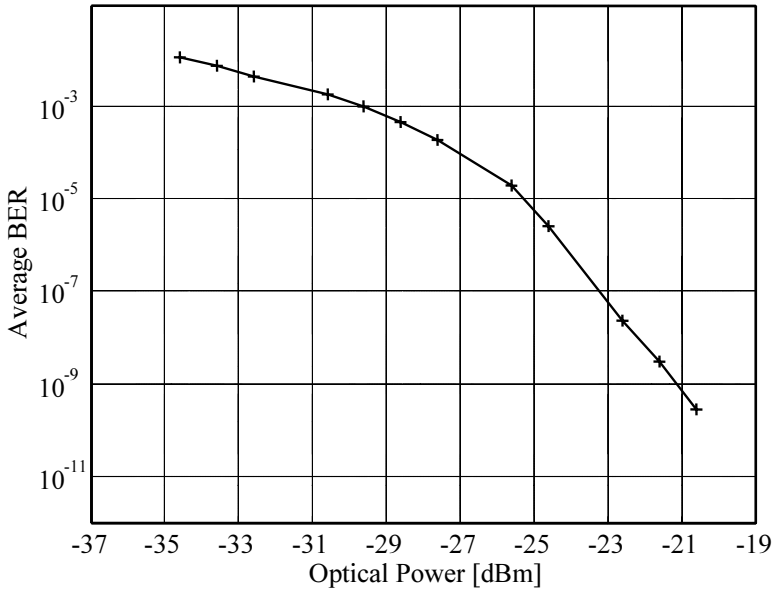

Figure 4.19: Average BER versus received optical power for a 20 Gbit/s QDB signal

The chromatic dispersion (CD) tolerance was measured for the generated 20 Gbit/s QDB signal. Figure 4.20 shows the OSNR after the optical preamplifier needed for a BER of 10^{-9} versus CD. An optical attenuator was used to vary the OSNR. The 1-dB tolerance at a BER of 10^{-9} was found to be ~140 ps/nm for 20 Gbit/s QDB. Although 20 Gbit/s QDB can tolerate CD up to ~140 ps/nm at the expense of an OSNR penalty of 1 dB, it can also tolerate up to ~250 ps/nm for an OSNR penalty of 1.8 dB, while 20 Gbit/s QASK can tolerate CD up to ~130 ps/nm at the expense of an OSNR penalty of 1 dB, it can only tolerate up to ~250 ps/nm at the expense of an OSNR penalty of 5.8 dB. Therefore QDB signals can tolerate more CD than QASK.

Figure 4.21 shows a photo of the 2×10 Gbit/s QDB transmitter setup using an optical QPSK modulator (Bookham), duobinary stub LPFs, and electrical modulator drivers (JDS Uniphase).

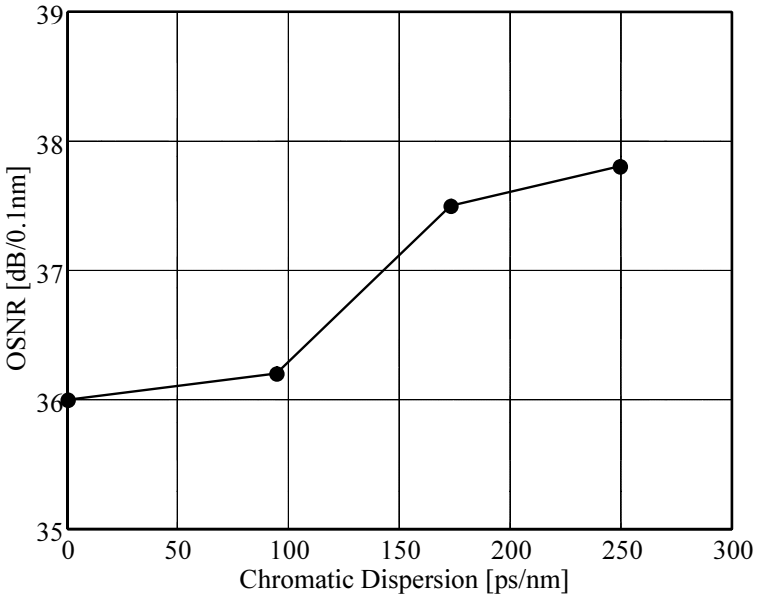

Figure 4.20: OSNR needed for a BER of 10^{-9} versus CD for a 20 Gbit/s QDB signal

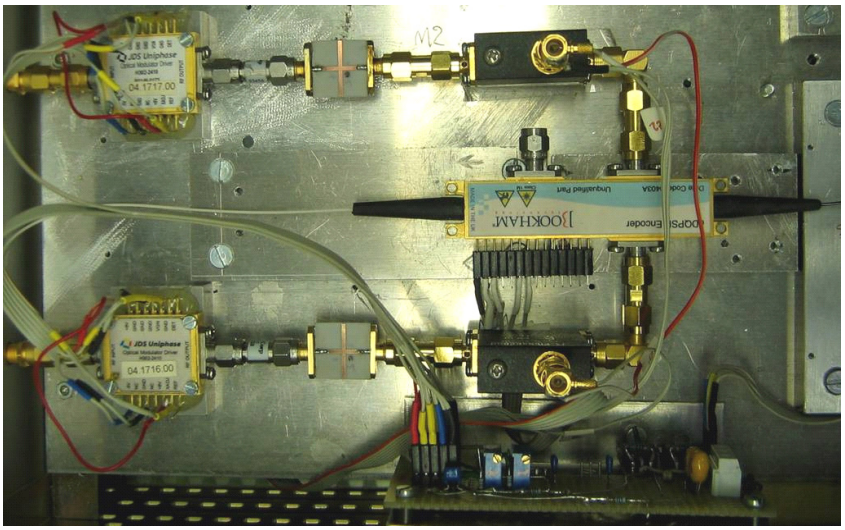

Figure 4.21: Photo of the 2×10 Gbit/s QDB transmitter based on the Bookham QPSK modulator

4.5 Quaternary Polarization Duobinary Modulation (QPolDB)

In the previous section the spectral efficiency for 20 Gbit/s quaternary intensity modulation was improved by generating a 9-constellation point quaternary duobinary signal (QDB) based on combining two 10 Gbit/s duobinary signals with unequal amplitudes in *quadrature phases* using a QPSK modulator [27, 6, 21]. It is possible to generate a similar 9-constellation point quaternary signal by combining two duobinary signals with unequal amplitudes in *orthogonal polarizations* instead of quadrature phases by using a polarization division multiplex setup (PolDM). This 9-constellation point quaternary polarization duobinary signal (QPolDB) [6, 29, 7] does not require that the two duobinary combined in orthogonal polarizations must have quadrature phases. A generated 20 Gbit/s QPolDB modulation signal has high spectral efficiency similar to QDB signals and has better CD tolerance compared to standard NRZ-ASK binary modulation, RZ-DQPSK, 4-IM, QASK, and QDB signals all operating at the same bit rate (20 Gbit/s). The generation scheme, receiver sensitivity and CD tolerance of the proposed QPolDB modulation format at 20 Gbit/s will be discussed in the following subsections.

4.5.1 Generation and Detection of 2×10 Gbit/s QPolDB Signals

The schematic of the transmitter used to generate QPolDB signals is shown in figure 4.22.

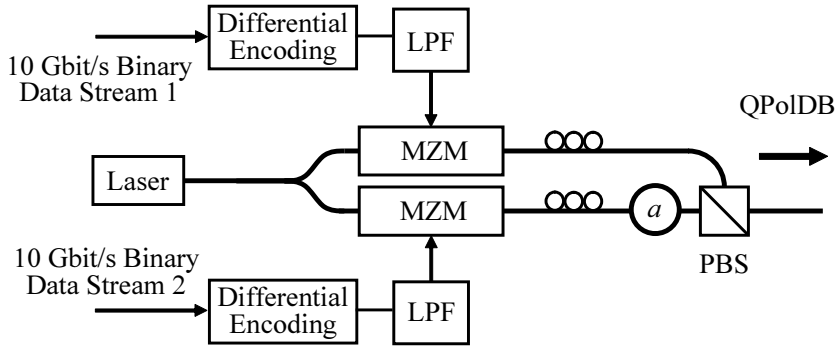

Figure 4.22: Schematic of the optical QPolDB signal generation scheme ($a = 1/\sqrt{2}$)

The laser signal is split into two branches where each branch consists of two Mach-Zehnder modulators biased at minimum transmission and driven by 10 Gbit/s electrical duobinary signals having peak-to-peak voltage amplitude of $2V_\pi$. In one of the branches the generated optical duobinary signal carries an electric field E_x with normalized amplitudes of {-1, 0, +1}. The optical duobinary signal in the other branch is optically attenuated by 3 dB ($a = 1/\sqrt{2}$) resulting in an electric field E_y with normalized electric field amplitudes of $\{-a, 0, +a\}$. The two resultant duobinary optical signals E_x and E_y carried in the two branches are then combined with orthogonal polarizations using a polarization beam splitter (PBS). Due to the uncertain phase relationship of the two polarizations, the Jones vector of this QPolDB signal is $E = \begin{bmatrix} E_x \\ e^{j\phi}E_y \end{bmatrix}$, where ϕ is the unknown and unimportant phase difference. The QPolDB 9-point signal constellation diagram is shown in figure 4.23. The resulting intensities are $\{0, a^2, 1, 1+a^2\}$ which corresponds to the symbols "0", "1", "2", "3"

respectively. To receive the transmitted data at the receiver, not only differential encoding is needed at the transmitter side, but also 4-IM decoding at the receiver side.

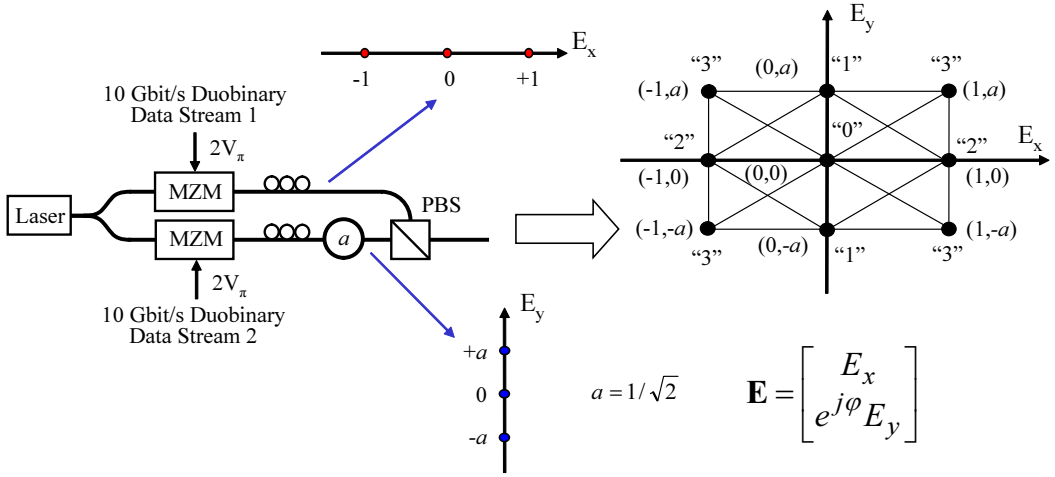

Figure 4.23: QPolDB electrical field signal constellation diagram (top-right) generated using a polarization division multiplex setup (left) with duobinary signals ($a = 1/\sqrt{2}$)

4.5.2 Experimental Results Measured for 2×10 Gbit/s QPolDB

The experimental setup used to generate and detect a 10 Gbaud (2×10 Gbit/s) QPolDB signal is shown in figure 4.24. For simplicity, only one optical duobinary signal was generated by passing a 10 Gbit/s binary data stream through a duobinary stub LPF having a frequency response dip at 5 $\mathrm{GH_z}$ (Stub-5), similar to that used for QDB generation. The differential encoding was neither implemented nor needed because a $2^7 - 1$ PRBS data stream was used. The generated electrical duobinary signal had a $2V_\pi$ peak-to-peak voltage swing and was used to drive a MZM biased at minimum transmission. At the output of the modulator an optical duobinary signal (Duobinary-5) was generated with an intensity eye diagram shown in figure 4.24 (top-left). Another duobinary stub LPF, producing impulses spaced by 83 ps and having a frequency response dip at 6 $\mathrm{GH_z}$, was used instead of the previous stub filter which resulted in the generation of the optical duobinary signal (Duobinary-6) with the intensity eye diagram shown in figure 4.24 (top-right). The frequency response of this filter (Stub-6) and a comparison with the frequency response of a duobinary Bessel LPF is given in appendix D. The generated optical duobinary signal is passed through an optical amplifier, polarization controller, and a polarizer. The output signal of the polarizer is split by a coupler into two branches. One of the branches, carrying the duobinary signal in the x-polarization E_x, delayed the signal by 31 symbol periods in an additional certain length of standard single mode fiber (SSMF) to decorrelate the two PRBS patterns. The signal in the orthogonal y-polarization E_y in the other branch was optically attenuated by 3 dB ($a = 1/\sqrt{2}$). The two electric fields E_x and E_y are orthogonally recombined in a subsequent PBS resulting in a 4-level quaternary polarization duobinary signal QPolDB. The 3 dB attenuation in the E_y branch was used to obtain equal eye openings in the intensity domain for the QPolDB signal.

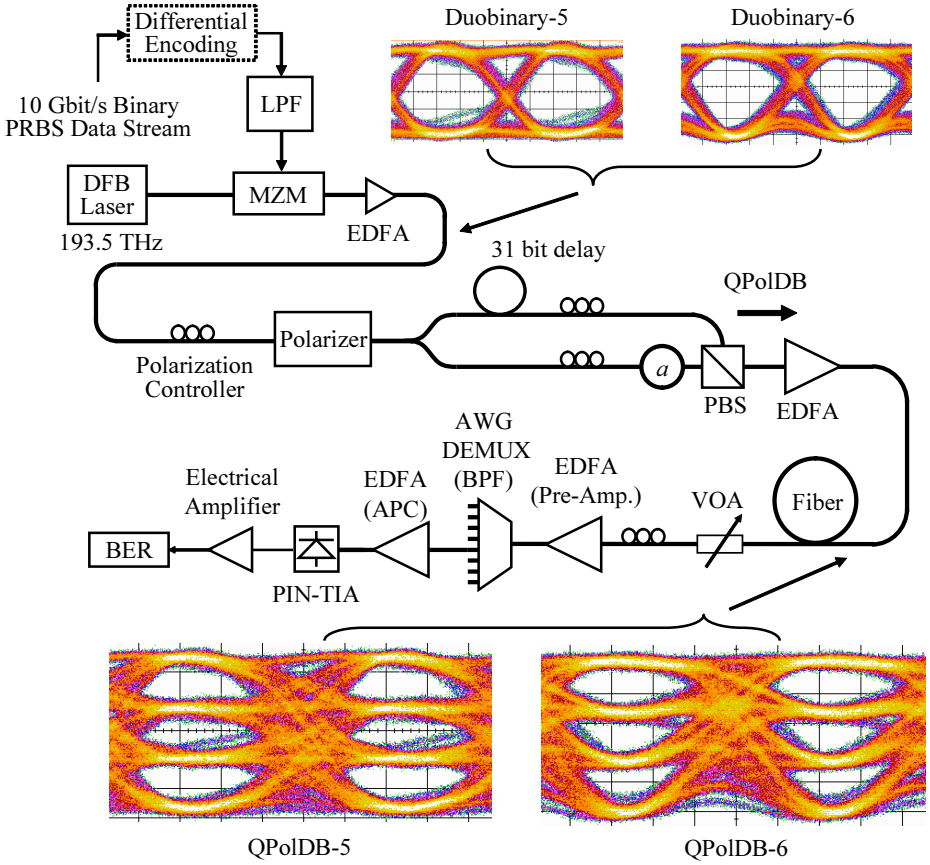

Figure 4.24: Schematic of the transmission setup used to generate and detect 2×10 Gbit/s QPolDB signals

The eye diagrams of the QPolDB signal generated using the two stub filters are shown in figure 4.24 (bottom). The extension -5 or -6 of the modulation format acronym QPolDB denotes the dip frequency of the respective stub filter in GHz. Later it will be seen that the QPolDB-5 signals yield better sensitivity but worse CD tolerance than the QPolDB-6 signals. Similar experience with differently shaped duobinary signals has been reported in [102, 24, 83, 82]. Figure 4.25 shows the heterodyned electrical spectrum of the QPolDB-6 signal. There is no carrier, and the bandwidth is equivalent to that of a single Duobinary-6 signal. The spectrum of the QPolDB-5 signal looks the same and has the same bandwidth as the heterodyned QDB spectrum shown in figure 4.17.

Similar to the experimental setup used in the previous sections the receiver employed an optical preamplifier followed by a 100 GH_zspaced, 40-channel, C-band dense wavelength division multiplexed (DWDM) demultiplexer (DeMux). This DeMux is of the Gaussian type and acts as a narrow bandpass optical filter. A variable optical attenuator (VOA) followed by a polarization controller placed before the optical preamplifier is used to vary the optical signal to noise ratio (OSNR) for sensitivity and CD tolerance measurements. The polarization controller was used to compensate the polarization dependent loss (PDL) of the optical preamplifier. For an automatic power control (APC), the detected photocurrent of an optical front end, a PIN photodiode integrated with a transimpedance amplifier (PIN-TIA), is stabilized by a feedback loop (not shown) that controls the pump current of the last

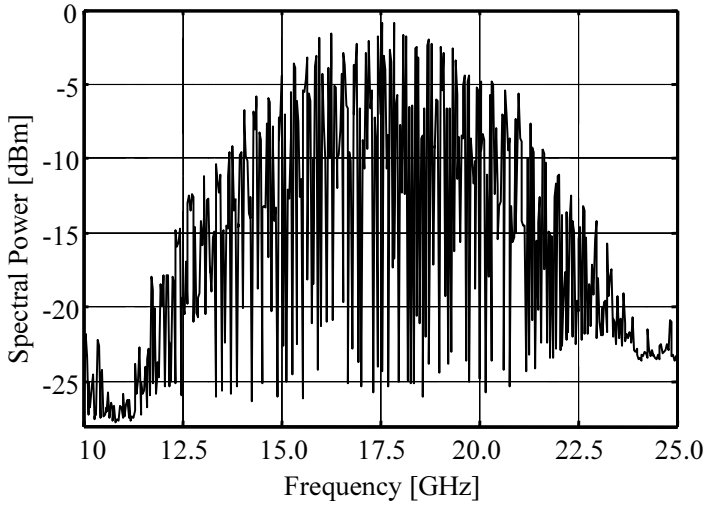

Figure 4.25: Heterodyned electrical spectrum of the 20 Gbit/s QPolDB-6 signal

erbium-doped fiber amplifier (EDFA). An electrical amplifier is used to amplify the received signal before it feeds an oscilloscope or a BER detector. The error detector was programmed with three different expected patterns corresponding to the top, middle, and bottom eye diagrams. To detect these patterns, different decision threshold settings of the error detector are used. Proper bit-error-rate (BER) averaging is performed to represent the mean BER of the received patterns. Figure 4.26 and figure 4.27, show the BER curves for the three received eyes (top, middle, and bottom) of the 20 Gbit/s QPolDB signals using LPF stubs with $5-\mathrm{GHz}$ dip (QPolDB-5), and $6-\mathrm{GHz}$ dip (QPolDB-6) respectively.

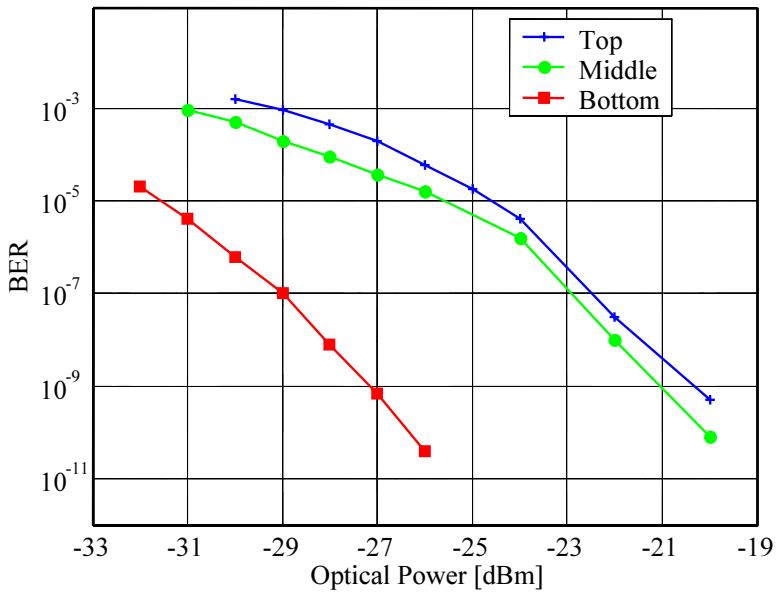

Figure 4.26: BER curves versus received optical power for the three received eyes (top, middle, and bottom) for a 20 Gbit/s QPolDB-5 signal

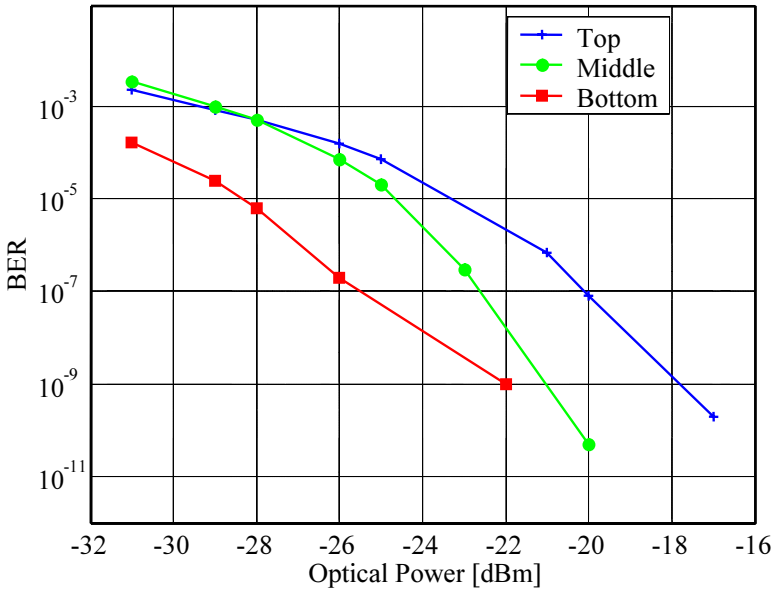

Figure 4.27: BER curves for the three received eyes (top, middle, and bottom) for a 20 Gbit/s QPolDB-6 signal

The average BER curves versus the received optical power measured at the optical preamplifier input for 20 Gbit/s QPolDB-5 and QPolDB-6 signals with PRBS length of $2^7 - 1$ are shown in figure 4.28. The measured receiver sensitivity using a PRBS length of $2^7 - 1$ at an average BER of 10^{-9} for the 20 Gbit/s QPolDB-5 and QPolDB-6 signals are ~-20.5 dBm, and ~-18.4 dBm, respectively.

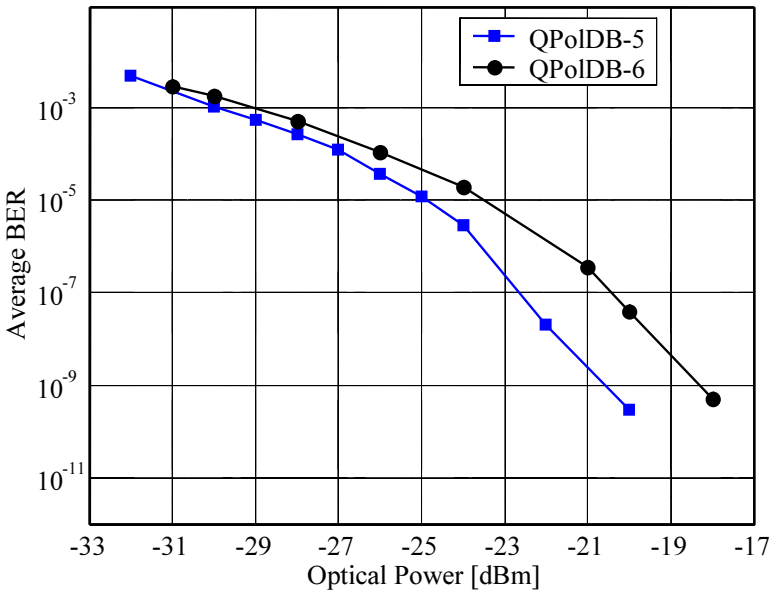

Figure 4.28: Average BER versus received optical power for 20 Gbit/s QPolDB-5 and QPolDB-6 signals

Figure 4.29 shows the average BER versus the received optical power measured at the

optical preamplifier input for 20 Gbit/s QPolDB-6 signal with PRBS length of $2^7 - 1$ (PRBS 7), $2^{10} - 1$ (PRBS 10) , and $2^{15} - 1$ (PRBS 15). The measured receiver sensitivity at an average BER of 10^{-9} for the 20 Gbit/s QPolDB-6 signal with PRBS lengths of $2^{10} - 1$ (PRBS 10) and $2^{15} - 1$ (PRBS 15) are ~-18 dBm, and ~-13 dBm, respectively.

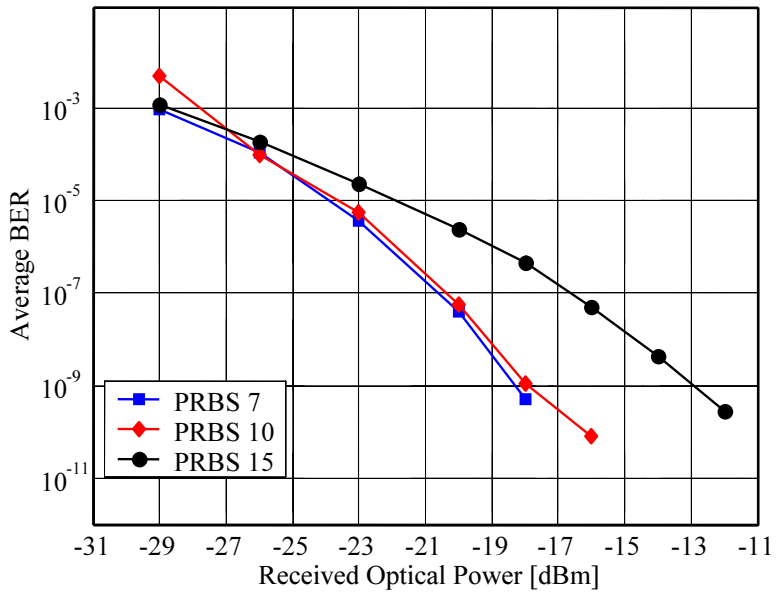

Figure 4.29: Average BER versus received optical power for 20 Gbit/s QPolDB-6 signal with PRBS 7, 10 and 15

The chromatic dispersion (CD) tolerance was measured for the generated 20 Gbit/s QPolDB signals (QPolDB-5 and QPolDB-6). Figure 4.30 shows the measured OSNR after the optical preamplifier needed for a BER of 10^{-9} versus CD for both 20 Gbit/s QPolDB-5 and QPolDB-6 signals. An optical attenuator was used to vary the OSNR. The 1-dB tolerances at a BER of 10^{-9} are ~340ps/nm and ~530ps/nm, for QPolDB-5 and QPolDB-6, respectively.

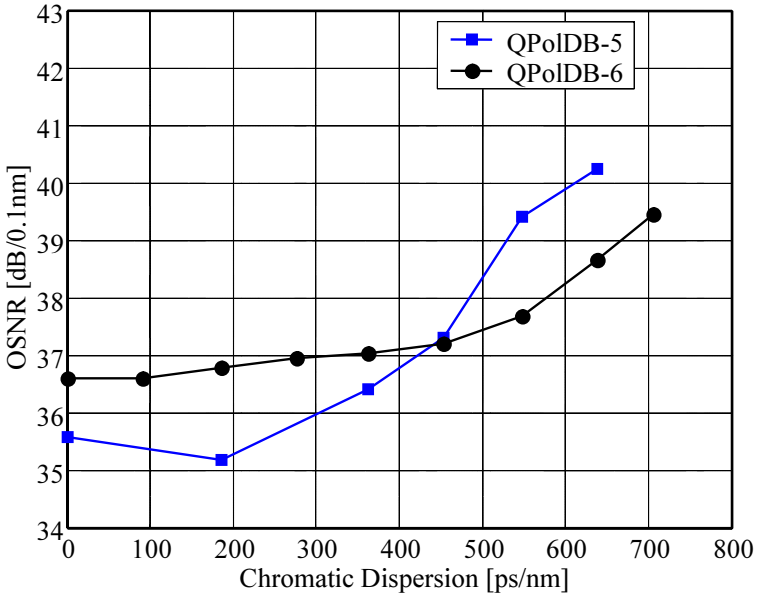

Figure 4.30: OSNR needed for a BER of 10^{-9} versus CD in ps/nm for 20 Gbit/s QPolDB-5 and QPolDB-6 signals

Figure 4.31 and figure 4.32 show the intensity eye diagrams at the sensitivity edge (BER =10^{-9}) for 20 Gbit/s QPolDB-5 and QPolDB-6 signals respectively after transmission over different lengths of SSMF (D ~ 17 ps/nm.km). It can be seen that by increasing the fiber length the chromatic dispersion increases and the quality of the QPolDB signal degrades. Since QPolDB-6 has better CD tolerance than QPolDB-5 it was possible to measure the intensity eye diagram at the sensitivity limit for the QPolDB-6 signal after transmission over 41.54 km of SSMF (~706ps/nm) as shown in figure 4.31 (f).

Figure 4.33 shows a photo of the polarization division multiplex (PolDM) setup used to generate the 20 Gbit/s QPolDB signals. It consists of 3 polarization controllers, a polarizer, a 3dB coupler, 2 optical attenuators, and a polarization beam splitter (PBS).

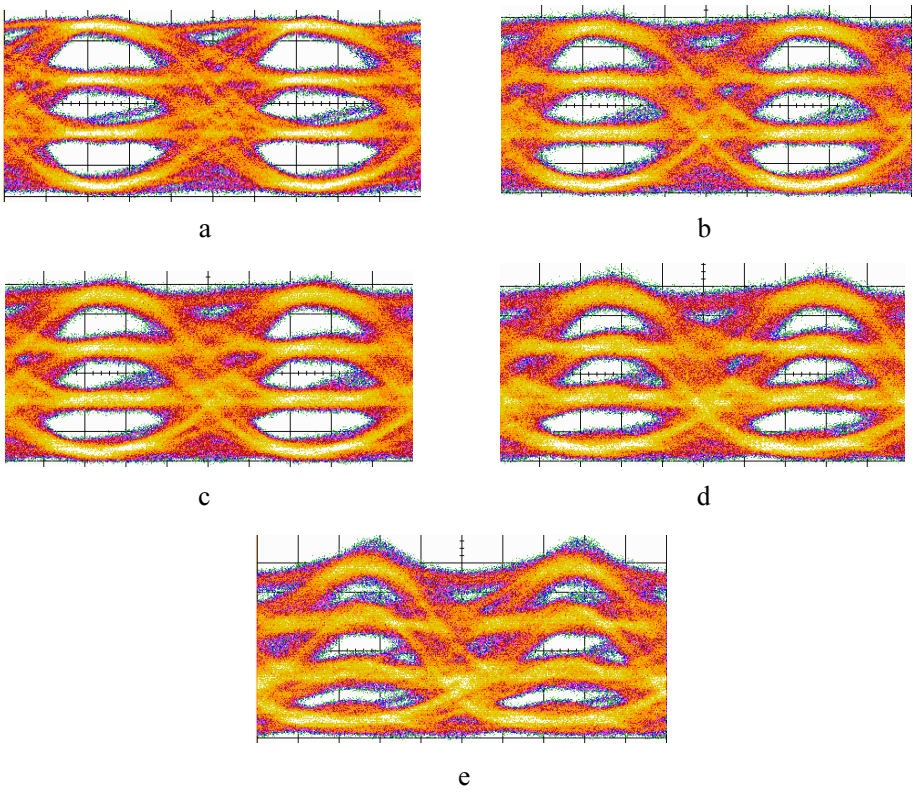

Figure 4.31: Intensity eye diagrams of the 20 Gbit/s QPolDB-5 signal measured at the sensitivity edge after transmission over (a) 0 km (back-to-back), (b) 10.9 km, (c) 16.24 km, (d) 26.65 km, and (e) 37.55 km of SSMF

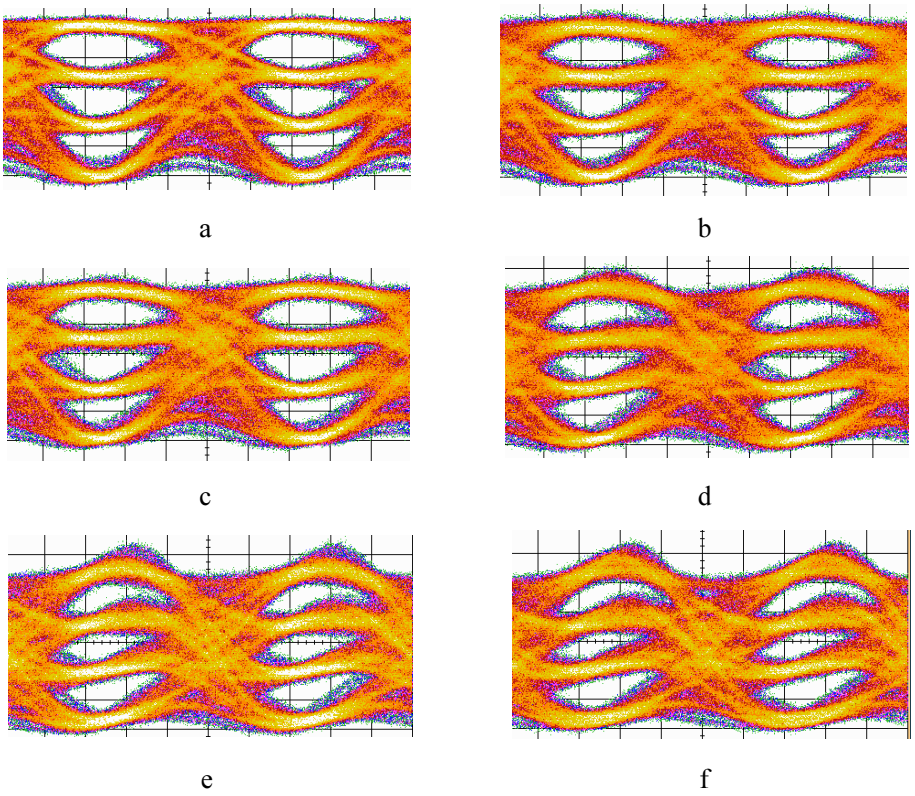

Figure 4.32: Intensity eye diagrams of the 20 Gbit/s QPolDB-6 signal measured at the sensitivity edge after transmission over (a) 0 km (back-to-back), (b) 10.9 km, (c) 16.24 km, (d) 26.65 km, (e) 37.55 km, and (f) 41.54 km of SSMF

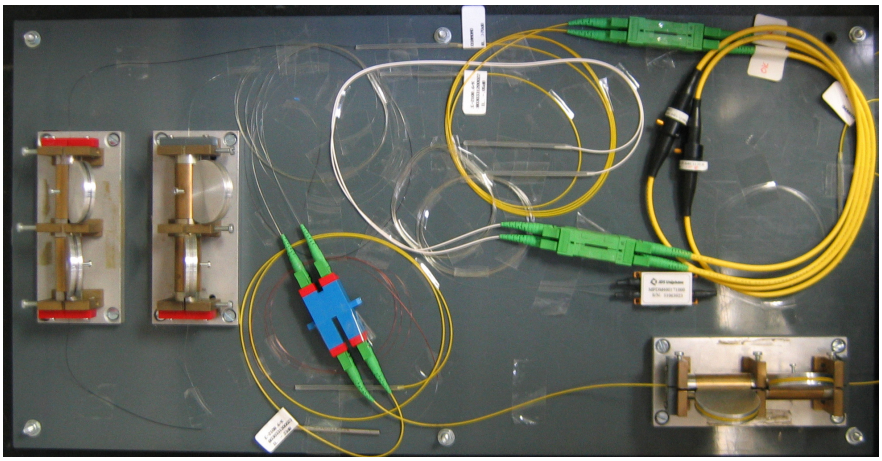

Figure 4.33: Photo of the PolDM transmitter setup used to generate the QPolDB signals

4.6 Other Quaternary Multilevel Modulation Formats

In addition to the quaternary modulation formats covered in the previous sections, there exist also other quaternary multilevel formats that use various combinations of phase- polarization- and amplitude-shift keying to achieve high spectral efficiency [19, 103, 18]. In the following subsections we will briefly cover some of the other reported quaternary modulation formats such as quaternary polarization amplitude shift keying (QPolASK) [23, 22] and quaternary differential phase amplitude shift keying (DP-ASK) [18, 19]. Both of these modulation formats double the transmission rate and have higher spectral efficiency than binary NRZ-ASK signals operating at the same bit rate.

4.6.1 Quaternary Polarization Amplitude Shift Keying (QPolASK)

Quaternary polarization amplitude shift keying modulation (QPolASK) is generated by optically combining two binary intensity modulated signals NRZ-ASK with unequal amplitudes in orthogonal polarizations [23, 22]. The resulting modulation format is similar to the QASK [20], but orthogonal polarizations are used to generate the 4-level signal instead of quadrature phases. The schematic of the QPolASK transmitter is similar to the QPolDB transmitter shown in figure 4.22 but with replacing the duobinary signals with binary signals as shown in figure 4.34.

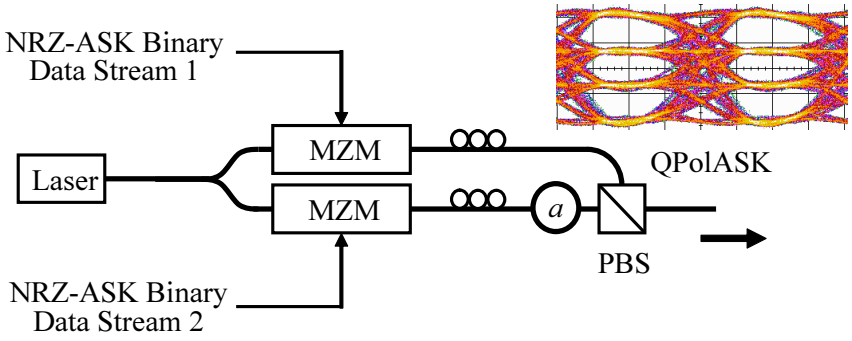

Figure 4.34: Schematic of the optical QPolASK signal generation scheme ($a = 1/\sqrt{2}$), eye diagram of 2×10 Gbit/s QPolASK signal (top-right).

The laser signal is split into two branches where each branch consists of a Mach-Zehnder modulator biased at the quadrature point and driven by an electrical binary NRZ-ASK signals having peak-to-peak voltage amplitude of V_π. In one of the branches the generated optical binary NRZ-ASK signal carries an electric field E_x with normalized field amplitudes of {0, +1}. The optical binary NRZ-ASK signal in the other branch is optically attenuated by 3 dB ($a = 1/\sqrt{2}$) resulting in an orthogonal electric field E_y with normalized field amplitudes $\{0, +a\}$. The two generated optical signals $E_x$and $E_y$carried in the two branches are then combined with orthogonal polarizations in a polarization beam splitter (PBS) generating a quaternary polarization amplitude shift keying modulation signal (QPolASK). The intensity eye diagram of a generated 2×10 Gbit/s QPolASK signal is shown in figure 4.34 (top-right). The QPolASK signal constellation diagram is given in figure 4.35. The QPolASK signal can be detected as a 4-IM with intensities $\{0, a^2, 1, 1 + a^2\}$ corresponding to

the levels labeled “0”, “1”, “2”, “3”. Similar decoding as in 4-IM is needed at the receiver side. The spectrum of the QPolASK signal is expected to contain a carrier component and equivalent to the 4-IM and the QASK spectrum. The spectral bandwidth of the QPolASK is about twice the bandwidth of the QPolDB signal. The measured receiver sensitivity for the QPolASK modulation format at 20 Gbit/s is ~-21 dBm.

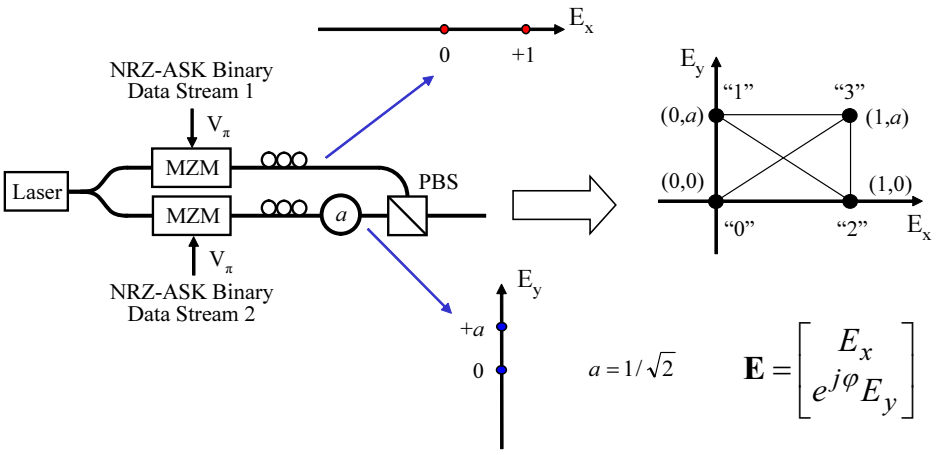

Figure 4.35: QPolASK electrical field signal constellation diagram (top-right) generated using a polarization division multiplex setup with binary signals ($a = 1/\sqrt{2}$)

4.6.2 Quaternary Differential-Phase ASK Modulation (DP-ASK)

It has been reported in [18, 19] on a quaternary differential-phase ASK modulation format based on independent DPSK and ASK modulation. The schematic of the DP-ASK transmitter and receiver setup are shown in figure 4.36. DP-ASK can be used to transmit independently two binary 10 Gbit/s data streams on the same optical carrier frequency by using two cascaded MZM modulators, one configured for ASK modulation and the other configured for DPSK modulation [18].

The DP-ASK signal constellation diagram in the optical domain is represented by four signal points on the real axis of the electric field as shown in figure 4.37 having two different amplitudes, a and b ($b > a > 0$), and two possible phase angles 0 and π [19]. The extinction ratio (ER) of the ASK branch ($ER = b/a$) must be optimized (~9.5 dB) in order to obtain equal receiver sensitivity for both the ASK and DPSK signals [18].

To receive the two transmitted data streams, the DP-ASK signal is split into two signals. One part enters a standard ASK receiver based on a single photodiode, and the other part enters a standard DPSK receiver based on a MZDI and a balanced detection photodiode receiver. One drawback of this method is the complicated receiver design and extra cost due to the need of both a DPSK balanced receiver and an ASK receiver. The reported receiver sensitivity and optical bandwidth for the DP-ASK modulation format at 20 Gbit/s were ~-30 dBm, and ~ 20 GHz respectively [18].

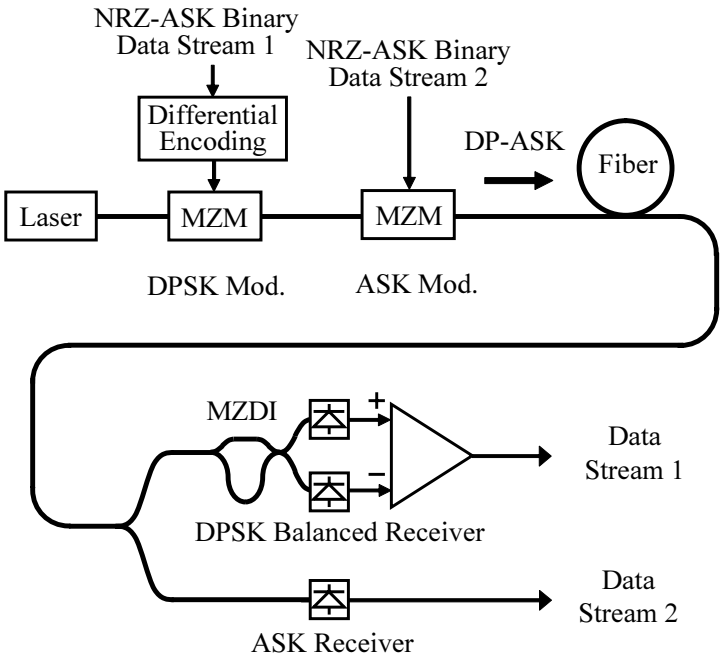

Figure 4.36: Schematic of quaternary DP-ASK transmitter and receiver

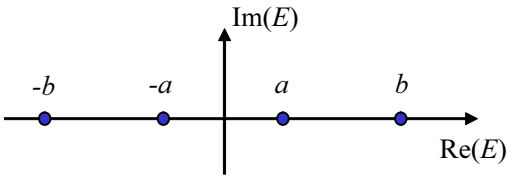

Figure 4.37: DP-ASK signal constellation diagram

Chapter 5

Results Discussion and Conclusion

5.1 Introduction

This chapter will discuss the experimental results obtained for the multilevel optical modulation formats obtained from chapter 3 and 4. These modulation formats are DQPSK, DQPSK PolDM, 4-IM, QASK, QDB, QPolDB-5 and QPolDB-6. A comparison between the different quaternary modulation formats with standard binary and duobinary modulation operating at 20 Gbit/s will also be given in a table in the following section. The advantages and disadvantages of each modulation format will also be highlighted. A brief conclusion of the overall work will be given in the last section of this chapter.

5.2 Results Discussion

The measured receiver sensitivities at an average BER of 10^{-9} for the quaternary modulation formats NRZ-DQPSK, RZ-DQPSK, 4-IM, QASK, QDB, QPolDB-5, and QPolDB-6 are -36.8 dBm, -38.3 dBm, -12.8 dBm, -21.6 dBm, -21.2 dBm, -20.5 dBm, and -18.4 dBm, respectively for 2×10 Gbit/s transmitted data with a PRBS length of $2^7 - 1$. Obviously the RZ-DQPSK modulation format achieved the best receiver sensitivity compared to the other modulation formats. The 4-IM had the worst receiver sensitivity. For $2\times2\times10$ Gbit/s DQPSK PolDM, the receiver sensitivities at an average BER of 10^{-9} for NRZ-DQPSK PolDM and RZ-DQPSK PolDM signals are -33.8 dBm and -34.7 dBm, respectively with a PRBS length of $2^7 - 1$. Figure 5.1 shows the BER curves obtained for all the quaternary multilevel modulation format experiments performed in chapter 4 (4-IM, QASK, QDB, QPolDB-5, and QPolDB-6) with a PRBS length of $2^7 - 1$.

The effects of very long PRBS pattern lengths ($\geq 2^{23} - 1$) could not be assessed since the expected patterns could not be uploaded to the BER detector with the available software and memory size. It is believed that the sensitivity for the QDB and QPolDB signals would be degraded when used with higher PRBS lengths since they are based on duobinary modulation which is known to be degraded when used with longer PRBS patterns [83, 84]. To confirm that conclusion it was possible to generate and detect a QPolDB-6 signal using 2×10 Gbit/s data streams with a PRBS length of $2^{10}-1$ and $2^{15}-1$ resulting into a measured average receiver sensitivity of ~-18 dBm and ~-13 dBm, respectively. It may be possible to improve the receiver sensitivity of the QPolDB signals by optimizing the generated duobi-

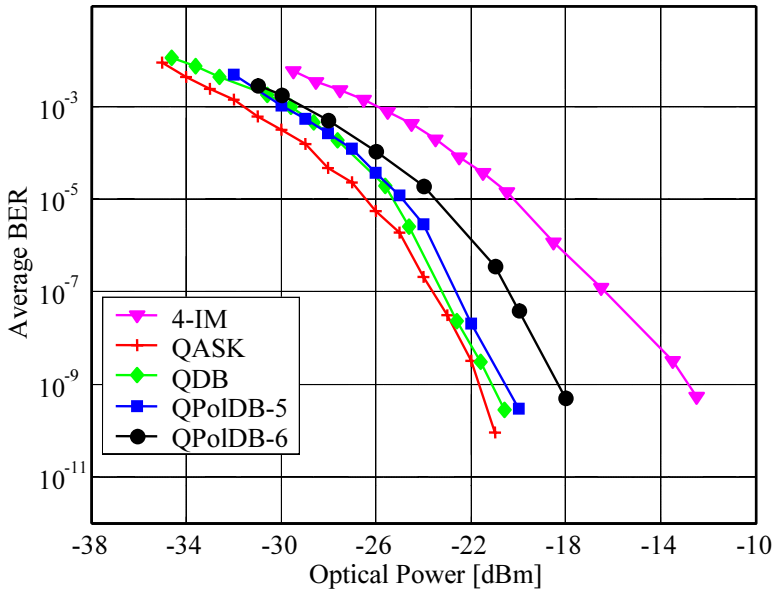

Figure 5.1: Average BER curves versus received optical power for 20 Gbit/s quaternary modulation signals (4-IM, QASK, QDB, QPolDB-5, and QPolDB-6).

nary signals by filtering it with a narrow bandwidth optical filter [83, 84, 104, 105]. As for DQPSK signals, the average receiver sensitivity for 2×10 Gbit/s DQPSK signals with a PRBS length of $2^{15} - 1$, is measured to be ~-36.4 dBm and ~-37.3 dBm for NRZ and RZ pulse shaping, respectively. As for 2×2×10 Gbit/s DQPSK PolDM signals with a PRBS length of $2^{15} - 1$, the average receiver sensitivity is measured ~-32.5 dBm and ~-34.2 dBm for NRZ and RZ pulse shaping, respectively.

In terms of chromatic dispersion tolerance, figure 5.2 shows the OSNR needed for an average BER of 10^{-9} versus CD in ps/nm for 20 Gbit/s quaternary modulation signals (QASK, QDB, QPolDB-5, and QPolDB-6). The measured 1 dB CD tolerance of the multilevel modulation formats at 20 Gbit/s for RZ-DQPSK, QASK, QDB, QPolDB-5, and QPolDB-6 are 360 ps/nm, 130 ps/nm, 140 ps/nm, 340 ps/nm, and 530 ps/nm respectively. The CD tolerance measurement was not possible for the 4-IM signal due to high noise and poor receiver sensitivity.

The QPolDB-6 modulation format had the best CD tolerance compared to the other modulation formats while the QASK scheme had the worst CD tolerance. This is due to the reduced bandwidth of the duobinary modulation used for the QPolDB signals. The analog QDB signal using duobinary signals with the QPSK modulator had a better sensitivity but a worse CD tolerance. The reduced CD tolerance of the QDB scheme may be understood from the fact that CD affects the phase. On the other hand QPolDB is of course affected by polarization-dependent loss, since unbalanced optical powers in the orthogonal polarizations result in unequal eye openings at the receiver side. The QDB signal is also affected by the fact that one of the Mach-Zehnder modulators is driven with a V_π voltage swing. In the presence of electrical intersymbol interference this results in a non-optimal optical generated duobinary signal in the modulator. A solution to this problem is to place an optical attenuator in one of the QPSK modulator branches [20] and to drive both Mach-Zehnder modulators with a full $2V_\pi$ voltage swing, where optical duobinary signal quality is best.

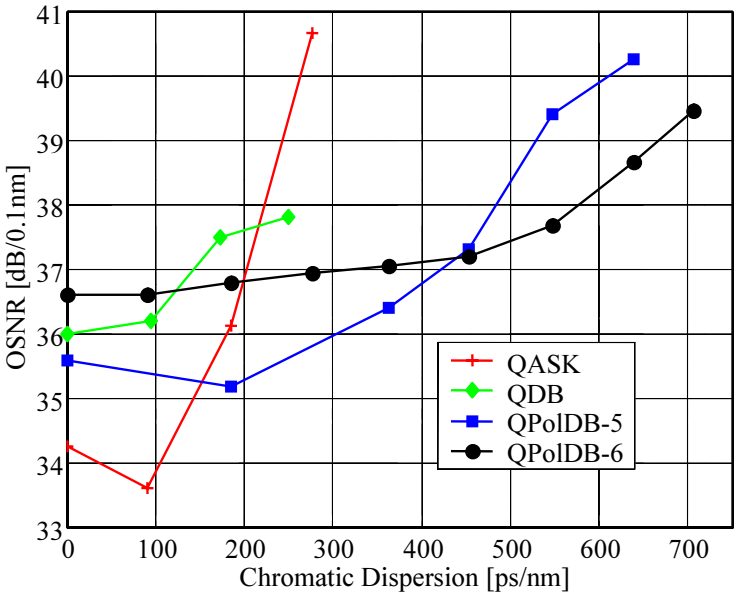

Figure 5.2: OSNR needed for a BER of 10-9 versus CD in ps/nm for 20 Gbit/s quaternary modulation signals (QASK, QDB, QPolDB-5, and QPolDB-6).

The modulation amplitudes in all the quaternary generation schemes were adjusted to optimize the 3 eye openings for the quaternary signal. Any change in the modulation amplitudes will cause unequal eye openings in the quaternary signal. It was also found that the $5-\mathrm{GHz}$ stub generated QPolDB-5 signals have better sensitivity but worse CD tolerance than the QPolDB-6 signals generated by using the $6-\mathrm{GHz}$ stub. This is due to the fact that two different methods were used to generate the two duobinary signals. The QPolDB-5 signals were similar to the duobinary signals generated by the conventional one-bit-delay and add method [24, 25, 26]. The QPolDB-6 signals were similar to the duobinary signals generated by the LPF method. It has been reported in [24, 82, 83] that the duobinary signals based on the LPF method better suppresses the optical spectrum side-lobes, tolerates more CD than the one bit delay method, but has a worse back-to-back sensitivity than the one-bit-delay and add method. A similar behavior was obtained for the QPolDB-5 and QPolDB-6 signals.

Table 5.1 compares different modulation formats at 20 Gbit/s in terms of receiver sensitivity, CD tolerance and optical bandwidth occupancy. For comparability all quaternary modulation experiments in table 5.1 refer to a PRBS length of 2^7-1.

From table 5.1 it is can be concluded that the 20 Gbit/s standard binary NRZ-ASK signal had the largest spectral bandwidth and therefore has worse spectral efficiency than all the other compared multilevel modulation formats operating at the same bit rate. The best spectral bandwidth was for QDB, QPolDB, and DQPSK PolDM signals. In terms of CD tolerance, DQPSK PolDM, duobinary modulation, then QPolDB-6 modulation had the best CD tolerance compared to all the other modulation formats operating at the same bit rate. In terms of receiver sensitivity, RZ-DQPSK and RZ-DQPSK PolDM had the best receiver sensitivity. The merits of DQPSK and DQPSK PolDM signals come at the cost and complexity of the extra components at the receiver (interferometer-based balanced photoreceiver with two photodiodes, polarization controller).

Table 5.1: Comparison between different modulation formats at 20 Gbit/s

Mod. Format (@ 20 Gbit/s)	Sensitivity (dBm)	CD tol. (ps/nm)	BW (GHz)	Reference
NRZ-ASK	-31.6	~260	~40	[48]
Duobinary	-28.5	600	~20	[24]
NRZ-DQPSK	-36.8	-	~20	(measured)
RZ-DQPSK	-38.3	360	>20	(measured)
NRZ-DQPSK PolDM	~-36.8	-	~10	(scaled)
RZ-DQPSK PolDM	~-37.7	~1440	>10	(scaled)
4-IM	-12.8	-	~20	[6]
QASK	-21.6	130	~20	[6]
QDB	-21.2	140	~10	[6]
QPolDB-5	-20.5	340	~10	[6]
QPolDB-6	-18.4	530	~12	[6]
QPolASK	-21	-	~20	(measured)
DP-ASK	-30	-	~20	[18]

5.3 Conclusion

The two duobinary QDB and QPolDB schemes which require only a single photodiode as a receiver are believed to represent intensity modulation with the narrowest reported spectrum reported to date ($10\mathrm{GHz}$). The polarization division multiplex based duobinary QPolDB-6 scheme doubles the transmission capacity and is believed to feature the largest reported CD tolerance (530 ps/nm) for 20 Gbit/s intensity modulation with such a narrow spectrum ($12\mathrm{GHz}$), which makes it attractive for DWDM systems applied for short reach (several kilo meters) to medium reach (several hundreds kilometers) transmission applications (metro applications). However, for long or ultra long haul optical fiber transmission systems, RZ-DQPSK modulation (with reported receiver sensitivity -38.3 dBm and CD tolerance 360 ps/nm at 20 Gbit/s) and Duobinary modulation (with reported receiver sensitivity -28.5 dBm and CD tolerance 600 ps/nm at 20 Gbit/s) are the potential candidates. Also RZ-DQPSK PolDM is a promising modulation format for ultra long haul DWDM optical fiber transmission systems with channels operating at high data rates ≥ 40 Gbit/s.

Appendix A

Optical Intensity Mach-Zehnder Modulator (MZM)

Several types of external optical intensity modulators have been developed over the past several decades for optical fiber communication applications. Most of the modern wide-bandwidth modulators are based on the linear electro-optic (EO) effect (also known as Pockels effect) which depends on the applied electric field which makes the modulator a voltage-controlled device [66]. EO effect denotes the change of the optical refractive index in nonlinear optical (NLO) crystals due to the presence of the electric field. The index change leads to change in the optical phase, which can be converted into intensity modulation in a Mach-Zehnder interferometer. Lithium Niobate ($LiNbO_3$) is the most widely used material for manufacturing electro-optic devices, including phase modulators and Mach-Zehnder intensity modulators (MZM). The Mach-Zehnder interferometer is the most popular device for implementing optical intensity modulation using EO effect. Figure A.1 shows a schematic drawing of such an interferometer .

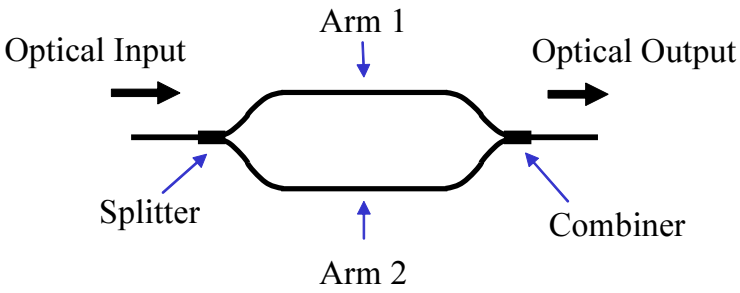

Figure A.1: Schematic drawing of a Mach-Zehnder interferometer

At its optical input port, there is an optical splitter that divides the input optical power into two equal portions. The divided power propagates in two separate waveguides that are often called "*two arms*". In a MZM, at least one of these two arms is designed as an EO waveguide, along which the optical phase can be modulated by an applied voltage. If the optical waves are in phase after propagating through the two arms, they combine as a single mode in the output optical combiner, which results in a maximum intensity output; whereas if the optical waves are out of phase after propagating through the two arms, they

combine as a higher order spatial mode near the optical combiner, therefore most of the optical power becomes an unguided wave beyond the combiner and the output intensity is minimum [44, 66]. The optical field amplitude E_o at the output of the MZM can be generally represented by [44, 66, 1, 35]:

$$E_o = \frac{1}{\sqrt{2}}\left(E_1 e^{j\Phi_1} + E_2 e^{j\Phi_2}\right), \tag{A.1}$$

where (E_1, E_2) and (Φ_1, Φ_2) represent the optical field amplitudes and optical phase delays in the two arms respectively. The output optical power P_o is:

$$P_o = |E_o|^2 = \frac{1}{2}\left[|E_1|^2 + |E_2|^2 + 2\,|E_1|\,|E_2|\cos\left(\Phi_1 - \Phi_2\right)\right]. \tag{A.2}$$

The phase difference $\Phi_1 - \Phi_2$ consists of two parts ($\Phi_1 - \Phi_2 = \Delta\Phi + \Phi_0$): one is the path difference Φ_0 at zero applied voltage and the other is the phase difference $\Delta\Phi$ due to the applied voltage. Assuming that the optical splitter splits the input electric field E_i into two equal electric fields of $E_i/\sqrt{2}$ each $\left(E_1 = E_2 = E_i/\sqrt{2}\right)$ and by neglecting the waveguide losses and ignoring the arm path delays and constant phase shifts ($\Phi_0 = 0$). The resulting output electric field of the MZM structure shown in figure A.1 when only arm one is modulated ($\Phi_2 = 0$, $\Phi_1 = \Delta\Phi$) can be written as:

$$E_o = \frac{E_i}{2}\left(e^{j\Phi_1} + 1\right) = \frac{E_i}{2}\left(e^{j\pi\frac{V(t)}{V_\pi}} + 1\right) = E_i\left[\cos\left(\frac{\pi}{2}\frac{V(t)}{V_\pi}\right)\right] e^{j\frac{\pi}{2}\frac{V(t)}{V_\pi}}, \tag{A.3}$$

where $V(t)$ is the applied voltage to the electrode of arm one, and V_π is the voltage value at which the voltage-induced phase difference reaches π (or 180^{o}) [66, 1]. However, in additional to the change of the optical intensity, the input and output relation of Eq. A.3 also accompanies with phase modulation of $e^{j\phi}$ where $\phi = \frac{\pi}{2}\frac{V(t)}{V_\pi}$. The ratio of the phase to amplitude modulation is called the chirp coefficient [1]. In addition to chirp, the unmodulated path (lower arm) of figure A.1 reduces the modulation efficiency of the modulator. When the microwave electrodes are properly designed, both paths of the Mach-Zehnder modulator can be modulated to improve the modulator efficiency. Figure A.2 shows the waveguide structure for a Mach-Zehnder modulator using $x-\text{cut}\ LiNbO_3$ crystal. The two paths of the Mach-Zehnder modulator are phase-modulated with opposite phase shifts in a push-pull structure. For this type of MZM structure, the V_π is reduced by half with respect to the MZM structure with only one modulated arm.

Because the two arm paths are modulated with opposite phases of $\pm\frac{\pi V(t)}{2V_\pi}$ so that $\Phi_1 = -\Phi_2$ and the output electric field of the MZM (push-pull) structure is:

$$E_o = \frac{E_i}{2}\left(e^{j\Phi_1} + e^{j\Phi_2}\right) = \frac{E_i}{2}\left(e^{j\pi\frac{V(t)}{2V_\pi}} + e^{-j\pi\frac{V(t)}{\pi}}\right) = E_i\left[\cos\left(\frac{\pi}{2}\frac{V(t)}{V_\pi}\right)\right]. \tag{A.4}$$

From Eq. A.4, it can be concluded that no phase modulation accompanies the amplitude modulation and therefore this single-drive x-cut push-pull modulator has zero-chirp. In terms of optical intensity for both of the previous mentioned structures of the Mach-Zehnder modulator (single arm and push-pull), the transfer characteristic equation (transfer function

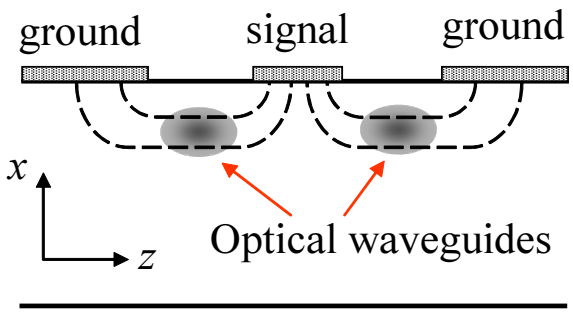

Figure A.2: Mach-Zehnder modulator (push-pull) structure using $x-\text{cut}\ LiNbO_3$

or optical intensity transmission) as a function of the applied voltage from equations A.3 and A.4 can be written as:

$$\frac{|E_o|^2}{|E_i|^2} = \cos^2\left(\frac{\pi}{2}\frac{V(t)}{V_\pi}\right) = \frac{1}{2}\left[1+\cos\left(\pi\frac{V(t)}{V_\pi}\right)\right]. \tag{A.5}$$

The transfer function of the MZM is a nonlinear sinusoidal function as shown in figure A.3. The voltage to turn the modulator from minimum to maximum transmission points is V_π. The input and output transfer characteristic of the MZM modulator may provide 0 and π phase modulation to an optical signal. For $V(t)$ from 0 to V_π, E_o and E_i have the same phase. For $V(t)$ from V_π to $2V_\pi$, E_o and E_i have opposite phases [1]. Because of some amount of constant shift ($\Phi_0 \neq 0$), the driving voltage $V(t)$ when equal to zero ($V(t) = 0$) in a practical modulator is not necessarily corresponding to the maximum transmission point as shown in figure A.3.

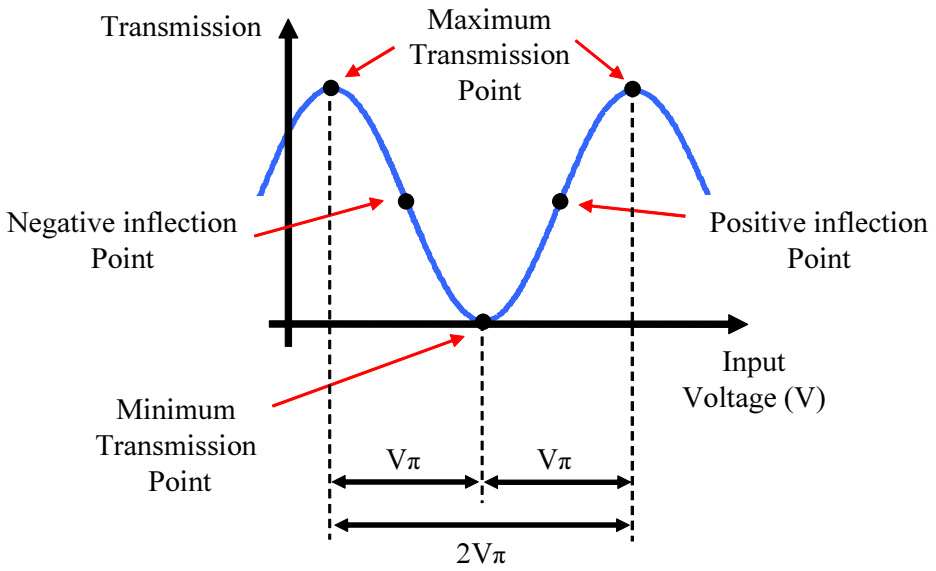

Figure A.3: Typical transfer characteristic curve of a Mach-Zehnder modulator

Phase modulation provided by zero-chirp modulators have the advantage that amplitude jitter does not give phase jitter, i.e., variation of drive voltage does not transfer to varia-

tion of output phase. However, the phase modulation is limited to 0 and π, equivalent to ± 1. For phase-modulation operation, to minimize loss and obtain optimal amplitude jitter compression, the modulator should operate between two maximum transmission points for a peak-to-peak voltage swing of $2V_\pi$ [1]. Currently, most commercially available $LiNbO_3$ amplitude modulators have a V_π from 4 to 6 V. In additional to $LiNbO_3$, semiconductor materials also have electro-optical effect and can be used to fabricate external modulators [1, 66]. For $LiNbO_3$ MZMs, the most remarkable advantages are the lowest optical loss and the highest optical power handling capability. Among all types of MZMs, $LiNbO_3$ modulators are still considered as the devices with the best performance. The main disadvantage for $LiNbO_3$ MZMs is the large size. It also has the bias-drifting issue, which requires bias control circuit. Also $LiNbO_3$ modulators are polarization sensitive, difficult to be integrated with other components and have a higher fabrication cost in terms of large volume production.

As for semiconductor $GaAs$ MZMs, its performance is now getting closer to that of $LiNbO_3$. Also $GaAs$ MZMs have smaller chip sizes, less bias-drifting problem, lower fabrication cost and can be integrated with a wide range of components, such as lasers, semiconductor optical amplifiers, photodetectors, passive optical circuits and even electronic drivers. However, $GaAs$ MZMs have a slightly smaller modulation efficiency and higher optical loss (several dB higher) in comparison to $LiNbO_3$ MZMs [66].

Appendix B

DQPSK Precoder

A schematic of a DQPSK transmission setup is shown in figure B.1. The DQPSK signal carries the information to transmit the two binary data streams $U(k)$ and $V(k)$ on the optical phase of the laser carrier signal. To receive the two data streams, the DQPSK signal is demodulated by two interferometers at the receiver side as shown in figure B.1 (right).

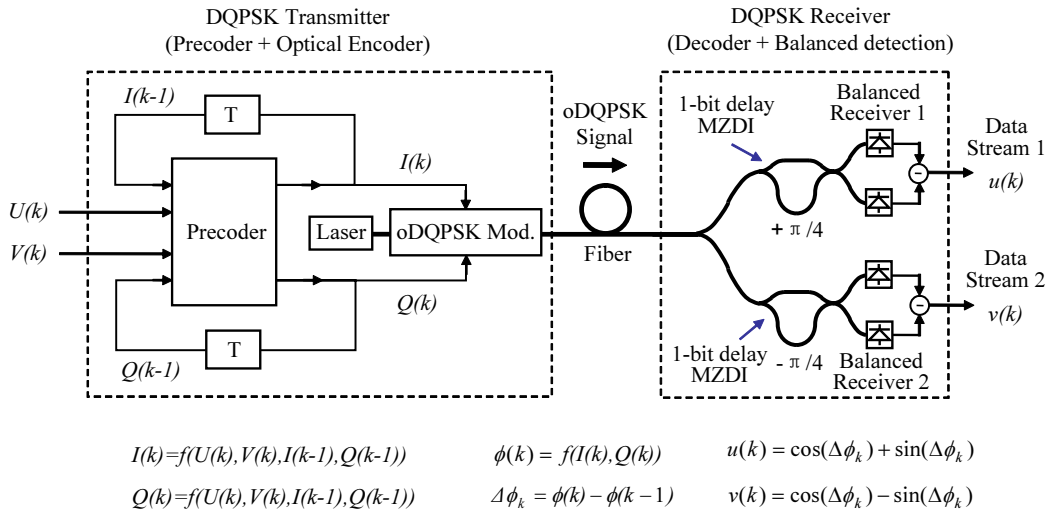

Figure B.1: Schematic of a DQPSK transmission system

Both interferometers need a 1 bit delay in one of their arms. The differential optical phase between the interferometer arms is to be set to $+\pi/4$ and $-\pi/4$ for the upper and lower branches respectively in order to receive the two transmitted data streams [15]. The received phase difference $\Delta\phi = \phi\,(k) - \phi\,(k-1)$ is decoded by the DQPSK receiver to two data bit outputs ($u(k)$ and $v(k)$) corresponding to the two original transmitted bits ($U(k)$ and $V(k)$) by the following relations [13, 94, 45, 44]:

$$u(k) = \cos(\triangle\phi_k) + \sin(\triangle\phi_k) \tag{B.1}$$

$$v(k) = \cos(\triangle\phi_k) - \sin(\triangle\phi_k). \tag{B.2}$$

The mapping of the received phase difference ($\triangle\phi_k$) to the received data streams ($u(k)$ and $v(k)$) are shown in table B.1.

Table B.1: Mapping of the phase change ($\triangle\phi_k$) to received data ($u(k)$ and $v(k)$) for DQPSK signals

Phase difference ($\triangle\phi_k$)	$u(k)$	$v(k)$
0	1	1
$\pi/2$	1	0
π	0	0
$3\pi/2$	0	1

A precoding function is required for the DQPSK system to provide a direct mapping of the data from the input at the transmitter side to the output at the receiver side after demodulation [13, 1]. The precoder block shown in figure B.1 (left) has four inputs where two of the four inputs are the input data streams ($U(k)$ and $V(k)$) and the other two are the time delayed version of the precoder outputs ($I(k-1)$ and $Q(k-1)$). The outputs of the precoder ($I(k)$ and $Q(k)$) are used to drive an optical (D)QPSK modulator (optical encoder) to generate different phase states $\phi(k) = f(I(k), Q(k))$ as shown in figure B.2.

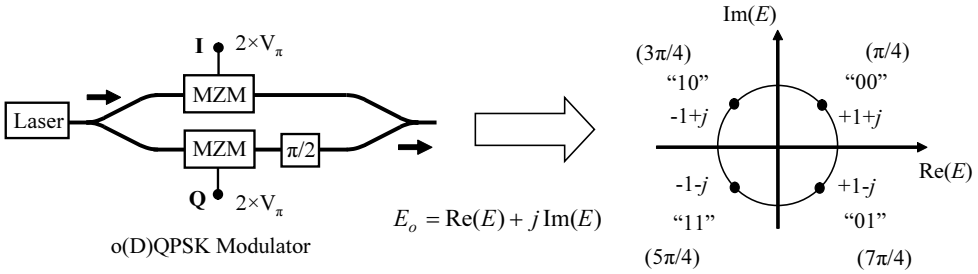

Figure B.2: QPSK modulator and generated phase states $\phi(k)$

The mapping of the optical (D)QPSK modulator input signals ($I(k)$ and $Q(k)$) to the output electric field (E_o) and generated phase state $\phi(k)$ are shown in table B.2.

Table B.2: Mapping of the input signals ($I(k)$ and $Q(k)$) to the output electric field (E_o) and generated phase state ($\phi(k)$) of the o(D)QPSK modulator

$I(k)$	$Q(k)$	O/P Electric Field E_o	Phase state ($\phi(k)$)
0	0	$+1+j$	$\pi/4$
0	1	$+1-j$	$7\pi/4$
1	0	$-1+j$	$3\pi/4$
1	1	$-1-j$	$5\pi/4$

Based on the DQPSK receiver decoder equations B.1 and B.2 and by using the information obtained from table B.1 and B.2, it is possible to generate a lookup table that maps the

precoder input signals ($U(k)$, $V(k)$, $I(k-1)$, and $Q(k-1)$) to the two output precoded signals ($I(k)$ and $Q(k)$) as shown in table B.3. From table B.3 and by using the Karnaugh maps shown in figure b.3 it is possible to find the simplified precoder logic equations that represent $I(k)$ and $Q(k)$ as follows [13, 1, 93]:

$$I(k) = \overline{U}(k)\overline{V}(k)\overline{I}(k-1)+\overline{U}(k)V(k)Q(k-1)+U(k)V(k)I(k-1)+U(k)\overline{V}(k)\overline{Q}(k-1) \tag{B.3}$$

$$Q(k) = \overline{U}(k)\overline{V}(k)\overline{Q}(k-1)+\overline{U}(k)V(k)\overline{I}(k-1)+U(k)V(k)Q(k-1)+U(k)\overline{V}(k)I(k-1). \tag{B.4}$$

Table B.3: DQPSK precoder look up table

$\Delta\phi_k$	$U(k)$	$V(k)$	$I(k-1)$	$Q(k-1)$	$\phi(k-1)$	$I(k)$	$Q(k)$	$\phi(k)$
π	0	0	0	0	$\pi/4$	1	1	$5\pi/4$
π	0	0	0	1	$7\pi/4$	1	0	$3\pi/4$
π	0	0	1	0	$3\pi/4$	0	1	$7\pi/4$
π	0	0	1	1	$5\pi/4$	0	0	$\pi/4$
$3\pi/2$	0	1	0	0	$\pi/4$	0	1	$7\pi/4$
$3\pi/2$	0	1	0	1	$7\pi/4$	1	1	$5\pi/4$
$3\pi/2$	0	1	1	0	$3\pi/4$	0	0	$\pi/4$
$3\pi/2$	0	1	1	1	$5\pi/4$	1	0	$3\pi/4$
$\pi/2$	1	0	0	0	$\pi/4$	1	0	$3\pi/4$
$\pi/2$	1	0	0	1	$7\pi/4$	0	0	$\pi/4$
$\pi/2$	1	0	1	0	$3\pi/4$	1	1	$5\pi/4$
$\pi/2$	1	0	1	1	$5\pi/4$	0	1	$7\pi/4$
0	1	1	0	0	$\pi/4$	0	0	$\pi/4$
0	1	1	0	1	$7\pi/4$	0	1	$7\pi/4$
0	1	1	1	0	$3\pi/4$	1	0	$3\pi/4$
0	1	1	1	1	$5\pi/4$	1	1	$5\pi/4$

The set of logic equations (B.3 and B.4) describe the operation of the precoder used for a DQPSK system using on an optical encoder based on the parallel MZM oDQPSK modulator as shown in figure B.2. The precoder equations can be realized using the logic circuit diagram shown in figure B.4 . It is also possible to use different circuits than in figure B.4 that are based on different logic gate arrangements that also follow the truth table B.3.

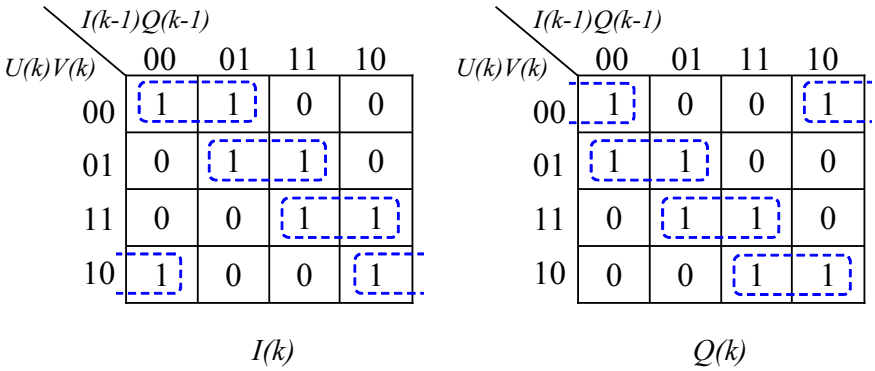

Figure B.3: Karnaugh-maps for the DQPSK precoder outputs $I(k)$ and $Q(k)$

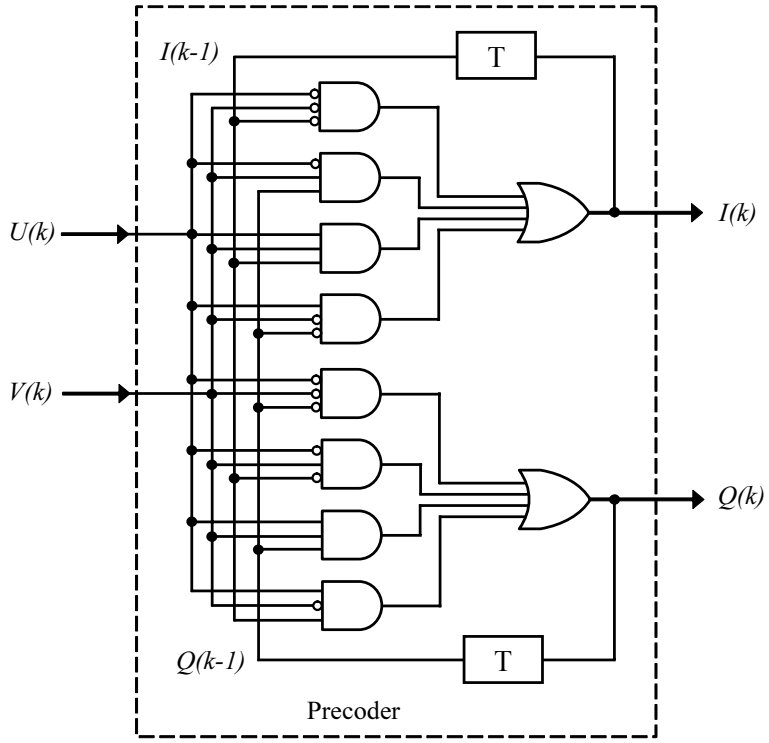

Figure B.4: DQPSK precoder circuit diagram

Appendix C

4-ary ASK Decoder

Figure C.1 shows a schematic of a 4-ary receiver [10, 101]. The input to the receiver is a 4 level quaternary signal (figure C.1 (left)) that contains three eye openings corresponding to three different patterns {Q1, Q2, Q3} representing the bottom, middle, and top eyes respectively. These three patterns {Q1, Q2, Q3} are separated by three decision circuits (D flip-flops) with the reference voltage on each flip set at the decision levels V1 ($0 \leftrightarrow 1$), V2 ($1 \leftrightarrow 2$), and V3 ($2 \leftrightarrow 3$), respectively. Suitable decoding is then needed to recover the two original transmitted data streams from the three detected patterns [101, 10, 6].

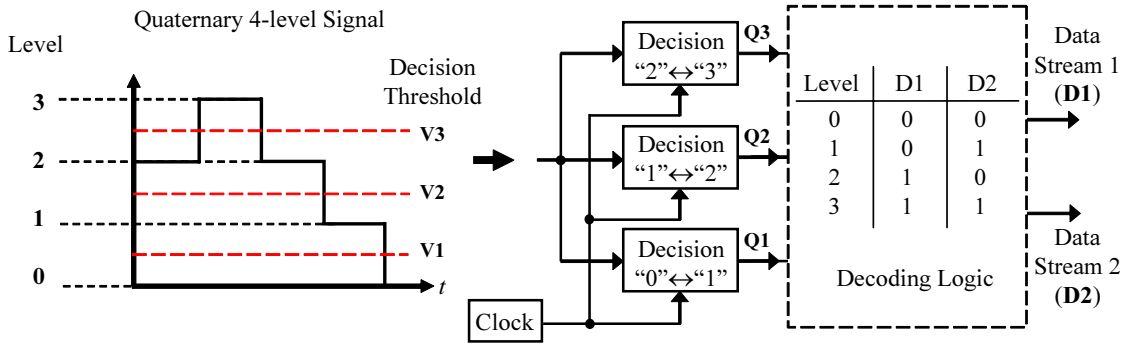

Figure C.1: Schematic of a 4-ary ASK receiver

The mapping of the four input signal levels {0, 1, 2, 3} to the three received patterns {Q1, Q2, Q3} and the two decoded data streams {D1, D2} that represent the recovered transmitted patterns are shown in table C.1.

From table C.1 and by using the Karnaugh maps shown in figure C.2 it is possible to find the simplified decoder logic equations that represent the received data streams D1 and D2 as follows:

$$\mathrm{D1} = \mathrm{Q2} \tag{C.1}$$

$$\mathrm{D2} = \mathrm{Q3} + \mathrm{Q1}\overline{\mathrm{Q2}}. \tag{C.2}$$

The schematic of the decoding logic circuit is shown in figure C.3.

Table C.1: Mapping of the input levels and the 3 received patterns to the decoded outputs for a 4-ary ASK receiver

Level	Q1	Q2	Q3	D1	D2
0	0	0	0	0	0
1	1	0	0	0	1
2	1	1	0	1	0
3	1	1	1	1	1

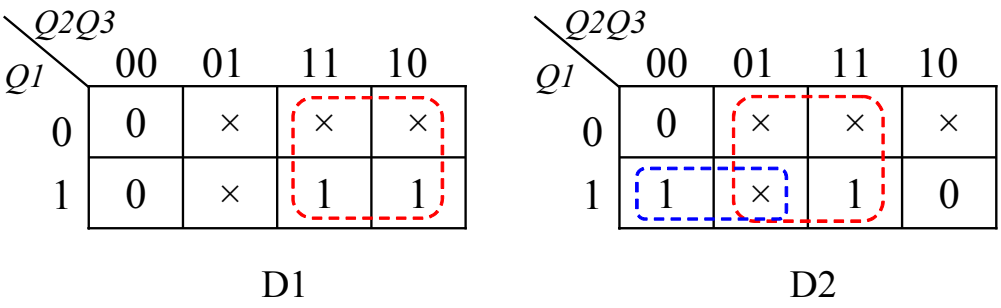

Figure C.2: Karnaugh-maps for the 4-ary ASK decoder outputs D1 and D2

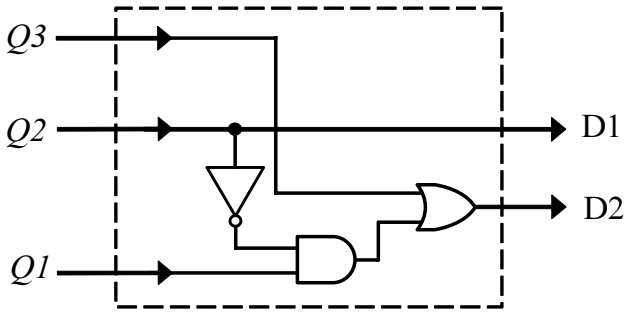

Figure C.3: 4-ary ASK decoder circuit diagram

Appendix D

Duobinary Filters

There exits two common methods to generate duobinary signals. They are; the electrical low-pass filtering (LPF) method [24, 79, 80] and the conventional electrical one-bit delay and add method [24, 25, 26]. The electrical LPF used in generating a duobinary signal is usually based on an electrical LPF having a 3 dB bandwidth of about $\frac{1}{4}$ of the of the bit rate [106, 78, 105]. The one-bit delay-and-add method can be constructed by splitting the electrical signal by an RF power divider and delaying one of the paths by 1 bit delay and then combining the two signals together in a RF power combiner. It is also possible to implement the one-bit delay-and-add duobinary encoder by using a transmission line with an open circuit (O.C.) stub connected parallel to it (Duobinary Stub filter) as shown in figure D.1.

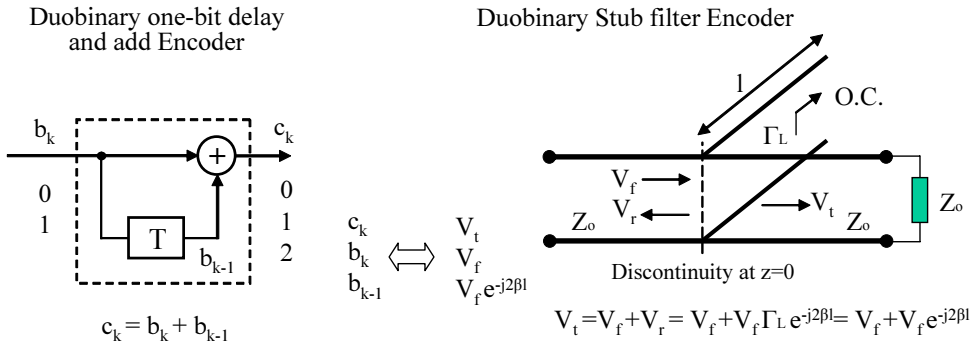

Figure D.1: Schematic of the one bit delay-and-add duobinary encoder versus the stub filter duobinary encoder

At the discontinuity, represented in figure D.1 by an open stub connected in parallel across the transmission line, the total voltages on either side of the junction must be identical. Therefore at the plane z=0, taken as a local reference plane $V_f + V_r = V_t + 0$ since there in no wave reflected from the matched load back to the discontinuity, where V_f, V_r and V_t are the forward, reverse and transmitted traveling wave voltages, respectively. With the transmission coefficient defined as $T = V_t/V_f$, it follows that $T = 1 + \Gamma$, where Γ is the voltage reflection coefficient just to the left of the open stub. Assuming lossless lines $\Gamma = \Gamma_l e^{-j2\beta l}$, where $\Gamma_l = \frac{Z_{O.C.}-Z_o}{Z_{O.C.}+Z_o} = 1$ is the reflection coefficient at the load side of the

open circuit stub, $\beta = \frac{2\pi}{\lambda} = 2\pi(\frac{f}{\upsilon})$ is the phase coefficient, λ is the wavelength, f is the frequency, l is the length of the open stub, $\upsilon = c/\sqrt{\varepsilon_r}$ is the phase velocity in the medium with the relative permittivity ε_r, $Z_{O.C.} = Z_L = \infty$ is the O.C. load impedance, and Zo is the characteristic impedance [107]. Therefore the transmitted voltage $V_t = V_f + V_f e^{-j2\beta l} = V_f + V_f e^{-j2\pi f(\frac{2l}{\upsilon})}$.

It was possible to realize a Duobinary Encoder for a 10 Gbit/s data signal by constructing a stub filter using open stubs with single-path delays of 50 ps ($\frac{l}{\upsilon} = 50\text{ps}$) by making the length of the O.C. stub ($l = \upsilon \times 50 = \frac{c}{\sqrt{\varepsilon_r}} \times 50 \simeq 8.15\text{mm}$) where $c = 2.997925 \times 10^8 m/s$ is the speed of light in free space, and $\varepsilon_r = 3.38$ is the dielectric constant for the material used to build the microstrip transmission lines (RO4003 from Rogers). This stub filter responds to an impulse by two impulses of equal height and 100 ps mutual delay (1 bit =$\frac{2l}{\upsilon} = 100\text{ps}$), thereby forming an idealized duobinary one-bit-delay and add filter as shown in figure D.2 (a). The simulated frequency response of the LPF stub used in this experiment had a ~ 35 dB dip at the frequency 5 GHz (Stub-5) as shown in figure D.3. The eye diagram for a generated 10 Gbit/s electrical duobinary signal shown in figure D.3 is measured after filtering a 10 Gbit/s electrical binary NRZ-ASK signal by the constructed stub (Stub-5).

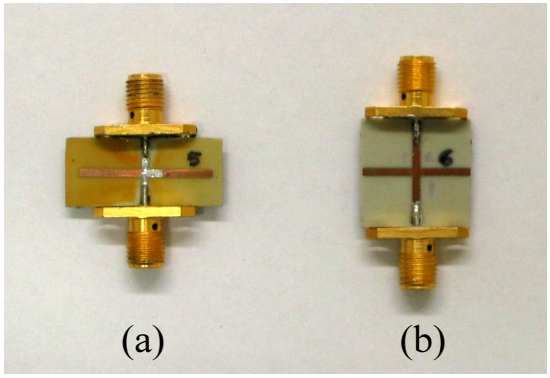

Figure D.2: Photo of constructed electrical stub LPFs, (a) Stub-5, (b) Stub-6

Another duobinary stub LPF, producing impulses spaced by 83 ps ($\frac{2l}{\upsilon} = 83\text{ps}$) and having a frequency response dip at 6 GHz (Stub-6), was also constructed as shown in figure D.2 (b). The frequency response of the LPF stub (Stub-6) is shown in figure D.4. The eye diagram shown in figure D.4 is for a 10 Gbit/s electrical duobinary signal generated by filtering a 10 Gbit/s electrical binary NRZ-ASK signal by this stub (Stub-6). Several versions of the Duobinary stub filters with slightly different lengths were built and tested in order to optimize the performance and response of the filter.

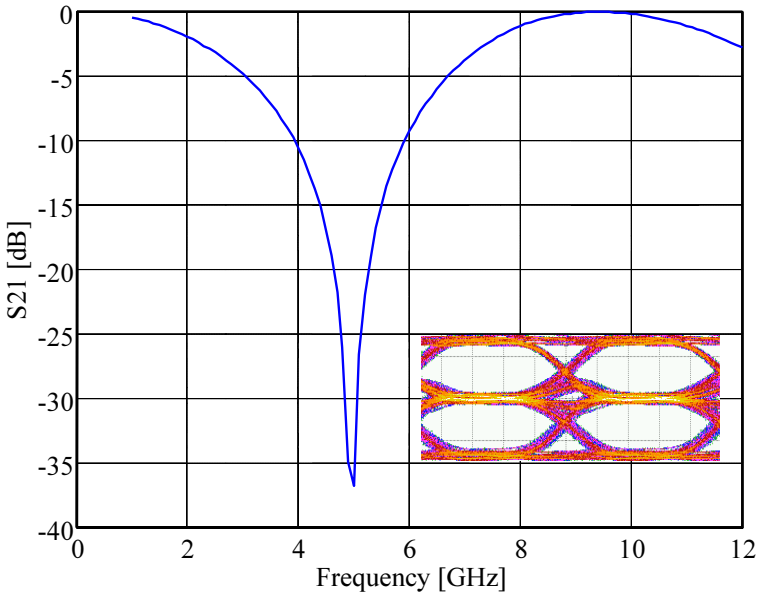

Figure D.3: Frequency response of the electrical stub LPF (Stub-5) and eye diagram of a generated 10 Gbit/s electrical duobinary signal

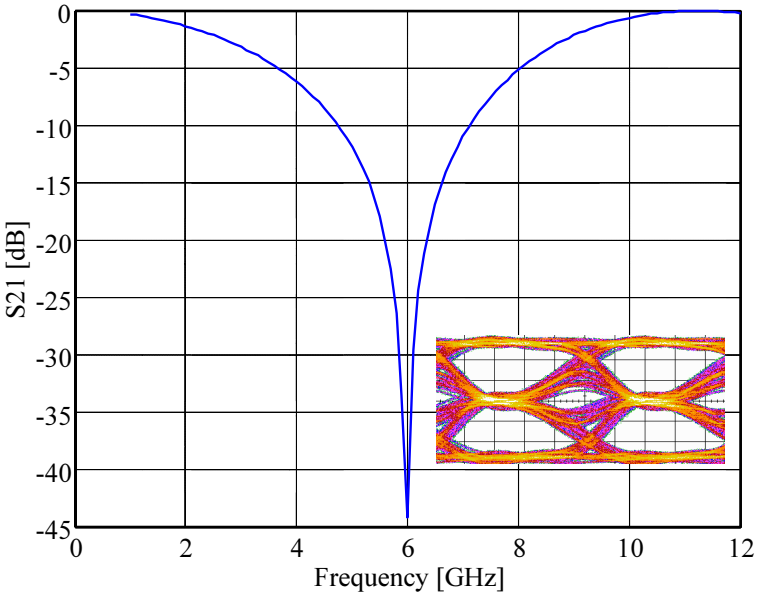

Figure D.4: Frequency response of the electrical stub LPF (Stub-6), and eye diagram of a generated 10 Gbit/s electrical duobinary signal

Figure D.5 and D.6 show the frequency response of a 5th order Bessel LPF with a 3 dB corner frequency at 2.8 GHz [82] plotted together with the frequency response of the Stub-5 and Stub-6 filters respectively. From figure D.6 it can be noticed that the 3 dB corner frequency of the Stub-6 was approximately the same as the Bessel filter, therefore the duobinary signal generated using the Stub-6 filter will perform more similar to a duobinary signal generated using the Bessel filter.

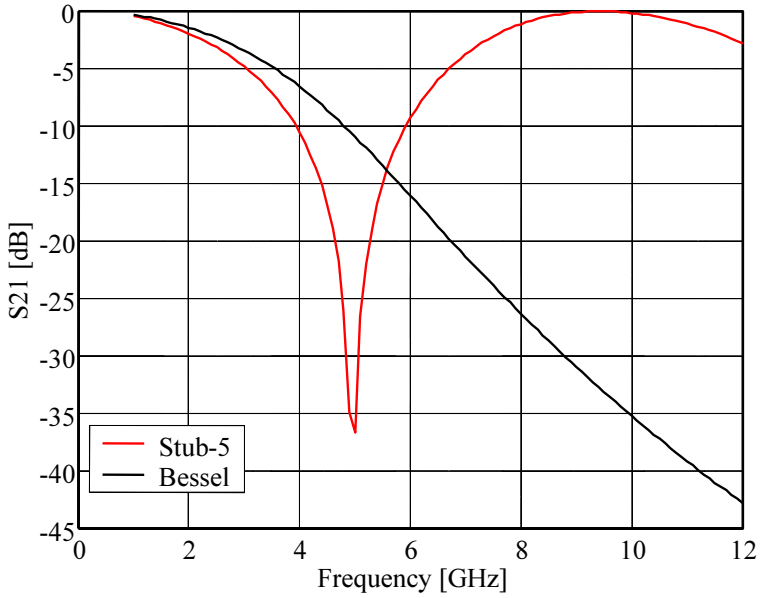

Figure D.5: Frequency response of a Stub-5 filter and 5th order Bessel LPF (3dB@2.8GHz)

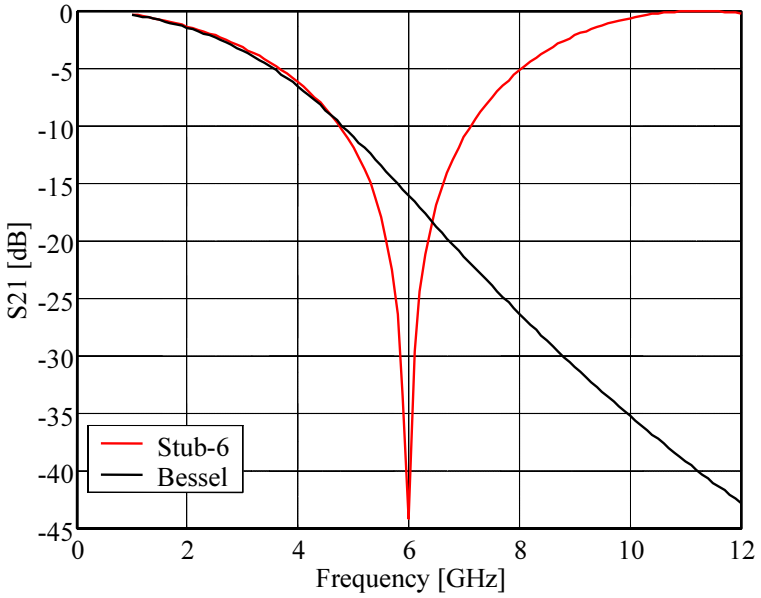

Figure D.6: Frequency response of a Stub-6 filter and 5th order Bessel LPF (3dB@2.8GHz)

Bibliography

[1] K.-P. Ho, *Phase-Modulated Optical Communication Systems*, Springer, 2005, ISBN 0-387-24392-5.

[2] J. M. Kahn and K.-P. Ho, "Spectral efficiency limits in DWDM systems", in *31st European Conference on Optical Communication (ECOC 2005),* Glasgow, vol. 4, pp. 843 – 846, September 2005.

[3] K. Petermann and S. Randel, "Strategies for spectrally efficient optical fiber communication systems with direct detection", in *International Conference on Transparent Optical Networks (ICTON 2003),* Warsaw, Poland, vol. 2, pp. 58 – 63, 2003.

[4] H. Louchet, K. Petermann, A. Robinson, and R. Epworth, "On the spectral information distribution in optical fibers", in *IEEE Lasers and Electro-Optics Society Annual Meeting (LEOS 2004),* Rio Grande, Puerto Rico, vol. 1, pp. 17 – 18, 2004.

[5] N. Kikuchi, "Amplitude and phase modulated 8-ary and 16-ary multilevel signaling technologies for high-speed optical fiber communication", in *SPIE Proceedings,* vol. 6021, pp. 17 – 18, 2005.

[6] S. K. Ibrahim, S. Bhandare, and R. Noé, "Performance of 20 Gbit/s Quaternary Intensity Modulation Based on Binary or Duobinary Modulation in Two Quadratures With Unequal Amplitudes", *IEEE Journal of Selected Topics in Quantum Electronics*, vol. 12, no. 4, pp. 596 – 602, 2006.

[7] S. K. Ibrahim, S. Bhandare, and R. Noé, "20 Gbit/s Quaternary Intensity Modulation Based on Duobinary Modulation with Unequal Amplitude in Two Polarizations", *IEEE Photonics Technology Letters*, vol. 18, no. 14, pp. 1482 – 1484, 2006.

[8] B. Wedding, W. Idler, B. Franz, W. Pöhlmann, and E. Lach, "40 Gbit/s quaternary dispersion supported transmission over 31 km standard singlemode fibre without optical dispersion compensation", in *24th European Conference on Optical Communication (ECOC 1998),* Madrid, Spain, vol. 1, pp. 523 – 524, September 1998.

[9] S. Walklin and J. Conradi, "A 10 Gb/s 4-ary ASK Lightwave System", in *23rd European Conference on Optical Communication (ECOC 1997),* Edinburgh, UK, pp. 255 – 258, September 1997.

[10] S. Walklin and J. Conradi, "Multilevel signaling for increasing the reach of 10 Gb/s lightwave systems", *IEEE Journal of Lightwave Technology*, vol. 17, no. 11, pp. 2235 – 2248, November 1999.

[11] H. Suzuki, J. Kani, T. Nakamura, M. Teshima, and K. Iwatsuki, "High-Spectral-Efficiency DWDM Access Network Supporting 10-Gbps Access Services", in *Optical Fiber Communications Conference (OFC 2003),* Atlanta, Georgia, USA, vol. 2, pp. 551 – 552, March 2003.

[12] A. Wonfor, J. K. White, E. E. Coulson, R. V. Penty, and I. H. White, "Uncooled operation of a 40Gb/s directly modulated multi-level laser for datacoms applications", in *29th European Conference on Optical Communication (ECOC 2003),* Rimini, Italy, Tu4.5.6, September 2003.

[13] R. A. Griffin and A. C. Carter, "Optical differential quadrature phase-shift key (oDQPSK) for high capacity optical transmission", in *Optical Fiber Communications Conference (OFC 2002),* Anaheim, California, USA, WX6, pp. 367 – 368, March 2002.

[14] C. Wree, J. Leibrich, J. Eick, and W. Rosenkranz, "Experimental investigation of receiver sensitivity of RZ-DQPSK modulation format using balanced detection", in *Optical Fiber Communications Conference (OFC 2003),* Atlanta, Georgia, USA, vol. 2, pp. 456 – 457, March 2003.

[15] A. H. Gnauck and P. J. Winzer, "Optical Phase-Shift-Keyed Transmission", *IEEE Journal of Lightwave Technology*, vol. 23, no. 1, pp. 115 – 130, January 2005.

[16] Y. Han and G. Li, "Differential Polarization-Phase-Shift Keying without Using Polarization Control", in , Anaheim, CA, USA, JWA39, March 2005.

[17] Y. Han and G. Li, "Direct detection differential polarization-phase-shift keying based on Jones vector", *Optics Express*, vol. 12, no. 24, pp. 5821 – 5826, November 2004.

[18] X. Liu, X. Wei, Y.-H. Kao, J. Leuthold, C. R. Doerr, and L. F. Mollenauer, "Quaternary differential-phase amplitude-shift-keying for DWDM transmission", in *29th European Conference on Optical Communication (ECOC 2003),* Rimini, Italy, vol. 4, pp. 1010 – 1011, September 2003.

[19] M. Ohm and J. Speidel, "Quaternary Optical ASK-DPSK and Receivers With Direct Detection", *IEEE Photonics Technology Letters*, vol. 15, no. 1, pp. 159 – 161, 2003.

[20] T. Nakamura, J.-I. Kani, M. Teshima, and K. Iwatsuki, "A quaternary amplitude shift keying modulator for suppressing initial amplitude distortion", *IEEE Journal of Lightwave Technology*, vol. 22, no. 3, pp. 733 – 738, March 2004.

[21] S. K. Ibrahim, S. Bhandare, H. Zhang, and R. Noé, "2×10 Gbit/s Quaternary Intensity Modulation Generation using an Optical QPSK modulator", in *SPIE Proceedings,* vol. 6021, December 2005.

[22] M. I. Hayee, M. C. Cardakli, A. B. Sahin, and A. E. Willner, "Doubling of bandwidth utilization using two orthogonal polarizations and power unbalancing in a polarization-division-multiplexing scheme", *IEEE Photonics Technology Letters*, vol. 13, no. 8, pp. 881 – 883, August 2001.

[23] M. I. Hayee, M. C. Cardakli, and A. E. Willner, "Power unbalanced polarization division-multiplexing for efficient bandwidth utilization", in *Conference on Lasers and Electro-Optics (CLEO 1999),* Baltimore, MD, USA, CTuQl, pp. 181 – 182, May 1999.

[24] T. Ono, Y. Yano, and K. Fukuchi, "Demonstration of high-dispersion tolerance of 20-Gbit/s optical duobinary signal generated by a low-pass filtering method", in *Optical Fiber Communications Conference (OFC 1997),* Dallas, USA, ThH1, pp. 268 – 269, February 1997.

[25] K. Yonenaga, S. Kuwano, S. Norimatsu, and N. Shibata, "Optical duobinary transmission system with no receiver sensitivity degradation", *IEE Electronic Letters*, vol. 31, no. 4, pp. 302 – 304, Feb. 1995.

[26] K. Yonenaga and S. Kuwano, "Dispersion-Tolerant Optical Transmission System Using Duobinary Transmitter and Binary Receiver", *IEEE Journal of Lightwave Technology*, vol. 15, no. 8, pp. 1530 – 1537, August 1997.

[27] S. K. Ibrahim, S. Bhandare, and R. Noé, "Narrowband 20 Gbit/s Quaternary Intensity Modulation Generated by Duobinary 10 Gbit/s Modulation in 2 Quadratures", in *31st European Conference on Optical Communication (ECOC 2005),* Glasgow, Scotland, vol. 4, pp. 909 – 910, September 2005.

[28] S. K. Ibrahim, S. Bhandare, H. Zhang, and R. Noé, "2×10 Gbit/s Quaternary Intensity Modulation Generation using an Optical QPSK modulator", in *Asia-Pacific Optical Communications Conference (APOC 2005),* Shanghai, China, 6021-44, November 2005.

[29] S. K. Ibrahim, S. Bhandare, and R. Noé, "Narrowband 2×10 Gbit/s Quaternary Intensity Modulation Based on Duobinary Modulation in Two Polarizations with Unequal Amplitudes", in *Optical Fiber Communication Conference (OFC 2006),* Anaheim, CA, USA, OThI2, March 2006.

[30] G. Jacobsen, *Noise in Digital Optical Transmission Systems*, Artech House, 1994, ISBN 0-89006-695-7.

[31] R. Noé, "Optical amplifier performance in digital optical communication systems", *Electrical Engineering*, vol. 83, pp. 15 – 20, February 2001.

[32] G. P. Agrawal, *Fiber-Optic Communication Systems*, Wiley, 1992, ISBN 0-471-54286-5.

[33] A. E. Willner, "Chromatic Dispersion and Polarization-Mode Dispersion: Managing Key Limitations in Optical Communication Systems", *Optics and Photonics News, OPN Trends, OSA*, vol. 13, no. 2, pp. 116 – 121, March 2002.

[34] A. F. Elrefaie, R. E. Wagner, D. A. Atlas, and D. G. Daut, "Chromatic Dispersion Limitations in Coherent Lightwave Transmission Systems", *IEEE Journal of Lightwave Technology*, vol. 6, no. 5, pp. 704 – 709, May 1988.

[35] A. Hodzic, *Investigations of high bit rate optical transmission systems employing a channel data rate of 40 Gb/s*, Ph.D. thesis, Technische Universität Berlin, Berlin, Germany, 2004.

[36] R. Noé, D. Sandel, S. Bhandare, F. Wüst, B. Milivojevic, and V. Mirvoda, "Chromatic dispersion monitoring by synchronous signal arrival time detection in the clock recovery PLL", *Journal of Optical Networking, OSA*, vol. 3, no. 8, pp. 589 – 600, 2004.

[37] P. J. Corvini and T. L. Koch, "Computer Simulation of High-Bit-Rate Optical Fiber Transmission Using Single-Frequency Lasers", *IEEE Journal of Lightwave Technology*, vol. 5, no. 11, pp. 1591 – 1595, November 1987.

[38] S. Ryu, *Coherent Lightwave Communication Systems*, Artech House, 1995, ISBN 0-89006-612-4.

[39] M. Ohm and J. Speidel, "Optimal Receiver Bandwidths, Bit Error Probabilities and Chromatic Dispersion Tolerance of 40Gbit/s Optical 8-DPSK with NRZ and RZ Impulse Shaping", in *Optical Fiber Communications Conference (OFC 2005),* Anaheim, CA, USA, OFG5, 2005.

[40] M. W. Chbat and D. Penninckx, "High-spectral-efficiency transmission systems", in *Optical Fiber Communications Conference (OFC 2005),* Baltimore, USA, TuJ1, pp. 134 – 136, March 2000.

[41] J. M. Kahn and K.-P. Ho, "Spectral efficiency limits and modulation/detection techniques for DWDM systems", *IEEE Journal of Selected Topics in Quantum Electronics*, vol. 10, no. 2, pp. 259 – 272, March/April 2004.

[42] S. Haykin, *Communication Systems*, Wiley, Fourth edition, 2001, ISBN 0-471-17869-1.

[43] J. D. Ralston, J. M. Kahn, and K.-P. Ho, "Advanced modulation and signal processing techniques for 40 Gb/s optical transmission systems", in *SPIE Proceedings,* vol. 4872, pp. 24 – 31, 2002.

[44] B. Milivojevic, *Study of Optical Differential Phase Shift Keying Transmission Techniques at 40 Gbit/s and beyond*, Ph.D. thesis, University of Paderborn, EIM-E, Paderborn, Germany, 2005.

[45] T. Tokle, *Optimised Dispersion Management and Modulation Formats for High Speed Optical Communication Systems*, Ph.D. thesis, Research Center COM, Technical University of Denmark, Denmark, 2004.

[46] P. J. Winzer and R.-J. Essiambre, "Advanced optical modulation formats", in *29th European Conference on Optical Communication (ECOC 2003),* Rimini, Italy, vol. 4872, pp. 1002 – 1003, 2003.

[47] S. Bigo, G. Charlet, and E. Corbel, "What has hybrid phase/intensity encoding brought to 40 Gbit/s ultralong-haul systems?", in *30th European Conference on Optical Communication (ECOC 2004),* Stockholm, Sweden, pp. 872 – 875, 2004.

[48] T. Kataoka, Y. Miyamota, K. Hagimoto, and K. Noguchi, "20 Gbit/s long distance transmission using a 270 photon/bit optical preamplifier receiver", *IEE Electronic Letters*, vol. 30, no. 9, pp. 715 – 716, April 1994.

[49] M. Daikoku, N. Yoshikane, and I. Morita, "Performance comparison of modulation formats for 40 Gbit/s DWDM transmission systems", in *Optical Fiber Communications Conference (OFC 2005),* Anaheim, CA, USA, OFN2, March 2005.

[50] A. Hodzic, B. Konrad, and K. Petermann, "Alternative Modulation Formats in N×40 Gb/s WDM Standard Fiber RZ-Transmission Systems", *IEEE Journal of Lightwave Technology*, vol. 20, no. 4, pp. 598 – 607, April 2002.

[51] W. Idler, A. Klekamp, R. Dischler, and B. Wedding, "Advantages of Frequency Shift Keying in 10 Gb/s Systems", in *IEEE Lasers and Electro-Optics Society Annual Meeting (LEOS 2004),* Rio Grande, Puerto Rico, FD3, 2004.

[52] T. Sakamoto, T. Kawanishi, T. Miyazaki, and M. Izutsu, "Novel modulation scheme for optical continuous-phase frequency-shift keying", in *Optical Fiber Communications Conference (OFC 2005),* Anaheim, CA, USA, OFG2, March 2005.

[53] B. Wedding, R. Jung, C. Haslach, and H. Söhnle, "10.7 Gbit/s FSK transmission with 61 dB power budget", in *29th European Conference on Optical Communication (ECOC 2003),* Rimini, Italy, Th1.5.5, September 2003.

[54] J. Mo, Y. Dong, Y. Wen, S. Takahashi, Y. Wang, and C. Lu, "Optical Minimum-Shift Keying Modulator for High Spectral Efficiency WDM Systems", in *31st European Conference on Optical Communication (ECOC 2005),* Glasgow, Scotland, Th1.2.3, September 2005.

[55] A. Gnauck, "40-Gb/s RZ-Differential Phase Shift Keyed Transmission", in *Optical Fiber Communications Conference (OFC 2003),* Atlanta, Georgia, USA, ThE1, March 2003.

[56] A. H. Gnauck, S. Chandrasekhar, J. Leuthold, and L. Stulz, "Demonstration of 42.7-Gb/s DPSK Receiver With 45 Photons/Bit Sensitivity", *IEEE Photonics Technology Letters*, vol. 15, no. 1, pp. 99 – 101, January 2003.

[57] A. Hirano, Y. Miyamoto, and S. Kuwahara, "Performances of CSRZ-DPSK and RZ-DPSK in 43-Gbit/s/ch DWDM G.6S2 Single-Mode-Fiber Transmission", in *Optical Fiber Communications Conference (OFC 2003),* Atlanta, Georgia, USA, vol. 2, pp. 454 – 456, March 2003.

[58] G. Bosco, A. Carena, V. Curri, R. Gaudino, and P. Poggiolini, "Modulation Formats Suitable for Ultrahigh Spectral Efficient WDM Systems", *IEEE Journal of Lightwave Technology*, vol. 10, no. 2, pp. 454 – 456, March/April 2004.

[59] H. Kim, "Differential Phase Shift Keying for 10-Gb/s and 40-Gb/s Systems", in *IEEE Lasers and Electro-Optics Society Annual Meeting (LEOS 2004),* Rio Grande, Puerto Rico, ThC1, pp. 13 – 14, 2004.

[60] A. Carena, V. Curri, R. Gaudino, N. Greco, P. Poggiolini, and S. Benedetto, "Polarization modulation in ultra-long haul transmission systems: a promising alternative to intensity modulation", in *24th European Conference on Optical Communication (ECOC 1998),* Madrid, Spain, WdA24, pp. 429 – 430, September 1998.

[61] A. S. Siddiqui, S. G. Edirisinghe, J. J. Lepley, J. G. Ellison, and S. D. Walker, "Dispersion-tolerant transmission using a duobinary polarization-shift keying transmission scheme", *IEEE Photonics Technology Letters*, vol. 14, no. 2, pp. 158 – 160, February 2002.

[62] S. G. Edirisinghe, J. J. Lepley, and A. S. Siddiqui, "Polarization shaped duobinary transmission scheme", *IEEE Photonics Technology Letters*, vol. 13, no. 11, pp. 1245 – 1247, November 2001.

[63] A. H. Gnauck, X. Liu, X. Wei, D. M. Gill, and E. C. Burrows, "Comparison of Modulation Formats for 42.7-Gb/s Single-Channel Transmission Through 1980 km of SSMF", *IEEE Photonics Technology Letters*, vol. 16, no. 3, pp. 1245 – 1247, March 2004.

[64] J. G. Proakis, *Digital Communications*, McGraw-Hill, Second edition, 1989, ISBN 0-07-050937-9.

[65] J. G. Proakis and M. Salehi, *Communication Systems Engineering*, Prentice Hall, 1994, ISBN 0-13-158932-6.

[66] G. L. Li and P. K. L. Yu, "Optical Intensity Modulators for Digital and Analog Applications", *IEEE Journal of Lightwave Technology*, vol. 21, no. 9, pp. 2010 – 2030, September 2003.

[67] W. A. Atia and R. S. Bondurant, "Demonstration of Return-to-zero Signaling in Both OOK and DPSK Formats to Improve Receiver Sensitivity in an Optically Preamplified Receiver", in *IEEE Lasers and Electro-Optics Society Annual Meeting (LEOS 1999),* San Francisco, CA, USA, TuM3, pp. 226 – 227, 1999.

[68] I. Lyubomirsky and C.-C. Chien, "DPSK Demodulator Based on Optical Discriminator Filter", *IEEE Photonics Technology Letters*, vol. 17, no. 2, pp. 492 – 494, February 2005.

[69] R. A. Griffin, R. L. Johnstone, R. G. Walker, J. Hall, S. D. Wadsworth, K. Berry, A. C. Carter, and M. J. Wale, "10 Gb/s optical differential quadrature phase shift key (DQPSK) transmission using GaAs/AlGaAs integration", in *Optical Fiber Communications Conference (OFC 2002),* Anaheim, California, USA, FD6, March 2002.

[70] C. Wree, J. Leibrich, and W. Rosenkranz, "RZ-DQPSK format with high spectral efficiency and high robustness toward fiber nonlinearities", in *28th European Conference on Optical Communication (ECOC 2002),* Copenhagen, Denmark, 9.6.6, September 2002.

[71] E. A. Swanson, J. C. Livas, and R. S. Bondurant, "High Sensitivity Optically Preamplified Direct Detection DPSK Receiver with Active Delay-Line Stabilization", *IEEE Photonics Technology Letters*, vol. 6, no. 2, pp. 263 – 265, February 1994.

[72] G. Bosco and P. Poggiolini, "The Impact of Receiver Imperfections on the Performance of Optical Direct-Detection DPSK", *IEEE Journal of Lightwave Technology*, vol. 23, no. 2, pp. 842 – 848, February 2005.

[73] D. Penninckx, H. Bissessur, P. Brindle, E. Gohin, and F. Bakhti, "Optical differential phase shift keying (DPSK) direct detection considered as a duobinary signal", in *27th European Conference on Optical Communication (ECOC 2001),* Amsterdam, The Netherlands, We.P.40, pp. 456 – 457, September 2001.

[74] X. Wei, X. Liu, S. Chandrasekhar, A. H. Gnauck, G. Raybon, J. Leuthold, and P. J. Winzer, "40 Gb/s duobinary and modified duobinary transmitter based on an optical delay interferometer", in *28th European Conference on Optical Communication (ECOC 2002),* Copenhagen, Denmark, 9.6.3, September 2002.

[75] T. Ono, Y. Yano, K. Fukuchi, T. Ito, H. Yamazaki, M. Yamaguchi, and K. Emura, "Characteristics of Optical Duobinary Signals in Terabit/s Capacity, High-Spectral Efficiency WDM Systems", *IEEE Journal of Lightwave Technology*, vol. 16, no. 5, pp. 788 – 797, May 1998.

[76] W. Kaiser, T. Wuth, M. Wichers, and W. Rosenkranz, "Reduced Complexity Optical Duobinary 10-Gb/s Transmitter Setup Resulting in an Increased Transmission Distance", *IEEE Photonics Technology Letters*, vol. 13, no. 8, pp. 884 – 886, August 2001.

[77] G. Charlet, J.-C. Antona, S. Lanne, P. Tran, W. Idler, M. Gorlier, S. Borne, A. Klekamp, C. Simonneau, L. Pierre, Y. Frignac, M. Molina, F. Beaumont, J.-P. Hamaide, and S. Bigo, "6.4Tb/s (159$\times$42.7Gb/s) Capacity over 21$\times$100 km using Bandwidth-limited Phase-Shaped Binary Transmission", in *28th European Conference on Optical Communication (ECOC 2002),* Copenhagen, Denmark, PD4.1, September 2002.

[78] W. Rosenkranz, "High Capacity Optical Communication Networks - Approaches for Efficient Utilization of Fiber Bandwidth", in *First Joint Symposium on Opto- & Microelectronic Devices and Circuits (SODC 2000),* Nanjing, China, pp. 106 – 107, April 2000.

[79] A. J. Price and N. L. Mercier, "Reduced bandwidth optical intensity modulation with improved chromatic dispersion tolerance", *IEE Electronic Letters*, vol. 31, no. 1, pp. 58 – 59, January 1995.

[80] A. J. Price, L. Pierre, R. Uhel, and V. Havard, "210 km Repeaterless 10 Gb/s Transmission Experiment Through Nondispersion-Shifted Fiber Using Partial Response Scheme", *IEEE Photonics Technology Letters*, vol. 7, no. 10, pp. 1219 – 1221, October 1995.

[81] D. Penninckx, "Dispersion-tolerant modulation techniques for optical communications", in *24th European Conference on Optical Communication (ECOC 1998),* Madrid, Spain, vol. 1, pp. 509 – 510, September 1998.

[82] D. Penninckx, "Effect of electrical filtering of duobinary signals on the chromatic dispersion transmission limitations", in *24th European Conference on Optical Communication (ECOC 1998),* Madrid, Spain, vol. 1, pp. 537 – 538, September 1998.

[83] H. Kim and C. X. Yu, "Optical Duobinary Transmission System Featuring Improved Receiver Sensitivity and Reduced Optical Bandwidth", *IEEE Photonics Technology Letters*, vol. 14, no. 8, pp. 1205 – 1207, August 2002.

[84] H. Kim, C. X. Yu, and D. T. Neilson, "Demonstration of Optical Duobinary Transmission System Using Phase Modulator and Optical Filter", *IEEE Photonics Technology Letters*, vol. 14, no. 7, pp. 1010 – 1012, July 2002.

[85] H. Kim and P. J. Winzer, "Robustness to Laser Frequency Offset in Direct-Detection DPSK and DQPSK Systems", *IEEE Journal of Lightwave Technology*, vol. 21, no. 9, pp. 1887 – 1891, September 2003.

[86] P. S. Cho, V. S. Grigoryan, Y. A. Godin, A. Salamon, and Y. Achiam, "Transmission of 25-Gb/s RZ-DQPSK Signals With 25-GHz Channel Spacing Over 1000 km of SMF-28 Fiber", *IEEE Photonics Technology Letters*, vol. 15, no. 3, pp. 473 – 475, March 2003.

[87] C. Wree, N. Hecker-Denschlag, E. Gottwald, P. Krummrich, J. Leibrich, E.-D. Schmidt, B. Lankl, and W. Rosenkranz, "High Spectral Efficiency 1.6-b/s/Hz Transmission (8×40 Gb/s With a 25-GHz Grid) Over 200-km SSMF Using RZ-DQPSK and Polarization Multiplexing", *IEEE Photonics Technology Letters*, vol. 15, no. 9, pp. 1303 – 1305, September 2003.

[88] N. Yoshikane and I. Morita, "1.14 b/s/Hz spectrally-efficient 50×85.4 Gb/s transmission over 300 km using copolarized CS-RZ DQPSK signals", in *Optical Fiber Communications Conference (OFC 2004),* Los Angeles, CA, USA, PDP38, February 2004.

[89] S. Bhandare, D. Sandel, B. Milivojevic, A. Hidayat, A. A. Fauzi, H. Zhang, S. K. Ibrahim, F. Wüst, and R. Noé, "5.94-Tb/s 1.49-b/s/Hz (40×2×2×40 Gb/s) RZ-DQPSK Polarization-Division Multiplex C-Band Transmission Over 324 km", *IEEE Photonics Technology Letters*, vol. 17, no. 4, pp. 914 – 916, April 2005.

[90] G. Kramer, A. Ashikhmin, A. J. van Wijngaarden, and X. Wei, "Spectral Efficiency of Coded Phase-Shift Keying for Fiber-Optic Communication", *IEEE Journal of Lightwave Technology*, vol. 21, no. 10, pp. 2438 – 2445, October 2003.

[91] A. H. Gnauck, P. J. Winzer, C. Dorrer, and S. Chandrasekhar, "Linear and Nonlinear Performance of 42.7-Gb/s Single-Polarization RZ-DQPSK Format", *IEEE Photonics Technology Letters*, vol. 18, no. 7, pp. 883 – 885, April 2006.

[92] R. A. Griffin, "Integrated DQPSK Transmitters", in *Optical Fiber Communications Conference (OFC 2005),* Anaheim, CA, USA, OWE3, March 2005.

[93] K.-P. Ho and H.-W. Cuei, "Generation of Arbitrary Quadrature Signals Using One Dual-Drive Modulator", *IEEE Journal of Lightwave Technology*, vol. 23, no. 2, pp. 764 – 770, February 2005.

[94] J. M. Gené, M. Soler, R. I. Killey, and J. Prat, "Investigation of 10-Gb/s Optical DQPSK Systems in Presence of Chromatic Dispersion, Fiber Nonlinearities, and Phase Noise", *IEEE Photonics Technology Letters*, vol. 16, no. 3, pp. 924 – 926, March 2004.

[95] D. van den Borne, S. L. Jansen, E. Gottwald, P. M. Krummrich, P. Leisching, G. D. Khoe, and H. de Waardt, "A robust modulation format for 42.8-Gbit/s long-haul transmission: RZ-DPSK or RZ-DQPSK?", in *7th ITG Fachtagung on Photonic Networks,* Leipzig, Germany, pp. 51 – 56, April 2006.

[96] S. Bhandare, D. Sandel, B. Milivojevic, A. Hidayat, A. Fauzi, H. Zhang, S. K. Ibrahim, F. Wüst, and R. Noé, "5.94 Tbit/s (40×2×2×40 Gbit/s) C-Band Transmission over 324 km using RZ-DQPSK Combined with Polarization Division Multiplex", in *6th ITG Fachtagung on Photonic Networks "Photonische Netze",* Leipzig, Germany, pp. 87 – 90, May 2005.

[97] D. van den Borne, S. L. Jansen, E. Gottwald, P. M. Krummrich, G. D. Khoe, and H. de Waardt, "1.6-b/s/Hz Spectrally Efficient 40×85.6-Gb/s Transmission Over 1,700 km of SSMF Using POLMUX-RZ-DQPSK", in *Optical Fiber Communications Conference (OFC 2006),* Anaheim, CA, USA, PDP34, March 2006.

[98] Y. Zhu, K. Cordina, N. Jolley, R. Feced, H. Kee, R. Rickard, and A. Hadjifotiou, "1.6 bit/s/Hz orthogonally polarized CSRZ-DQPSK transmission of 8×40 Gbit/s over 320 km NDSF", in *Optical Fiber Communications Conference (OFC 2004),* Los Angeles, CA, USA, TuF1, February 2004.

[99] B. Milivojevic, A. F. Abas, A. Hidayat, S. Bhandare, D. Sandel, R. Noé, M. Guy, , and M. Lapointe, "1.6-b/s/Hz 160-Gb/s 230-km RZ-DQPSK Polarization Multiplex Transmission With Tunable Dispersion Compensation", *IEEE Photonics Technology Letters*, vol. 17, no. 2, pp. 495 – 497, February 2005.

[100] P. S. Cho, G. Harston, C. J. Kerr, A. S. Greenblatt, A. Kaplan, Y. Achiam, G. Levy-Yurista, M. Margalit, Y. Gross, and J. B. Khurgin, "Investigation of 2-b/s/Hz 40-Gb/s DWDM Transmission Over 4×100 km SMF-28 Fiber Using RZ-DQPSK and Polarization Multiplexing", *IEEE Photonics Technology Letters*, vol. 16, no. 2, pp. 656 – 658, February 2004.

[101] S. S. Walklin, *Multilevel Signaling for Increasing the Capacity of High-Speed Optical Communication Systems*, Ph.D. thesis, University of Alberta, Canada, 1997.

[102] J.-P. Elbers, H. Wernz, H. Griesser, C. Glingener, A. Faerbert, S. Langenbach, N. Stojanovic, C. Dorschky, T. Kupfer, and C. Schulien, "Measurement of the dispersion tolerance of optical duobinary with an MLSE receiver at 10.7 Gb/s", in *Optical Fiber Communications Conference (OFC 2005),* Anaheim, CA, USA, OThJ4, March 2005.

[103] S. Hayase, N. Kikuchi, K. Sekine, and S. Sasaki, "Proposal of 8-state per symbol (binary ASK and QPSK) 30-Gbit/s optical modulation/demodulation scheme", in *29th European Conference on Optical Communication (ECOC 2003),* Rimini, Italy, Th2.6.4, September 2003.

[104] I. Lyubomirsky and C.-C. Chien, “Tailoring the Duobinary Pulse Shape for Optimum Performance”, *IEEE Journal of Lightwave Technology*, vol. 23, no. 11, pp. 3732 – 3736, November 2005.

[105] I. Lyubomirsky and C.-C. Chien, “Ideal Duobinary Generating Filter for Optically Amplified Systems”, *IEEE Photonics Technology Letters*, vol. 18, no. 4, pp. 598 – 600, February 2006.

[106] M. Wichers and W. Rosenkranz, “Optical duobinary modulation schemes using a Mach-Zehnder transmitter for lightwave systems”, in *International Conference on Transparent Optical Networks (ICTON 1999),* Kielce, Poland, We.B.1, pp. 15 – 18, June 1999.

[107] E. H. Fooks and R. A. Zakarevicius, *Microwave Engineering Using Microstrip Circuits*, Prentice Hall, 1990, ISBN 0-13-691650-3.